Joint mAster of Mediterranean Initiatives on renewabLe and sustainAble energy

Palestine Polytechnic University

Deanship of Graduate Studies and Scientific Research

Master Program of Renewable Energy and Sustainability

Hybrid Olive Pomace-CSP Power Plant Investigation and Analysis for Electricity Generation in Palestine

---

By
Eman Ajlouni

Supervisor
Dr. Zuhdi Salhab

Thesis submitted in partial fulfillment of requirements of the degree

Master of Science in Renewable Energy & Sustainability

April, 2021

The undersigned hereby certify that they have read, examined, and recommended to the Deanship of Graduate Studies and Scientific Research at Palestine Polytechnic University and the Faculty of Science at Al-Quds University the approval of a thesis entitled:

Hybrid Olive Pomace-CSP Power Plant Investigation and Analysis for Electricity Generation in Palestine

Submitted by
Eman Ajlouni

in partial fulfillment of the requirements for the degree of Master in Renewable Energy & Sustainability.

Graduate Advisory Committee:

Prof./Dr. ……,……..
(Supervisor), University (typed)
Signature: ———————— Date: ————————

Prof./ Dr. ……, ……..
(Co-supervisor), University (typed)
Signature: ———————— Date: ————————

Prof./Dr……,……..
(Internal committee member), University (typed).
Signature: ———————— Date: ————————

Prof./Dr. ……,……..
(External committee member), University (typed).
Signature: ———————— Date: ————————

Thesis Approved by:

Name:

Dean of Graduate Studies & Scientific Research

Palestine Polytechnic University

Signature:……

Date:……

Name:

Dean of Faculty of Graduate Studies

Al-Quds University

Signature:……

Date:……

ABSTRACT

This research aims to develop and investigate a power plant model from hybridization between CSP technology and olive pomace as a biomass resource for electricity generation in Palestine. And study the annual performance of the hybrid power plant. The hybrid Power plant model with a thermal efficiency of 36.76% was developed using EBSILON simulation software, using both Linear Fresnel (LF) Solar Field and Parabolic Trough (PT) Solar Field based on the same power block, for the same solar field land area, and under the same design conditions. EBSILON time series simulation was used to evaluate the annual electricity generation, the annual operation characteristics, and performance of the proposed hybrid power plant for both LF and PT solar fields relevant to variation of Direct Normal Irradiance and ambient temperature. Results showed the most acceptable capacity of the hybrid power plant is 7 MW, which its annual consumption compatible with the annual average amounts of olive pomace generated annually in Palestine. The LF hybrid power plant showed superiority over the PT hybrid power plant in electricity generation but with the advantage of more allowable area occupation of reflectors than PT, but also PT solar field showed higher thermal efficiency than hybrid power plant LF solar field. The hybridization using LF and PT found to be capable of producing 60,321 and 60,251 MWh of electricity respectively.

Simulations showed that the levelized cost of energy, for both LF hybrid power plant and the PT hybrid power plant were 0.0969 and 0.0971 $/kWh. The levelized cost of energy was calculated taking into consideration all investment and operational costs, and the cost was below the max threshold of 0.1212 S/kWh. Sensitivity analysis were carried out to investigate the increase in the levelized cost of energy versus the increase of olive pomace prices, Islamic profit rate, and land cost. Sensitivity analysis showed that with changing these parameters, the levelized cost of energy still below the max generation cost threshold in Palestine.

فحص ودراسة تحليلية لمحطة هجينة من جفت الزيتون و الطاقة الشمسية المركزة لتوليد الكهرباء في فلسطين

إيمان عجلوني

ملخص

يهدف هذا البحث إلى تطوير وفحص نموذج لمحطة طاقة كهربائية من التهجين بين تقنية الطاقة الشمسية المركزة وجفت الزيتون كمصدر للكتلة الحيوية لتوليد الكهرباء في فلسطين. ودراسة الأداء السنوي لمحطة توليد الكهرباء الهجينة. تم بناء المحطة باستخدام تكنولوجيا عواكس الـــ LF و الـ PT تحت نفس مساحة الارض المخصصة للحقل الشمسي وتحت نفس الظروف التشغيلية على قدرات تشغيلية متعددة ، لنفس مساحة أرض الحقل الشمسي ، وتحت نفس شروط التصميم. تم تطوير نموذج للمحطة الهجينة بكفاءة 36.76% و استخدام محاكاة السلاسل الزمنية في برنامج EBSILON لتقييم توليد الكهرباء السنوي ، وخصائص التشغيل السنوية ، وأداء محطة الطاقة الهجينة المقترحة لكل من الحقول الشمسية LF و PT ذات الصلة باختلاف الإشعاع العادي المباشر ودرجة الحرارة المحيطة. أظهرت النتائج أن أكثر قدرة مقبولة لمحطة توليد الطاقة الهجينة هي 7 ميجاوات ، ويتناسب استهلاكها السنوي مع المتوسط السنوي لكميات جفت الزيتون المنتجة سنويًا في فلسطين. أظهرت محطة توليد الطاقة الهجينة بحقل شمسي يعمل بـ LF تفوقًا على محطة توليد الطاقة الهجينة التي تعمل على الـ PT في توليد الكهرباء ولكن مع ميزة شغل مساحة أكبر من العاكسات مقارنةً بـ PT ، ولكن أيضًا أظهر الحقل الشمسي الذي يعمل على الـ PT كفاءة حرارية أعلى من المجال الشمسي لمحطة الطاقة الهجينة .وجد أن التهجين باستخدام LF و PT قادر على إنتاج 60321 و 60.251 ميجاوات ساعة من الكهرباء على التوالي. أظهرت نتائج المحاكاة أن التكلفة المستوية للطاقة لكل من محطة توليد الطاقة الهجينة LFومحطة الطاقة الهجينة PT كانت 0.0969 و 0.0971 دولار/ كيلو واط ساعة. و تم حساب التكلفة الموحدة للطاقة مع الأخذ في الاعتبار جميع تكاليف الاستثمار والتشغيل ، وكانت التكلفة أقل من الحد الأقصى البالغ 0.1212 دولار/ كيلو واط ساعة . تم إجراء تحليل الحساسية للتحقق من الزيادة في التكلفة الموحدة للطاقة مقابل ارتفاع أسعار ثفل الزيتون ومعدل الربح الإسلامي وتكلفة الأرض. أظهر تحليل الحساسية أنه مع تغيير هذه المعايير ، فإن التكلفة المعيارية للطاقة لا تزال أقل من الحد الأقصى لتكلفة التوليد في فلسطين.

DECLARATION

I declare that the Master Thesis entitled "Hybrid Olive Pomace-CSP Power Plant Investigation and Analysis for Electricity Generation in Palestine." is my own original work, and hereby certify that unless stated, all work contained within this thesis is my own independent research and has not been submitted for the award of any other degree at any institution, except where due acknowledgment is made in the text.

Student Name……..

Signature: ———————————— Date:————————

STATEMENT OF PERMISSION TO USE

In presenting this thesis in partial fulfillment of the requirements for the joint Master's degree in Renewable Energy & Sustainability at Palestine Polytechnic University and Al-Quds University, I agree that the library shall make it available to borrowers under the rules of the library.

Brief quotations from this thesis are allowable without special permission, provided that accurate acknowledgment of the source is made.

Permission for extensive quotation from reproduction or publication of this thesis may be granted by my main supervisor, or in his absence, by the Dean of Faculty of Graduate Studies when, in the opinion of either, the proposed use of the material is for scholarly purposes.

Any copying or use of the material in this thesis for financial gain shall not be allowed without my written permission.

Student Name:…….

Signature: _____ Date:_____

DEDICATION

I would like to thank Allah, who gave me strength, love of knowledge, and faith,

To all prisoners in the occupation prisons,

To the spirit of Nizam al-Malik, the Seljuk minister who was one of the first founders of the scientific research system in the history of the Arab-Islamic civilization,

To my beloved husband, who has always been my greatest supporter,

To my sons Abdel-Rahman, Lamees, and Sondos, perhaps they will find their way to knowledge and creativity.

For my mother and father, all deep thanks.

ACKNOWLEDGEMENT

First, I would like to thank my thesis supervisor Dr. Zuhdi Salhab for his guidance for this work.

I also deeply thank Dr. Marwan Almokhtar, for sharing his technical and scientific background in solar thermal applications in this work.

I also thank STEAG Energy company for making EBSILON Professional available for the scholars in thermal energy studies. To support introducing more refined research in thermal engineering applications.

I would like to thank all those who have helped in some way or another, to make this work come out to light.

List of Abbreviations

CSP	Concentrated Power technology
PTC	Parabolic Trough Collector
LFR	Linear Fresnel Reflector
LF	Linear Fresnel
PT	Parabolic Trough
DNI	Direct Normal Irradiance
LCOE	Levelized Cost of Energy
SPT	Solar Power Tower
DSG	Direct Steam Generation
TES	Thermal Energy Storage
SAM	System Advisor Model software
OMSW	Olive Mill Solid Waste
LFRs	Linear Fresnel Reflectors
PTCs	Parabolic Trough Collectors
GCV	Gross Calorific Value
(N)	Nitrogen
(C)	Carbon
(O)	Oxygen
(H)	Hydrogen
(N_C)	Mole Number of Carbon
(N_{H_2})	Mole Number of Hydrogen
(N_{o_2})	Mole Number of Oxygen
(N_{N_2})	Mole Number of Nitrogen
A/F	Air Mass to Fuel Mass Ratio
λ	The Excess Air Ratio
PCBS	Palestinian Central Bureau of Statistics
E	Energy

Q	Any Type of Energy Generated or Consumed per Second Including Thermal Energy
W	Work
M	Mass Flow Rate
H	Enthalpy
V	Velocity
g	Gravitational Field
z	Height above a Reference Level
$\dot{Q}$	The Heat Transfer Rate To The System
$\dot{W}$	The Work done per time
"o" subscript	The Values at The Output
"i" subscript	The Values at The Inlet
q	Heat Transfer per Unit Mass
w	Work per Unit Mass
T	Temperature
s	Entropy
v	**S**pecific Volume
P	Pressure
H_n	The Enthalpy at State n
P_n	The Pressure at State n
η_{th}	Thermal Efficiency
$\eta_{th,carnot}$	The Carnot Efficiency
T_{max}	Thermal Energy Source Reservoir Temperature of power plant
T_{min}	Thermal Energy Sink Reservoir Temperature of power plant
M_s	Mass Flow rate of Steam Entering the condenser
H_s	Enthalpy of Steam Entering the Condenser
H_c	Enthalpy of Water Leaving the Condenser
M_w	The Mas Flow Rate of Cooling Water
$C_{p,w}$	Specific Heat of Water

U	The Heat Transfer Coefficient per Unit of Time, Unit of Surface, and Degree of Temperature Difference
ΔT	The Temperature Difference
A	Area
HP	High-Pressure
LP	Low-Pressure
HTF	Heat Transfer Fluid
WF	Working Fluid
PD	Parabolic Dish
PDC	Parabolic Dish Concentrators
NCV	Net Calorific Value
(S)	Sulfur
M_{Live}	The Mass Flow Rate of The Live Steam
M_{Reheat}	The Mass Flow Rate of Steam that Enters the Reheat Line in The Boiler
$H_{live,in}$	The Enthalpy at The Live Steam Inlet Line in The Boiler
$H_{Reheat,out}$	The Enthalpy at The Reheat Steam Outlet Line in the Boiler
$H_{Reheat,in}$	The Enthalpy at The Reheat Steam Inlet Line in the Boiler
η_{is}	The Isentropic Efficiency
η_{all}	Overall Efficiency
η_{mech}	Mechanical Shaft Efficiency
η_{motor}	Motor Efficiency
FWH	Feed Water Heater
γ_s	Solar Azimuth Angle
α_s	Solar Elevation Angle
θ_z	Zenith Angle
γ_c	Collector Azimuth Angle
β_c	Collector Axis Tilt Angle
θ_i	Incident Angle
RPHIIINC	Incident Angle Symbol in EBSILON
IAM	Incident Angle Modifier
QEFF	Thermal Energy Input into The Heat Transfer Fluid from Solar Energy

QSOLAR	Energy Transferred to The Heat Transfer Fluid from Solar without Losses
ANET	Net Aperture Area of the Collector
FOPT 0	Peak Optical Efficiency
ETASHAD	Factor to Include Shading Losses
ETACLEAN	Factor to Correct for Actual Mirror Cleanliness
ETAENDL	Factor to Correct End Loss Effects
$RPHITRAN$	Transversal Angle
ROWDIST	The Distance between Parallel Collectors.
QLOSS	The Thermal Losses of the Collector
q_{LOSS}	The Thermal Losses of the Collector per Unit Length
T_{HTF}	The Temperature of the Heat Transfer Fluid
T_{amb}	Ambient Temperature
FOPT	The Optical Efficiency of The Collector
LMTD	The Logarithmic Mean Temperature Difference
T_{fuel}	Fuel Temperature
$\eta_{combustion}$	Combustion Efficiency
P_{live}	Live Steam Pressure
T_{live}	Live Steam Temperature
η_G	Generator Efficiency
T_L	Low temperature side of the cycle
T_H	High temperature side of the cycle
$\eta_{th,solar\ field}$	Solar Field Efficiency
A_{net}	Total of The Aperture Area of Solar Reflectors or Concentrators in The Solar Field
Q_{Gen}	Power Plant Capacity for Electricity Generation per Time
Q_{Aux}	The sum of the all electrical consumption equipment in the Power plant
DC	Direct costs
IDC	Indirect costs
O&M	Operation and Maintenance
CRF	Capital Recovery Factor
i	The Interest Rate

n	Number of years
AN	The Annual due Payment from Borrowed Investment Cost
Pr	Profit Amount
TC	The Required Finance Amount for Investment
r_m	Average Profit (Rate) Percentage
Sp	The Bank Selling Price Used to Calculate the Annual Payment
I	The Added Exchange Insurance Amount to The Financed Amount Beside Profit
i_{ex}	The Applied Percentage for Exchange Insurance

List of Figures

List of Tables

Table of Contents

CHAPTER 1

Introduction

1.1 Preamble

The world is moving in fast steps toward adopting renewable energy solutions instead of traditional fossil resources (Dincer, 2000). That's due to the many complications caused by the vast reliance on burning fossil fuels for energy. It's now known that burning fossil fuels has played a great role in the current global warming phenomenon (Bartsch et al., 2000). Moreover, many other factors nowadays reduced the potential of relying on these resources, such as the volatile prices of fossil resources and their direct affection by political stability, their harmful footprint on the quality of air, the drop in newly discovered reserves, and many other factors (Bartsch et al., 2000). As a result, most countries are moving to adopt more authentic resources of energy, that can provide sustainable energy supplies at reasonable prices. Driven by extensive scientific research and investments; renewables are now providing 26.3% of the world total generated electricity, which values 1.4 times compared to 18.7% 20 years ago. In Palestine, renewables covered 2.63% of the total consumed electricity in 2018 (PCBS, 2018).

Palestine is in great need to exploit renewable resources. Due to the occupation, Palestine is banned from free energy trade with the neighboring countries and the occupation provides nowadays about 93.9% of the electricity for Palestine (Ismail et al., 2013). As a result, energy prices in Palestine are the highest among the neighboring countries. That led to unfair prices of electricity on the Palestinians and hindered the development of the country as a whole (Ismail et al., 2013). Palestine is located in the sun-belt region that features considerable sun insolation. most of Palestine receives solar radiation about 3000 hours annually (Abu Hamed et al., 2012), and the average solar radiation values range from 5.4 kWh/m^2.day to 6.0 kWh/m^2.day. These values show a reasonable potential for exploitation feasibility compared to other places worldwide such as Madrid-Spain 4.88 kWh/m^2.day, Sydney-Australia 4.64 kWh/m^2.day (Ajlouni and Alsamamra, 2019). Palestine is also one of the Mediterranean countries that the olive

industry is a major contributor to its agricultural profile. This produces considerable amounts of olive pomace annually (Musalam et al., 2017b).

1.2 Motivation and Objectives

Palestine needs to generate its electricity from authentic resources to reduce its vast reliance on imported electricity from the occupation and neighboring countries, securing a portion of the required electricity consumption and increase the renewables energy portion share in electricity. This leads to investigating the use of indigenous renewable resources away from occupational control like solar energy and biomass resources to generate electricity in Palestine.

Some researchers investigated the hybridization between biomass and Concentrated Solar Power technology (CSP) and there are many assessments of CSP and biomass combustion plants. in Palestine, there is no investigation for hybridization between any type of biomass and CSP technology for electricity generation in a steam power plant. Moreover, there is no comparison of annual energy yield between Parabolic Trough Collector (PTC) technology and Linear Fresnel Reflector (LFR) under the same land area and the same conditions for electricity generation.

The main objectives of this research:

1- To establish a strategy and approach for hybridization between CSP and olive pomace for electricity generation in Palestine. that can be applied for hybridization between CSP and other biomass resources that suitable for combustion in Palestine in steam power plants for future researches.
2- To introduce and investigate a proposed power plant for hybridization between CSP (Linear Fresnel (LF) and Parabolic Trough (PT)) and olive pomace in electricity generation by Using EBSILON simulation software.
3- To study the annual operation of the proposed hybrid power plant models for both LFR and PT under different capacities around the estimated power generation capacity. that can be achieved from CSP and olive pomace under specific design

conditions relevant to variation of Direct Normal Irradiance (DNI) and ambient temperature. Performed using EBSILON time series annual simulation.

4- Hybridization comparison between two CSP technologies: LFR and PTC. Comparing their thermal output performance, their effect of the Levelized Cost of Energy (LCOE).
5- To study the solar field performance in the hybrid power plant for both the LFR hybrid model and PTC hybrid model under variable DNI and ambient temperature.
6- To study the olive pomace boiler expended energy and the performance of the boiler under the variation of DNI and ambient temperature
7- To evaluate the energy share of olive pomace boiler and CSP from annual energy production
8- To evaluate for both LFR and PTC the net electricity annual production from hybrid power plant under different capacities, and to calculate the LCOE for the most appropriate capacity.
9- To investigate the hybridization potential share to the electricity consumption in Palestine

1.3 Methodology

Research methodology can be introduced by the following:

1. Examining the previous work related to the hybridization between biomass and CSP
2. Gathering the related data about the olive pomace in Palestine
3. Gathering the CSP and steam power plants.
4. Site selection
5. Gathering metrological data regarding the selected site.
6. Developing a hybrid power plant model for both LFR and PT solar fields.
7. Annual simulation using all the input gathered data.
8. Results and conclusions.

Figure 1.1 introduces the flow chart of the research methodology.

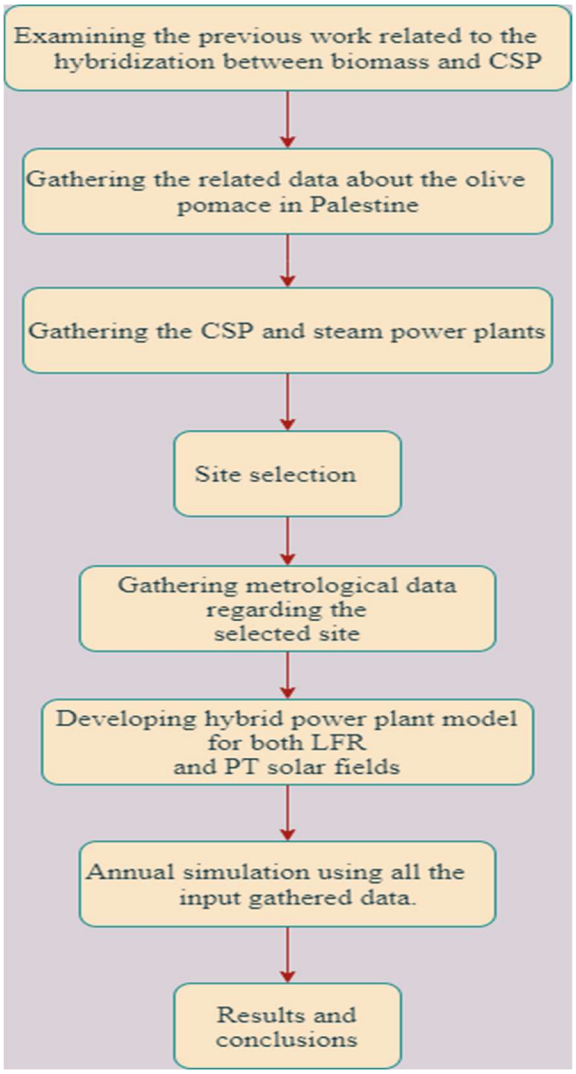

Figure 1.1: Thesis methodology flow chart

1.4 Literature Review

1.4.1 CSP for Power Generation

CSP technologies have been a hot topic for many researchers in the last few years. Investigating aggressively the potential of employing this technology and tracing its development from studies to real-world application. Islam et al (Islam et al., 2018) introduced a comprehensive review of the state-of-the-art of CSP technologies, investigating the current status and trends. They mentioned that the most investing countries in CSP technologies nowadays are Spain and the USA. For instance, the California Energy Commission approved the erection of five CSP power plants with a total

capacity of 2284 MW in 2014. By 2016, the total installed CSP plants in Spain was 2304 MW. The researchers found that the most dominant systems are the Parabolic Trough Collectors (PTC) and Solar Power Tower (SPT) respectively. The world total installed CSP power plants up to 2016 was around 4.8 GW. Which is about 13.7 times the CSP installed capacity in 2006, which is around 352MW. Finally, the paper concluded the Direct Steam Generation (DSG) systems are promising in power generation. Siyatar et al, (Krunal H. Siyatar, 2017) conducted a comprehensive review of different CSP technologies, they concluded that the best advantage of the CSP technology is their resemblance to the working fossil power plants. Stating that the can be a direct alternative with modification of the boiler section. Chaanaoui et al (Chaanaoui et al., 2016), their sensitivity analysis indicated that PTC systems with thermal oil and molten salt storage at 50 MW were the most mature system, and SPT plants are promising and might have the greatest potential by early 2018. In another study conducted by Giovannelli (Giovannelli, 2015), discussed the application of small-scale CSP for industrial and rural electrification applications.

The CSP applications in power generation were also a topic for research and investigation in the middle east area. Wael Alkouz et al (Wael Al-Kouz, 2020) conducted a study to predict the performance of a smaller model (140 MW) of a power plant installed in Gila Bend-Spain in Ma'an-Jordan. The simulation results including the monthly capacity factors suggest the annual operation in Ma'an may be even better than the operation in Gila Bend, for an annual average capacity factor of about 41% for Ma'an vs. a capacity factor of about 39% for Gila Bend. Elshazely (ElShazly, 2011) carried out a study to assess the potential of CSP power generation in Egypt. The study yielded that CSP represents a reliable and sustainable source of energy for Egypt with different outputs that can be used. and the private sector needs to be involved in this process.

In Palestine, Yasin (Yasin, 2019a) conducted a study to compare a 1 MW PV power plant to a PT-CSP power plant of the same capacity. He found that CSP power plants overwhelmed PV power plants in case of including 14.5 hr to 18.5 hr Thermal Energy Storage (TES). Which increases the capacity factor by up to 57%. Taleb also investigated the performance of a 5.4 MW PT-CSP system in Gaza Strip (Taleb, 2014) using SAM

(System Advisor Model) software. The investigation found that electricity could be generated 3.5% cheaper than current prices without trading saved CO2 emissions. In 2016, Draidi carried out a feasibility study to identify the potential of employing CSP for power generation in Palestine (Draidi, 2016b), taking into consideration many factors. The study found the viability of the potential relies on factors such as real state prices where the plant could be erected. This has excluded the feasibility of erection in Gaza due to the extremely high prices of the real state. The study covered the main cities in Palestine. LCOE was from 0.2-0.5 $/kWh without TES and 0.19-0.47 $/kWh employing TES, with payback period between 7-25 years.

1.4.2 Olive Pomace as a Source of Energy

The olive pomace is a by-product of the olive oil industry. Mediterranean countries produce about 98% of olive oil consumed around the world (Oktay, 2006). Due to its considerable calorific value, researchers investigated its potential in substituting fossil fuels in boilers. Cliff et al (Cliffe and Patumsawad, 2001), investigated the co-combustion of olive pomace beside coal in a fluidized bed boiler designed for burning coal. The study concluded that a 20% mix can be used with only a 5 % drop in boilers efficiency, and a 10% mixture produced less CO emissions than coal-burning only. Dally et al (Dally and Mullinger, 2002) prepared a report to assess the potential of using olive husks (pomace) for energy generation in South Australia Province. The report mentioned that the potential is estimated by 250 000MWh yearly from South Australia only. That's to be accomplished in different ways including gasification and co-combustion with the existing coal plants. And this exploitation is in favor of encouraging olive agriculture in Australia. Vourdoubas investigated the possibilities that olive pomace has for power generation in Crete island in Greece (Vourdoubas, 2017), the estimation of potential reached 24% of the total energy needs of the island. Oktay (Oktay, 2006) applied a similar study on Turkey. He estimated the potential as 150,000 tons of oil (toe). Majdoub (Majdoub, 2018) simulated a 10 MW power plant that operates 100% on the olive pomace as a source of energy. The LCOE was promising for more investments.

In Palestine, many research efforts aimed to study olive pomace and its potential in energy production. Qaraman et al (Qaraman et al., 2017) studied the thermal properties of

a composite fuel of olive pomace 40% and diesel 40% besides intense olive chemical residues as a solution for power generation in Gaza Strip. Abu Hamed et al (Abu Hamed et al., 2017), conducted a study to investigate the potential of power generation from the olive pomace in Palestine. their study found a high-energy potential that can be derived from the olive pomace and that powering olive mills by small-scale generators using OC is feasible. Saving 1.3% of annual electricity consumption based on 2009 data. Gannam et al (Ghannam et al., 2005), stated that utilization techniques of olive pomace have the potential to be feasible in Palestine should be considered to get the benefits of high energy content and avoid the environmental problems of dumbing olive pomace or using it as fertilizer without chemical treatment. Co-composting and anaerobic digestion of olive mill solid wastes to produce energy have the potential to be feasible and can be recommended for Palestine.

1.4.3 Biomass-CSP Power Generation

The combined power generation of electricity from CSP and biomass was investigated by researchers from different parts of the world and for different purposes. The core value is to use a carbon-neutral available resource such as biomass to overwhelm the intermittent nature of solar energy. Combining these two resources for power generation compensates for each other disadvantages. Nixon et al (Nixon et al., 2012), conducted a study checking for the feasibility of hybrid biomass-CSP power generation in India. The study endorsed the potential of this hybridization in successful electricity generation. 29% of biomass combustion could be reduced by employing solar thermal technologies and achieved 1.8-5.2 cent/kWh. Peterseim et al (Peterseim et al., 2014), ran a study to investigate economically and technically the hybridization of biomass power and the molten salt solar tower power system in Australia. The study yield was that a 30 MWe hybrid plant can produce 160,300 MWh of electricity at a levelized price of 155 AU$/MWh. The erection costs were 43% lower than erecting a standalone CSP power plant with 15h TES. Soares et al (Soares et al., 2018), compared two identical 1 MWe hybrid power generation plants in Tunisia. One for electricity generation only. And the other includes heat sources besides electricity. LCOE for both plants was 175.4 Euro/MWh and 126.3 Euro/MWh respectively. For both cases, the LCOE was competitive with the local market fairs. Srinivas et al

(Srinivas and Reddy, 2014), carried out a multi-technical sensitivity analysis for the combining of biomass and CSP technologies in power generation. The study found that with more employing of CSP, less boiler pressure is required. And fuel efficiency increases. And the optimal thermal efficiency under standard conditions could reach up to 27%. Servert et al (Servert and San Miguel, 2011), ran a technical and economic assessment of the hybrid solar-biomass power generation. The study results show that the erection costs drop by 24% better than the erection of two stand-alone power plants. In contrast, operational and maintenance costs are higher than using only solar or biomass sources by 2.77 times. the study considered 10 MWe for investigation and used SAM to run the required simulations and optimizations. In Palestine, there were no studies considering investigating the hybridization of biomass-CSP systems for power generation. Which is going to be the sole purpose of this thesis.

1.5 Thesis Design

The thesis consists from eight Chapters, after this chapter, Chapter 2 study the status of olive pomace in Palestine and its amounts per year and introduce the result of testing the heating value of multi-samples from olive pomace in Palestine. Next, Chapter 3 introduces the basic concept of steam power plants and their efficiency development, Followed by Chapter 4 that illustrates all types of concentrated solar power technologies. Chapter 5 introduces EBSILON® Software that will be used in our research as a design and simulation tool for the power plant processes. Chapter 6 presents the main approach and the main assumptions for hybridization between olive pomace and both Linear Fresnel Reflectors (LFRs) technology and Parabolic Trough Collectors (PTCs) technology for electricity generation, also in Chapter 6 proposed models of the hybrid power plant will be introduced for both LFR and PTC based on efficiency improvement criteria and technical requirements, furthermore, Chapter 6 demonstrates the operation strategy of the hybrid power plant for both LFR solar field and PTC solar field. The output results from simulation from hybridization will be demonstrated in Chapter 7 and a comparison between the hybridization that uses LFR technology and the hybridization that uses PTC technology under the same conditions besides the evaluating of levelized cost of energy. at the end Chapter 8 presents conclusions from a summary of achieved results, recommendations, and future work.

CHAPTER 2

Olive Pomace Potential for Energy Generation in Palestine

2.1 Preamble

In this chapter we will introduce the olive pomace status, heating value, gathered data from Palestine, and quantities as a major biomass resource that will be used besides the solar energy source extracted by concentrator solar technology for producing electricity by hybridization model.

Investing in energy production from authentic resources is a vital choice to mitigate the consequences of the occupation restrictions in Palestine, Biomass is one of these important authentic renewable resources of energy in Palestine that can be employed to match (or to meet) a variety of energy needs in many applications, such as heating, transportation, and electricity generation.

As most developing countries are characterized by an agriculturally-themed economy, people consume more than 85% of solid biomass fuels, using this source essentially for cooking, heating, and even lighting (Jebril and Khatib, 2018). Biomass combustion is carbon dioxide neutral. Since the released amounts of Carbon Dioxide are the same absorbed during growing the biomass source. Moreover, the amounts of used biomass for energy are always less than the originally grown quantities, which leads to more reduction in carbon dioxide emissions (Amro, 2016).

Biomass in Palestine (Gaza and West Wank) comes from the following sources: agricultural waste, municipal organic waste, animal manure, wood and charcoal waste, organic oils, lubricants waste, industrial organic waste, wastewater, and sewage (Jebril and Khatib, 2018). Palestine is also one of the Mediterranean countries that olive industry is a major contributor to its agricultural profile. About 45 % of cultivated lands in Palestine are occupied by olive trees. This produces considerable amounts of olive pomace annually that can be employed as a fuel for electricity generation (Musalam et al., 2017a). Also, according to Imraish and Abu Safa (Imraish and Safa, 2017), olive trees count for 75.6% of total arable lands in Palestine.

Olive presses generate three main outcomes: olive oil, olive pomace, and olive wastewater called (Zibar). While olive oil is the main outcome of the olive pressing, the other outcomes are considered lateral products that need utilizing or treatment. Zibar mainly consists of water and other non-oily content of the olives. This product is usually stored within a press septic tank and treated later for retrieving a low-quality olive oil and after that is treated and dumped. Olive pomace forms the rest parts of the olives. It's characterized by its high thermal content thus it is used for domestic heating applications, especially in winter.

Despite olive pomace is used widely for heating purposes. Considerable amounts of it are dumbed causing environmental issues; such as soil contamination and polluting water aquifers. The proper exploitation of this resource can resolve both energy and environmental issues at the same time. Figure 2.1 depicts the energy balance resources in Palestine, showing olive pomace as an energy source that provides about 0.69% of the total energy consumption in Palestine. (Juaidi et al., 2016).

2.2 Olive Pomace in West Bank & Gaza Strip

Based on the latest report from the Palestinian Central Bureau of Statics about agricultural areas in Palestine (PCBS, 2020), the total land in West Bank and Gaza Strip cultivated with horticulture trees (which includes olive trees), vegetables, and field crops are about 365,900 dunams, 326,345 dunams in the West Bank and 39,555 dunams in Gaza Strip. The percentage area in West Bank and Gaza cultivated with horticulture trees is about 53.17%, followed by field crops are about 34.15%, followed by vegetable crops are about 12.68%.

Olive trees have the largest percentage with 57% of the total number of horticulture trees, where the olive trees represent 93% of horticulture trees in West bank, and it represents 7% of horticulture trees in Gaza, and according to statistics in 2011, the total olive trees in the West Bank and Gaza are about 3,477,222 trees.

Olive cultivated areas are intense in Ramallah & AlBierh, Salfit, Qalqilya, Bethlehem, Jenin, and Nablus governorates. As mentioned in Figure 2.2.1 (Imraish and Safa, 2017). On the other hand, according to statistics in 2014, the olive press activity that is generating the olive pomace was concentrated in Jenin and Tubas as shown in Figure 2.2. The olive pomace that is generated after the olive oil extraction is dried and used for domestic heating purposes in most of Palestine areas, most of the olive pomace about 84.15 % are returned to owners without taking into consideration the best ways to dispose of it if it not used for heating purposes (Imraish and Safa, 2017).

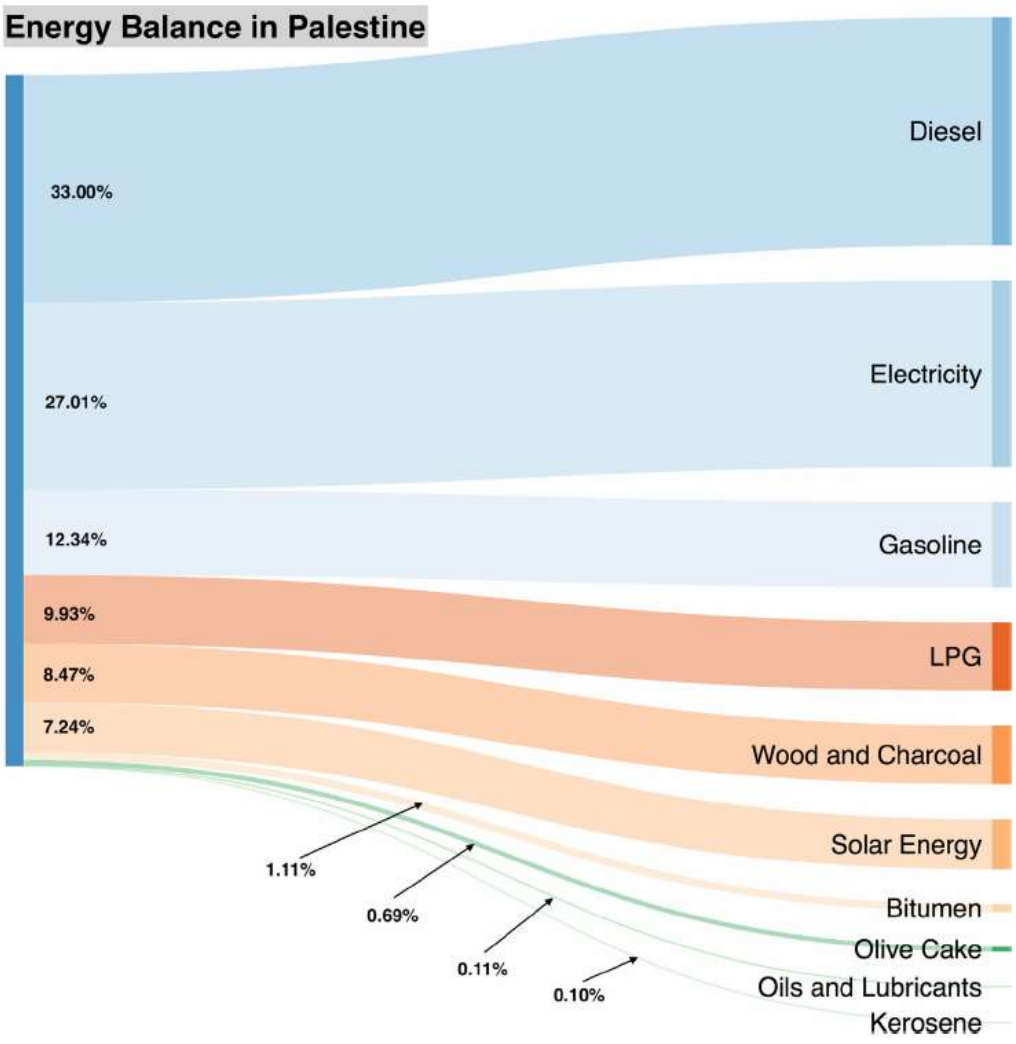

Figure 2.1: Sanky Diagram of Energy Balance in Palestine (Juaidi et al., 2016)

Olive cultivated areas are intense in Ramallah & AlBierh, Salfit, Qalqilya, Bethlehem, Jenin, and Nablus governorates. As mentioned in Figure 2.2.1 (Imraish and Safa, 2017). On the other hand, according to statistics in 2014, the olive press activity that is generating the olive pomace was concentrated in Jenin and Tubas as shown in Figure 2.2. The olive pomace that is generated after the olive oil extraction is dried and used for domestic heating purposes in most of Palestine areas, most of the olive pomace about 84.15 % are returned to owners without taking into consideration the best ways to dispose of it if it not used for heating purposes (Imraish and Safa, 2017).

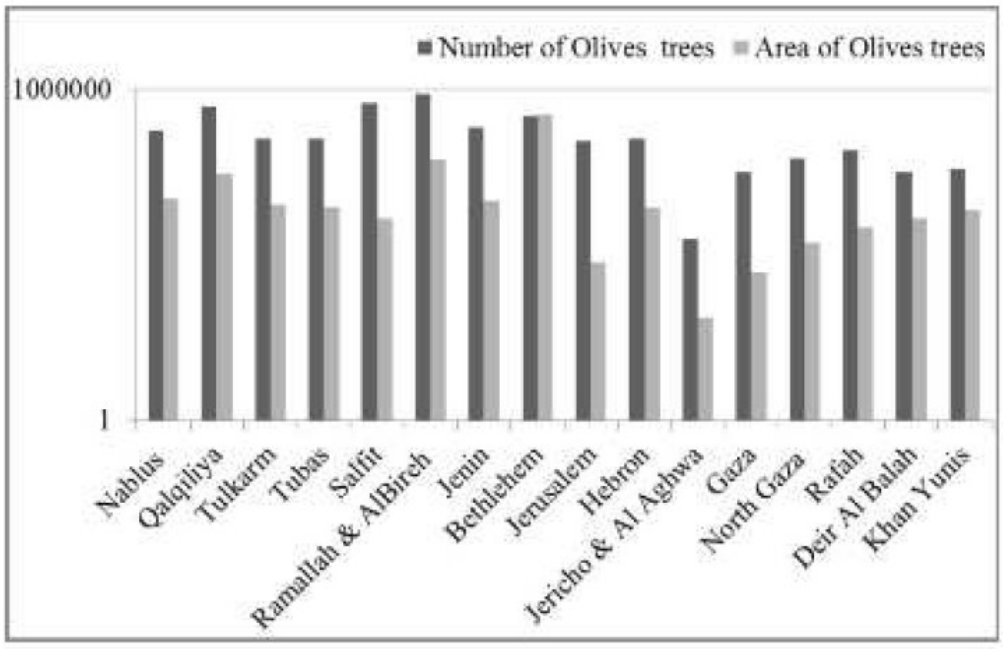

Figure 2.2: Olive trees statistics in Palestine, (Imraish and Safa, 2017)

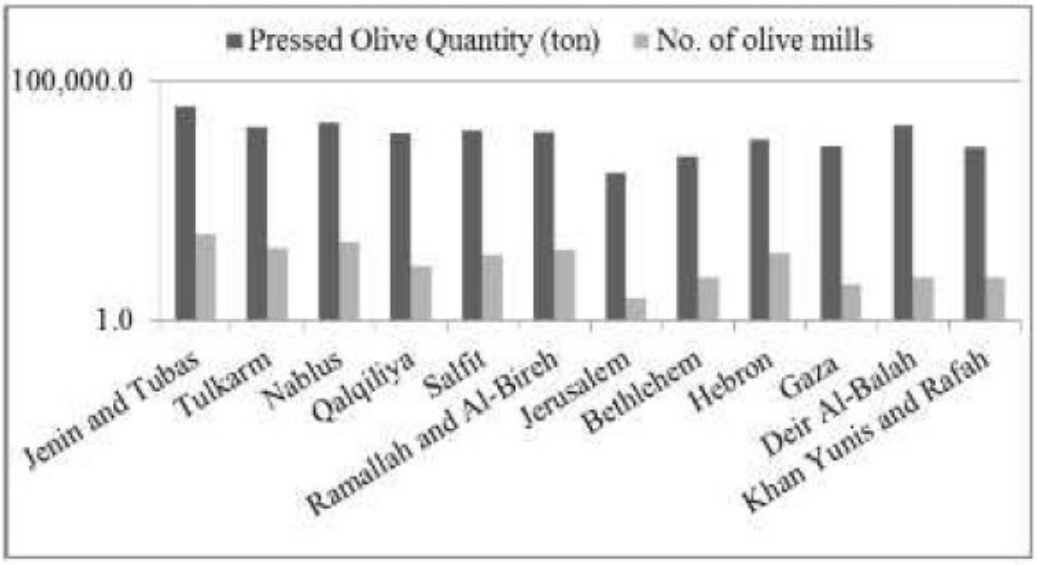

Figure 2.3 Statistics of pressed olive in Palestine (Imraish and Safa, 2017)

2.3 Olive Pomace Properties as an Energy Resource

Olive pomace is the solid remains of the olive oil extraction process. It constitutes the olive skin, pit or stone, bulb, and water. The water content of the olive pomace comes from the olive itself and the processing water used in the olive press (Amro, 2016). Moisture content in the olive pomace after pressing directly is around 44.8%. and varies depending on the olive press used technology (Imraish and Safa, 2017), and it is an essential criterion that should be considered before utilizing olive pomace.

Olive pomace can be utilized by digestion due to its composition. But it contains a high percentage of polyphenols that should be treated to lower the polyphenols (Abdo and Khatib, 2018). It's suitable to use olive pomace as a solid biofuel in combustion or gasification processes. There are significant amounts of olive pomace in Palestine to use for electricity generation. Combustion is the simplest energy conversion process that will be considered in this research.

The calorific value is the main property that characterizes any fuel and is an important indicator of fuel efficiency. The Gross Calorific Value (GCV) of Four samples of dried olive pomace was measured in the Palestine Polytechnic University laboratories in an

oxygen bomb calorimeter, the first sample was in 2019, the three other samples were in 2020. The GCV of the tested samples is detailed in Table 2.3.1. the average value of the GCV for the tested samples is 17.095 MJ/kg.

Table 2.1: Tested samples from different regions in Palestine

Sample	Harvest Season of Olive	GCV (MJ/Kg)	Sample location
Sample 1	2019	16.54	Salfiet
Sample 2	2020	18.35	Salfiet
Sample 3	2020	16.14	Hebron
Sample 4	2020	17.35	Berziet

The ultimate analysis of olive pomace as detailed in Table 2.3.1 is considered from a tested sample of olive pomace in Jordan which has similar environmental and soil conditions of olive trees in Palestine, the considered sample from Jordan have nearly similar average calorific value of the tested samples in Palestine Polytechnic University laboratories (Tawarah and Rababah, 2013).

Table 2.2: The ultimate analysis of olive pomace, (Tawarah and Rababah, 2013)

Constituent	Nitrogen (N)	Carbon (C)	Hydrogen (H)	Ash	Oxygen (O)
Percentage%	0.97%	48.42%	5.96%	10.56%	34.09%

For 1 kg of pomace the mole numbers of the constituent of the olive pomace can be calculated by dividing the mass of each constituent by the molar mass as following:

$$Mole\ number\ of\ carbon\ (N_C) = \frac{0.4842\ kg}{12\ kg/kmol} = 0.04035\ kmol$$

$$Mole\ number\ of\ hydrogen\ (N_{H_2}) = \frac{0.0596\ kg}{2\ kg/kmol} = 0.0298\ kmol$$

$$Mole\ number\ of\ oxygen\ (N_{O_2}) = \frac{0.03409\ kg}{32\ kg/kmol} = 0.01065\ kmol$$

$$Mole\ number\ of\ nitrogen\ (N_{N_2}) = \frac{0.0097\ kg}{28\ kg/kmol} = 0.00035\ kmol$$

The equation of combustion of 1 kg of olive pomace relative to the olive pomace composition:

$$(0.04035\ C + 0.0298\ H_2 + 0.01065\ O_2 + 0.00035\ N_2\ ) + 0.0446\ (O_2 + 3.76N_2) \longrightarrow 0.04035\ CO_2 + 0.0298\ H_2O + 0.168046\ N_2 + Ash + Energy$$

A major ratio that is used for the combustion process is the air-fuel ratio (A/F) which is the ratio between the mass of air and mass fuel during the combustion process or the ratio between the mass flow rate of air and the mass flow rate of fuel. The ideal air-fuel ratio is known as the stoichiometric air-fuel ratio for complete combustion.

Actually, in real combustion processes, it is needed to use the air-fuel ratio more than the stoichiometric air-fuel ratio to maximize the possibilities of complete combustion or to manage the combustion temperature. The symbol λ used for the amount of excess air to the air to fuel stoichiometric amount, it is also known as excess air ratio (Çengel, 2008):

$$\text{Stoichiometric air to fuel ratio} = \frac{(Mole\ Number\ of\ air\ in\ kmol) X\ Molar\ mass\ of\ air\ (\frac{kg}{kmol})}{1\ kg\ of\ olive\ pomace} \quad (2.1)$$

$$\text{Stoichiometric air to fuel ratio} = \frac{0.0446\ X\ [(16\ X2) + 3.76X\ (14X2)]}{1}$$

$$\text{Stoichiometric air to fuel ratio for olive pomace} = 6.1\ \text{kg}\ air\ /\ kg\ olive\ pomace$$

2.4 Olive Pomace Amounts in the Last 8 Years.

According to the statistics gathered by the Palestinian Central Bureau of Statistics PCBS (PCBS, 2020), Figure 2.4.1 represents the generated amounts of olive pomace for the years 2010 to 2018. These statistics were gathered using the olive press statistics

distributed in Palestine. The average annual generated amount of olive pomace is near 40,000 tons.

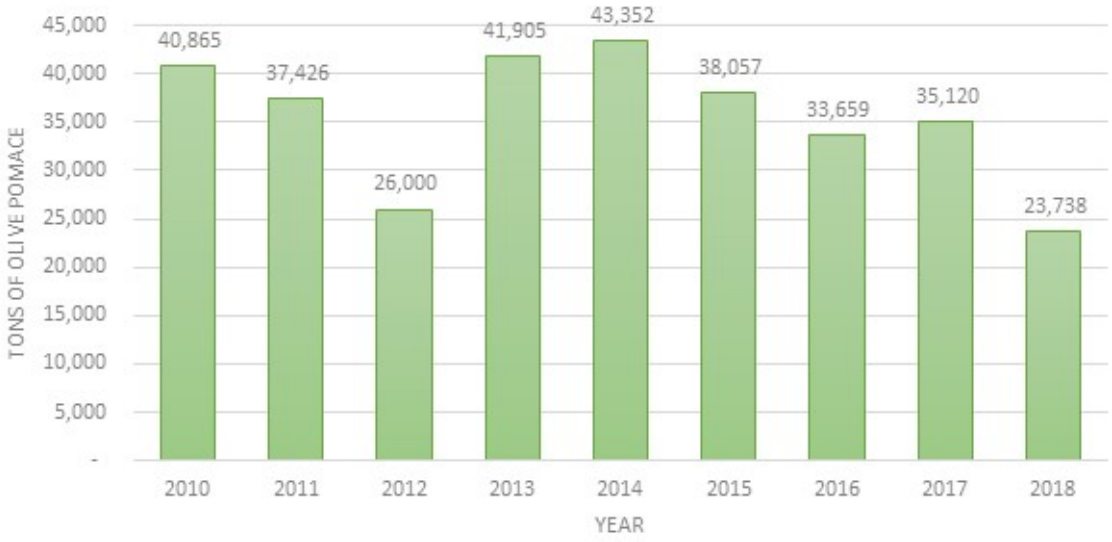

Figure 2.4: Generated olive pomace amounts between 2010 and 2018. (PCBS, 2020)

CHAPTER 3

Steam Power Plants

3.1 Preamble

In the previous chapter, we provided all gathered and necessary information about the olive pomace in Palestine, which is needed to use it in direct combustion in a steam power plant is provided and detailed. This chapter will introduce the basic concept of the steam power plant that will convert the thermal energy from the sun and the olive pomace combustion to the shaft mechanical power for electricity generation by a generator.

There are different types of power plants based on the power cycle used in them. There are two types of power cycles: gas power cycles and steam-powered cycles. Steam power plants are very common in the energy industry. Coal-fired plants, nuclear plants, and natural gas plants all are referred to as steam power plants. Steam could be produced for other resources rather than mentioned (Çengel, 2008). In steam-powered plants, heat is converted into mechanical work that drives an electrical generator to produce electricity. Steam-powered plants rely on the concept of the Rankine power cycle. Which is a thermodynamic cycle developed in 1859 by a Scottish engineer William J.M Rankine (Nag, 2015). Although there are other working fluids used to operate the Rankine power cycle such as organic fluids, still water is preferred due to many desired criteria. Such as its low cost, availability, and high specific heats (Çengel, 2008).

Biomass is a common fuel used for energy. A direct combustion system feeds a biomass feedstock (such as wooden pellets) to be combusted for steam generation. Some other technologies gasify the biomass feedstock and use the generated syngas as fuel to generated steam. Then the steam is allowed to expand in a steam turbine. Which in turn rotates an electric generator to produce electric power. In the United States, direct combustion of biomass is the most commonly used method to produce heat from biomass. For a small-scale biomass-powered plant, the erection cost is 3,000$ to 4,000$ per kW, and a levelized cost of energy of 0.15 $ to 0.8 $ / kWh (FEMP, 2016).

Concentrated Solar Power (CSP) plant uses different technologies for reflecting sunbeams into a focal point or line, generating the required heat for driving the plant's boiler. Solar thermal systems usually are equipped with thermal storage systems to retrieve the excess collected solar thermal energy, extending the plant's working hours. CSP plants suffer from the intermittency of solar radiation, especially in winter or cloudy days. Biomass power plants have a major logistic problem in providing the required amounts of biomass feedstock to the plant, whereas it is obtained seasonally. Hybrid systems between CSP and Biomass may provide the solution to these limitations, maximizing the energy potential of these resources, increasing process efficiency, and reliability, providing greater security of supply, and reducing overall costs (Servert and San Miguel, 2011).

3.2 Rankine Cycle

The Rankine cycle is the post-used thermodynamic cycle used in power generation plants that utilizes water as a working fluid. It consists of four main processes: two isobaric and two isentropic processes. And involves four components: boiler, turbine, condenser, and pump. As detailed in Figure 3.1, representing the major parts of the Rankine cycle. The cycle starts from pumping low-pressure water into the boiler. The water is heated in the boiler at constant pressure till it becomes superheated steam.

After that, high temperature and pressure steam are allowed to expand using a turbine. Transforming portion of the steam enthalpy to mechanical work. The steam reaches the saturation state of the cycle is ideal. Then the exhausted steam is led to the condenser to be condensed into water again. Rejecting heat to the surrounding. After that water is pumped into the boiler again and so on. The ideal Rankine cycle does not involve any internal irreversibilities and consists of the following four processes: Isentropic compression in a pump, Constant pressure heat addition in a boiler, Isentropic expansion in a turbine, Constant pressure heat rejection in a condenser (Çengel, 2008).

The steam turbine is an engine in which a steam flow, at high pressure and temperature, is expanded transforming its energy into kinetic energy, which is as well converted into work by moving the rotational parts of the turbine (Nag, 2015).

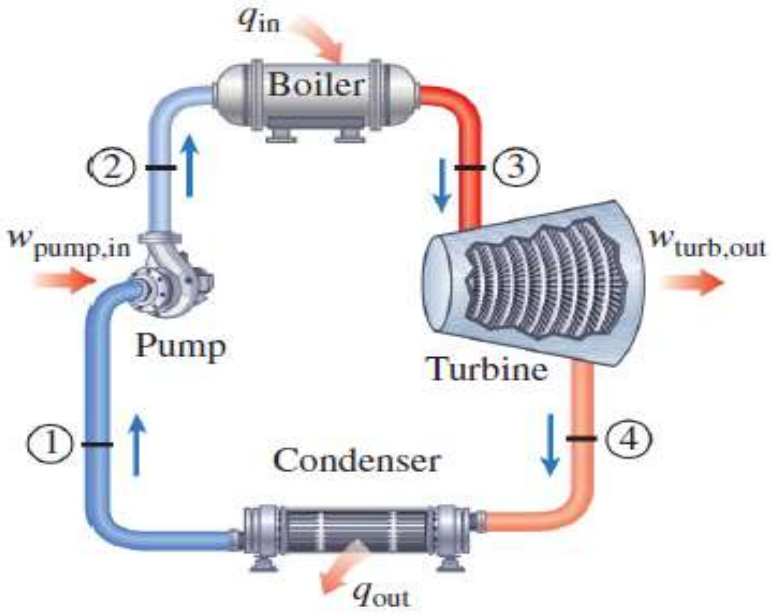

Figure 3.1: The Ideal Rankine cycle.

In an Ideal Rankine cycle, the processes performed by the pump and the turbine is considered isentropic. This means that there is no entropy generated during the working fluid compression and expansion processes. In a non-isentropic process, entropy is generated causing the work required by the pump to increase and the generated work of the turbine. As well, the processes of heat addition and rejection in the boiler and the condenser is isobaric. So, no pressure is lost during the heat addition and rejection (Çengel, 2008).

3.3 Energy Analysis of Simple Ideal Rankine Cycle

According to the first law of thermodynamics: the increase of the energy of a system is equal to the net work interaction of the system and the net of heat interaction on that system:

$$\Delta E = \Delta Q + \Delta W \tag{3.1}$$

Where E is the total change of the energy of a system, Q is the net heat interaction on the system, and W is the network interaction on the system.

Also, the first law of thermodynamics can be mentioned for an open system as:

$$\frac{dE}{dt} = \left(\sum M_{in}\left(H_i + \frac{V_i^2}{2} + gz_i\right)_{in} + \dot{Q}\right) - \left(\sum M_o\left(H_o + \frac{V_o^2}{2} + gz_o\right)_{out} + \dot{W}\right) \tag{3.2}$$

Noted that:

M is mass flow rate, H : is the enthalpy, V: is the velocity (related to kinetic energy), g and z: are respectively the local gravitational field, and the height above a reference level (related to the potential energy), $\dot{Q}$ is the heat transfer rate to the system, $\dot{W}$ is the work performed by the system. The subscripts "o" " indicates the values at the output and "i" indicates the values at the inlet (STSmed, 2015).

For steady-state cases, properties are not varied with time, then the left-hand side of the previous equation reduces to zero, then the relation for one stream of fluid entering and leaving a control volume will be:

$$M_{in}\left(H_i + \frac{V_i^2}{2} + gz_i\right) + \dot{Q} = M_{out}\left(H_o + \frac{V_o^2}{2} + gz_o\right) + \dot{W} \tag{3.3}$$

Also, when applying a mass balance $M_{in} = M_{out} = M$, the first law per unit mass reduce to:

$$\left(H_i + \frac{V_i^2}{2} + gz_i\right) + q = \left(H_o + \frac{V_o^2}{2} + gz_o\right) + w \tag{3.4}$$

Where q and w are the heat transfer and work per unit mass respectively (STSmed, 2015).

The relation between the entropy s and the temperature T during the simple ideal Rankine cycle is represented in Figure 3.2

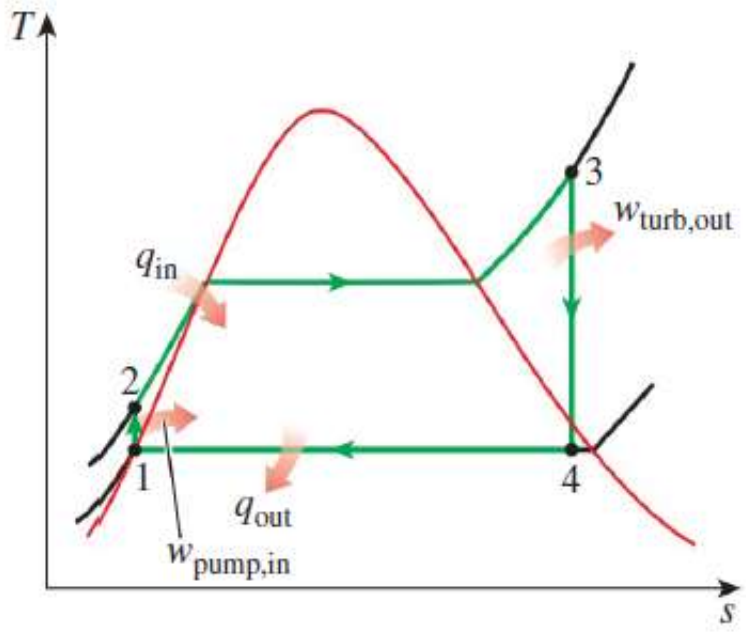

Figure 3.2: T-s Diagram for a Simple Ideal Rankine Cycle. (Çengel, 2008)

All components of the Rankine cycle are steady-flow devices and all four processes in the cycle can be analyzed as steady-flow processes, moreover, the kinetic and potential energy changes of the steam are very negligible relative to the work and heat transfer changes, thus the kinetic and potential energy changes are neglected (Çengel, 2008).

Referring to the T-s diagram and by using equation (3.4) for all devices of the Rankine cycle, and also by neglecting the changes in the kinetic and potential energies, the energy analysis for the cycle will be as the following:

Pump (Process 1-2):

$$q = 0$$
$$w_{pump} = H_2 - H_1 \tag{3.5}$$

Boiler (Process 2-3):

$$w = 0$$
$$q_{in} = H_3 - H_2 \tag{3.6}$$

Turbine (Process 3-4):

$$q = 0$$
$$w_{turbine} = H_3 - H_4 \tag{3.7}$$

Condenser (Process 4-1):

$$w = 0$$
$$q_{out} = H_4 - H_1 \tag{3.8}$$

Also

$$w_{pump} = \nu\,(p_2 - p_1) \tag{3.9}$$

ν is the specific volume, p_1 is the pressure at state 1, p_2 is the pressure at state 2, H_n, P_n represents the enthalpy and the pressure at state "n" in the T-s diagram. Notice that Q is used for any type of energy generated or transfer or consumed per second including thermal energy, $\dot{Q}$ is used especially for thermal energy.

In any thermodynamic cycle, the final state is the same as the initial state. As a result, using the first Law of Thermodynamics to a control volume containing the heat engine (STSmed, 2015):

$$\dot{W}_{net} = \dot{Q}_{in} - \dot{Q}_{out} \tag{3.10}$$

The thermal efficiency which is the most important indicator of the Rankine cycle effectiveness is given by the following expression:

$$\eta_{th} = \frac{(\dot{W}_{net})}{\dot{Q}_{in}} = \frac{(\dot{W}_{turbine} - \dot{W}_{pump})}{\dot{Q}_{in}} \approx \frac{\dot{W}_{turbine}}{\dot{Q}_{in}} \tag{3.11}$$

Since pump work is negligible compared to the turbine generated work. It's common to irradicate it from the thermal efficiency formula.

By Substituting $W_{net} = \dot{Q}_{in} - \dot{Q}_{out}$ in the previous equation you get:

$$\eta_{th} = 1 - \frac{\dot{Q}_{out}}{\dot{Q}_{in}}$$

(3.12)

The Carnot efficiency $\eta_{th,carnot}$, which is the highest efficiency of the thermodynamic cycle working between the thermal energy reservoirs at temperatures T_{min} and T_{max} can have is mentioned as the following: (Çengel, 2008)

$$\eta_{th,carnot} = 1 - \frac{T_{min}}{T_{max}} \tag{3.13}$$

3.4 Categories of Condensers in Steam Power Plants

The most common types of condensers used in steam power plants are water-cooled condensers. Air-cooled condensers are used widely where water surfaces are not available such as lakes, rivers, or sea. In the condenser, the steam leaving the turbine is condensed to water (Nag, 2015). The amount of heat removed $\dot{Q}_{out}$ by the condenser is expressed by the following equation:

$$\dot{Q}_{out} = \mathrm{M}_s\,(H_s - H_c) \tag{3.14}$$

M_s represents the mass flow rate of steam entering the condenser, H_s represents the enthalpy of the steam entering the condenser, and H_c represents the enthalpy of the water leaving the condenser (Nag, 2015).

In condensers, dealing either with water or with air, the amount of extracted heat from the steam is the same that cooling fluid receives:

$$\mathrm{M}_s\,(H_s - H_c) = M_{air}\,(H_o - H_i) = M_w\,C_{p,w}\,(T_o - T_i) \tag{3.15}$$

M_{air} and M_w stands for the mass flow rate of the cooling air and the cooling water. The subscripts "o" and "i" refer to the values at the condenser output and inlet (Da Rocha, 2010). $C_{p,w}$ is the specific heat of water at constant pressure.

Another criterion that is used for representing the performance of a condenser. The overall thermal transmittance U. in a condenser is the amount of heat transmitted per unit of time, the unit of surface, and the degree of temperature difference. The thermal transmittance is described by the following formula:

$$U = \frac{M_w \ C_{p,w}}{A} \ln\left(\frac{\Delta T_i}{\Delta T_o}\right) \tag{3.16}$$

Where ΔT_i is the temperature difference between the steam and the cooling water entering the condenser, and ΔT_o is the temperature difference between the steam and the cooling water after passing through the condenser. A is the area at which heat transfer takes place (Da Rocha, 2010).

- Water Cooled Condenser

As the name suggests, cooling water is used as a coolant to remove the heat from the steam entering the condenser. This condenser consists of a bundle of pipes that cooling water runs inside, while steam flows over the pipes. Figure 3.4.1.1 depicts a schematic of a water-cooled condenser. Cooling water is pumped from natural water surfaces such as rivers or lakes. In some cases, a cooling tower is provided to cool the hot cooling water coming out of the condenser. In such a case, a make-up water source is required (Da Rocha, 2010).

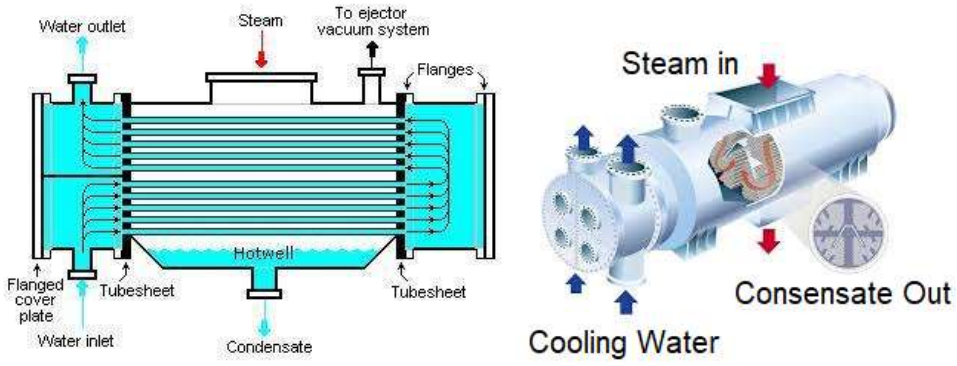

Figure 3.3: Steam Water-Cooled Condenser

- Air Cooled Condenser

An air-cooled condenser is employed where a natural cooling water source is scarce or makeup water is not available to compensate for a cooling tower. Generally, it is an expensive alternative to the water-cooled condenser. The high ambient temperatures cause the efficiency of the air-cooled condenser to decrease. But on the other hand, air-cooled condensers, since they deal with air as a coolant, have no problems with water quality requirements. As a result, air-cooled condensers require less maintenance than other types but the service life is shorter than water-cooled condensers due to the cooling coil degradation (Da Rocha, 2010).

Air-cooled condensers are a finned heat exchanger that the steam flows inside, whereas air flows are induced through fans. Figure 3.4.2.1 shows the major construction of the air-cooled condenser (Drbal et al., 2012).

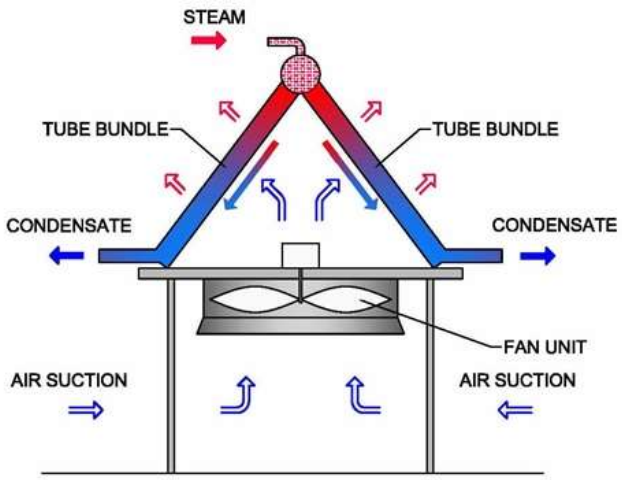

Figure 3.4: Steam air-cooled condenser

3.5 Increasing the Efficiency of the Rankine Cycle

Steam power plants generate most of the electric power in the world, increasing the efficiency of the power plant yields tremendous amounts of saving fuel (Çengel, 2008). The main concept of efficiency enhancement is to increase the average temperature at

which heat is injected through the boiler, and lowering the average temperature at which heat is rejected from the condenser (Çengel, 2008). That concept is relying on the Carnot ideal efficiency. With increasing the ideal cycle efficiency, the actual ideal efficiency increases.

There are three main procedures to enhance the efficiency of the Rankine cycle:

1- Reducing the condenser pressure (reduce T_{min}).
2- Superheating the steam to high temperatures before entering the turbine (increasing T_{max}).
3- Raising the Boiler pressure (increasing T_{max}).

Figure 3.5 depicts the T-s diagrams that show the effect of these three methods on the power cycle (Çengel, 2008).

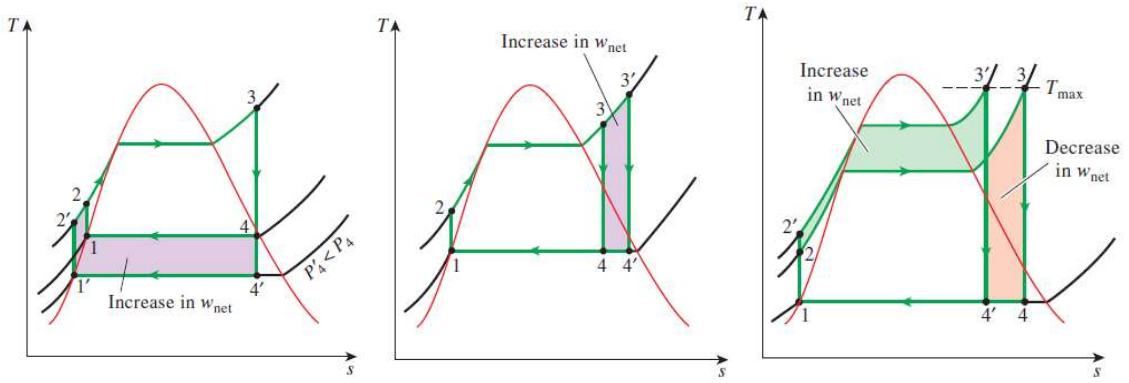

Figure 3.5: From left to right, the effect of reducing condenser's pressure, superheating the steam in the boiler, and increasing boiler's pressure.

But some limits apply to the previously mentioned methods (Nag, 2015):

- Reducing condenser pressure can be used to a certain pressure, after that the moisture content of the exhausted steam from the turbine increases. Such moisture plays a major role in turbine deterioration.
- Superheating the steam in the boiler could enhance the efficiency of the cycle, but it obligates the designer to use more reliable and expensive materials to endure the high temperatures.

- Increasing the boiler pressure also means using more pressure-enduring materials and designs, which are more expensive.

3.6 The Reheat Rankine Cycle

This configuration is proposed as a refinement to the simple ideal Rankine cycle to improve cycle efficiency. In a reheat Rankine cycle, the steam is allowed to expand in two turbines: A High-Pressure (HP) turbine and a Low-Pressure (LP) turbine. In between, a reheat is applied to the steam coming out from the HP turbine. This configuration lowers the pressure of the boiler. At the same time, the steam is not expanding till moist appears, it is reheated thus the next expansion in the LP turbine occurs close to the saturation condenser pressure (Çengel, 2008). Figure 3.6 represents the *T-s* diagram and a schematic of the ideal reheat cycle.

In the reheated cycle two turbines work in series and after the first expansion in the high-pressure turbine, the steam re-enters the boiler and is reheated almost until the maximum temperature of the cycle. Then pass through the second, lower pressure turbine. Among other advantages, this prevents the vapor from condensing during its expansion which can seriously damage the turbine blades, and improves the efficiency of the cycle (Nag, 2015).

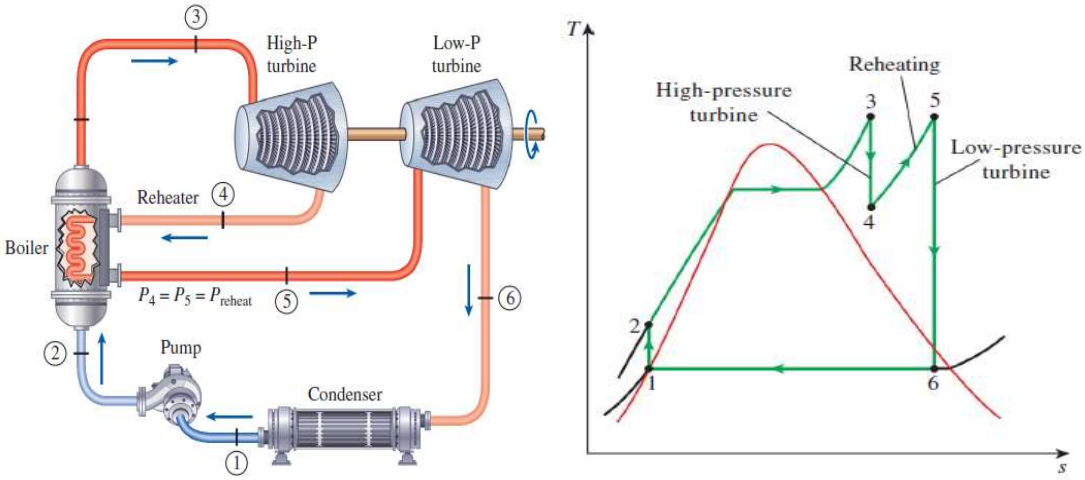

Figure 3.6: Ideal reheat Rankine cycle schematic and *T-s* Diagram (Çengel, 2008)

3.7 The Regenerative Rankine Cycle

In a simple ideal Rankine cycle, the heat is transferred to the working fluid at low temperature as depicted in the *T-s* diagram of the Rankine cycle in Fig 3.3.1 Which leads to lower, in turn, cycle efficiency. To tackle this disadvantage, the working fluid is heated internally from the cycle before entering the boiler, thus the temperature of heat addition is increased, which in turn enhances the cycle efficiency (Nag, 2015).

This could be achieved by bleeding a portion of the steam and mix it in a feedwater heater with the condensed working fluid coming out from the condenser. Or by performing this without mixing via a closed water heater. Which is a heat exchanger that transfers heat from the bleed steam to the condensed water coming from the condenser. Figures 3.7 and 3.8 represent both direct or indirect regeneration (Çengel, 2008).

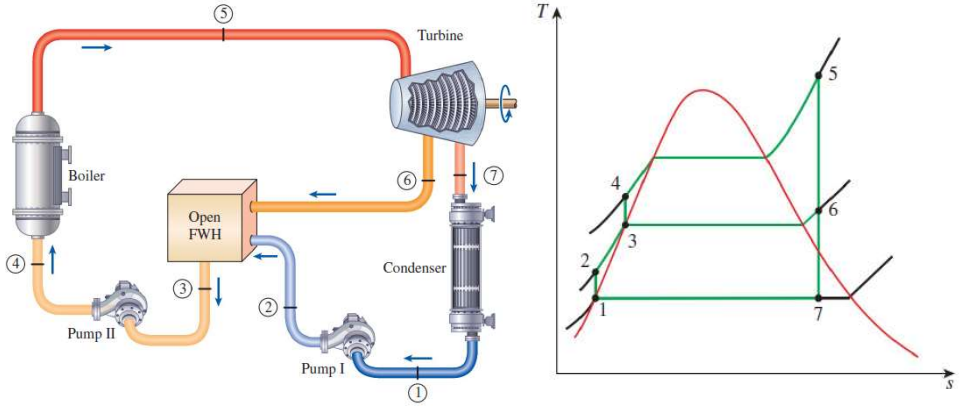

Figure 3.7: Regenerative Rankine cycle T-s diagram, with open feedwater heater (Çengel, 2008)

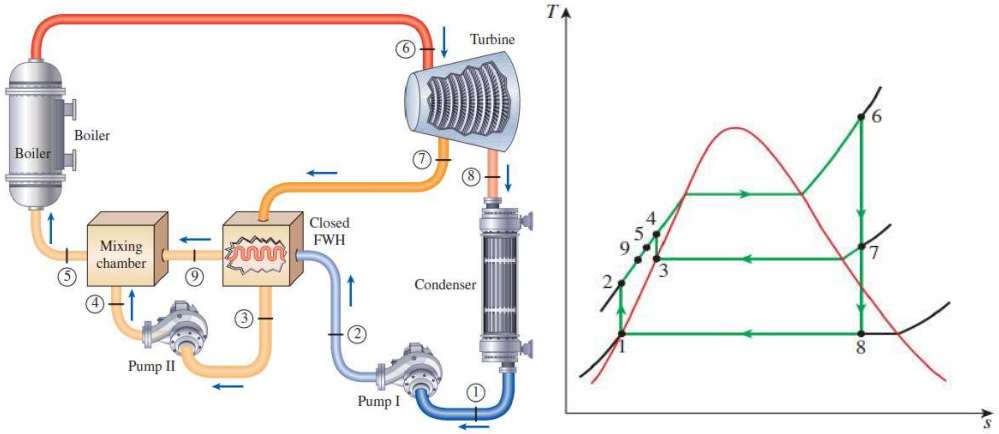

Figure 3.8: Regenerative Rankine cycle T-s diagram, with closed feedwater heater (Çengel, 2008)

Open feedwater heaters are simpler in construction and relatively inexpensive, they got an acceptable heat transfer profile. The closed feedwater heaters are considered more sophisticated because of the required tubing for heat exchange, thus they become more expensive. Heat transfer in them is less than an open feedwater heater. In large power plants, both are used and their advantages are added (Çengel, 2008).

CHAPTER 4

Concentrated Solar Power Technologies

4.1 Preamble

In Chapter Three, the steam power cycles were introduced. Discussing the different thermodynamic aspects of them. To be used later in developing the power plant model.

Concentrated Solar Power (CSP)Technology saw its first leap of commercial evolution between 1984 and 1995.

The technology used in CSP power plants is the same used in conventional power plants, except that the sun is the heating source in these plants. Instead of using fossil fuels, the heat energy captured from the sun is used to power a steam turbine to produce electricity from a clean renewable source without emissions. These plants have a low operating cost and the ability to produce electricity from an authentic renewable energy source away from any need for energy importation (Da Rocha, 2010).

CSP technology employs mirrors to concentrate the Direct Normal irradiance (DNI) at a receiver filled by thermal fluid. The thermal fluid can be either a Heat Transfer Fluid (HTF) -Like Thermal Oils-, which acts as an energy carrier to heat the power cycle Working Fluid (WF) -like water- that used in the power cycle, or the working fluid is directly heated by CSP for direct steam generation for power generation. Since CSP systems able to capture only direct normal irradiance from the sun, CSP technology is a promising choice for areas with high annual clear sky days (Draidi, 2016a).

Solar energy has its disadvantages compared to fossil fuels. It is not available around the clock. The available amount of solar energy depends on many parameters, such as solar time, latitude, and sky clearance. Such many parameters decrease the reliability of solar energy. However, such disadvantages could be tackled by switching to a fossil fuel source, to compensate for the shortage in solar energy, or storing solar thermal energy for later use when the sun is unavailable or to make up any fluctuation in sun radiation (Da Rocha, 2010).

CSP power plants involve two main systems: the solar field and the power block part. The solar field consists of mirrors, receivers, and thermal-fluid networks. The power block is a Rankine power cycle.

There are two principles for concentrating sun rays (Draidi, 2016a, STSmed, 2015):

1- Line focus principle: It depends on concentrating DNI in a focal line instead of a point. Parabolic Trough and Linear Fresnel systems are examples of it.
2- Point focus principle; It depends on concentrating DNI in a fixed focal point. Solar Tower and Dish Stirling Systems are examples of it.

Figure 4.1 represents different photos regarding each system (Feldhoff, 2012)

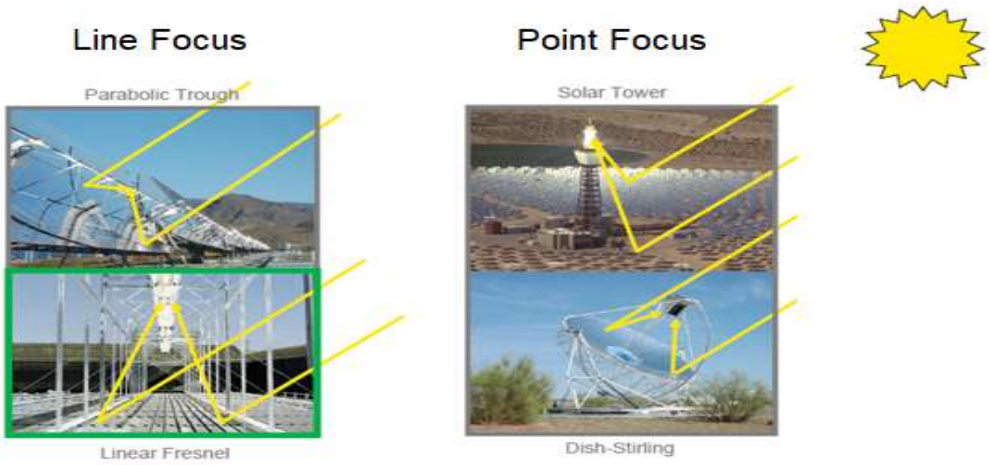

Figure 4.1: Main Categories of CSP Systems (Feldhoff, 2012)

4.2 Line Focus CSP

4.2.1 Parabolic Trough Collectors (PTC)

The first commercial CSP were parabolic trough systems installed in the United States in the 1980s and are the most proven, developed, and commercially-ready CSP technologies (Da Rocha, 2010).

PTC systems as depicted in Figure 4.2, consists of a focal-lined receiver and a parabolic-shaped mirror, this mirror concentrates the sunrays onto an absorber tube that is

constructed in the focal line of a parabola. The absorber tube contains the Heat Transfer Fluid (HTF). HTF could be heated to high temperatures up to 400 C^{o} (STSmed, 2015). Although PTC can achieve better efficiency in DSG more than HTF (synthetic oil) systems, but due to the high pressure and temperatures of the system, the complexity, and the existence of flexible connections makes disadvantages for DSG through PTC (Feldhoff et al., 2011).

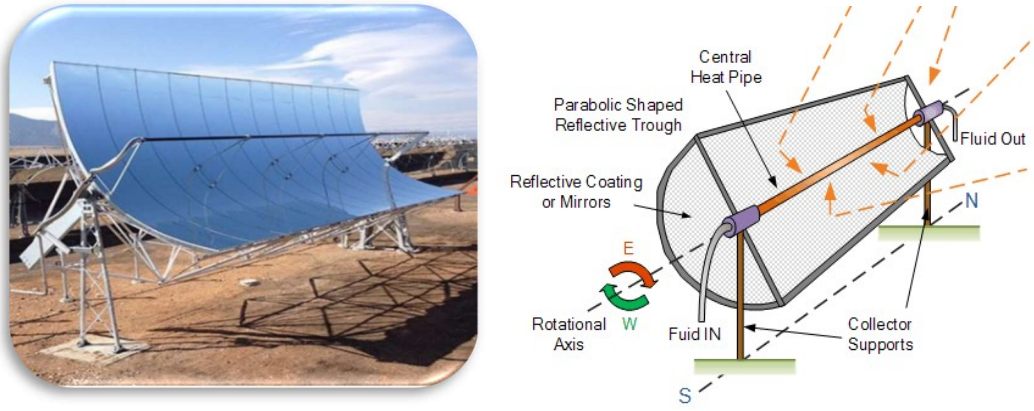

Figure 4.2: Parabolic trough collectors.

Figure 4.3 represents a schematic layout for the PTC system used for DSG in power generation.

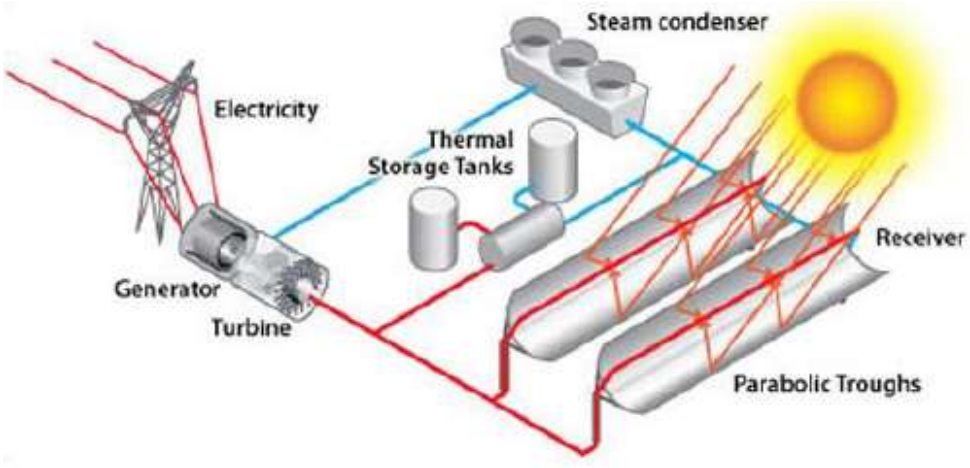

Figure 4.3: Parabolic trough collectors for DSG

4.2.2 Linear Fresnel Reflectors (LFR)

Fresnel reflectors, as illustrated in Figure 4.2.1.1, focus sun rays using thin, flat mirror strips onto the receiver filled by thermal fluid (STSmed, 2015).

Flat mirrors in LFR allow more reflective surfaces in the same amount of space as a parabolic reflector, thus capturing more of the available sunlight, and They are much cheaper than parabolic reflectors. Fresnel reflectors can be used in various size CSPs (STSmed, 2015).

The first commercializing of LFR in power generation was in Europe, by Novatec Solar AG. It was in Murcia-Spain with an electric power capacity of 1.4 MW (Makhlouf et al., 2017).

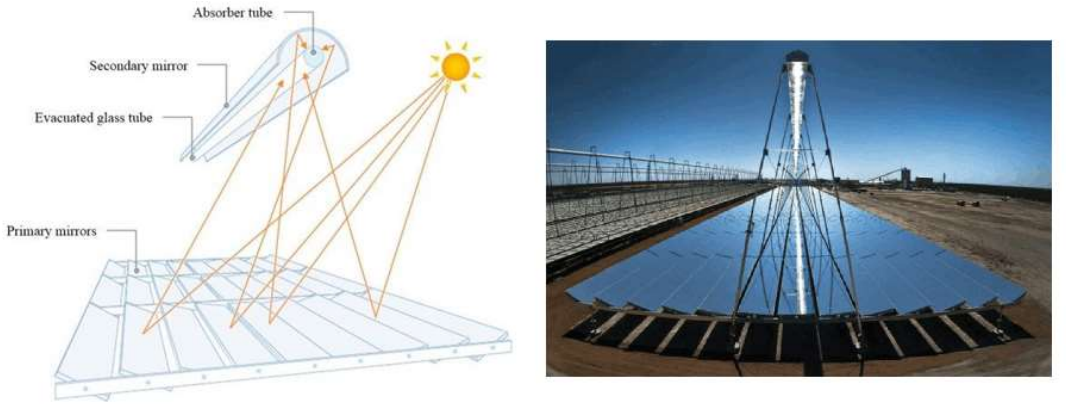

Figure 4.4: Linear Fresnel Reflector (LFR) principle

The major feature of linear Fresnel systems is the simplicity and flexibility of their design which facilitates the Direct Steam Generation (DSG) approach. On the other hand, LFR systems are less efficient than PTC Systems (Draidi, 2016a). Figure 4.5 illustrates DSG with LFR.

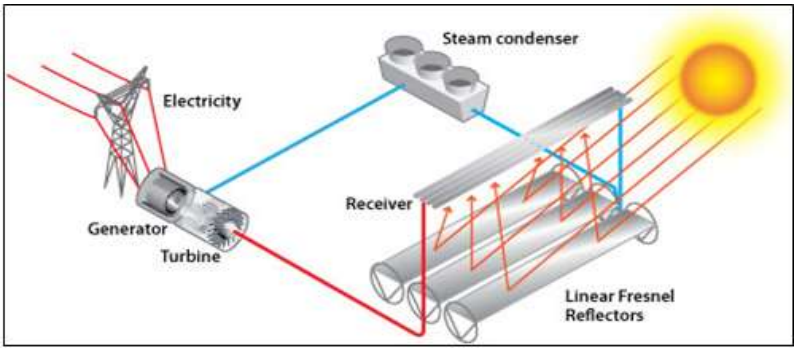

Figure 4.5: Linear Fresnel System for DSG

4.3 Point Focus CSP

4.3.1 Parabolic Dish (PD)

They are also known as Parabolic Dish Concentrators (PDC) or Stirling dish. A dish concentrator is a parabolic-shaped surface (a dish) that tracks the sun along both axes to concentrate the DNI onto a single point where a thermally-driven engine is fixed. So that engine uses the focused heat to produce electric power. The heat receiver of the engine is located in the focal point of the PDC and all the structure (the dish and the engine) moves together tracking the sun. Stirling and Brayton's engines are used nowadays for power conversion (Draidi, 2016a).

PDCs are independent units. Each dish produces its electric output, which allows higher modularity and gives a major advantage in the case of unit failure. In a nutshell, if a PDC failed within a PDC solar field that would not matter the operation of the field dramatically. Another principal advantage is their high efficiency which is over 30% for both the dish and the engine, which is the highest among all CSP systems. The PDCs eliminates the need for HTF or steam-powered power block. Which simplifies the solar field dramatically (Da Rocha, 2010).

Despite the many advantages, PDC's has their disadvantages: they are vulnerable to high-speed wind and wind gusts. The incurred costs are expensive compared to other CSP systems. They are incompatible with Thermal Storage Systems (TES) or hybridization with other energy systems. Promoters claim that with more production of PDCs, the cost will go down and the LCOE will improve. Figure 4.6 depicts a schematic of PDC's solar system (Draidi, 2016a).

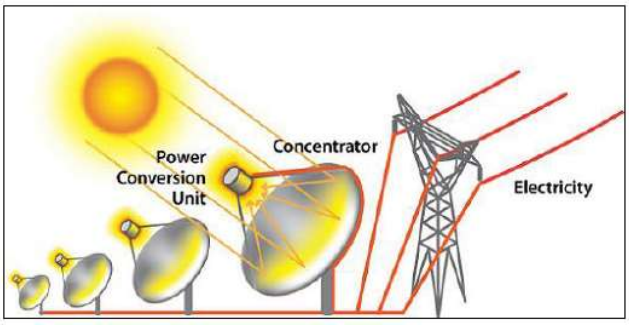

Figure 4.6: Dish Stirling Systems

4.3.2 Solar Power Tower (SPT)

It is known also as the central receiver system. The solar tower is conceptually a large Stirling dish whose reflector is divided into several reflectors that reflect sun rays to a single elevated point on the top of a tower. Each reflector is called a heliostat. The receiver then transforms the heat to generate steam or to heat a synthetic oil. Even though heliostats are the discrete form of the paraboloid dish, the heliostats don't concentrate sun rays as much as an ideal paraboloid does (Da Rocha, 2010). Figure 4.7 represents a schematic layout of a solar power tower.

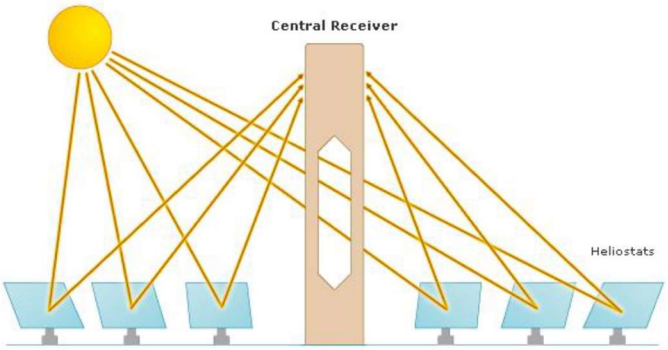

Figure 4.7: Schematic layout of Solar Power Tower

Heliostats are either flat or concaved reflectors that track the sun in two axes. The reflected radiation is absorbed by the receiver and heat is transferred to the HTF. After that, HTF is used to generate the required steam to drive a Rankine power plant. Some solar towers are designed for DSG without the need for HTF. Since solar towers could achieve very high temperatures, that enables higher temperatures for plant operation. Which in turn increases the plant efficiency in power transformation and reduces the cost of the thermal storage systems. Solar towers are flexible in design, many types of heliostats could be selected, the same is available for the receiver and HTF. The system could be flexibly designed to drive the power block (Draidi, 2016a).

At the first investigations about this technology, the question was what is the appropriate HTF to use. The superheated steam was an attractive candidate to avoid using heat exchangers and enabling the immediate connection to the steam turbines. However, it was difficult to control the generation of superheated steam steadily under different

radiation conditions. Also, heat storage from superheated steam incurred high loss rates (Da Rocha, 2010).

Another alternative was proposed later. Alkali salts were proposed to be the candidate HTF in their liquid manner. The advantages were the good heat transfer properties and the possibility of storing heat in them at low pressure in a well-insulated storage tank. The use of alkali metals salts obligates the use of auxiliary heaters to prevent salt freezing in circumstances where the solar radiation is not available or sufficient so that HTF piping is not blocked (Da Rocha, 2010). Figure 4.8 shows an aerial photo of PS10 and PS20 solar power towers in Sevilla, Spain.

Figure 4.8: shows an aerial photo of PS10 and PS20 solar power towers in Sevilla, Spain.

4.4 Comparison of CSP Technologies

According to the related literature, the main features of CSP technologies are depicted comparatively in Table 4.1.

Every type of CSP technology is characterized by some features, advantages, and disadvantages. Table 4.2 illustrates the advantages and disadvantages of each type of CSP (Draidi, 2016a, STSmed, 2015, Răboacă et al., 2019, Moser et al., 2013, Pablo del Río et al., 2018). Where the ratio of solar concentration is the area of collector aperture to the area of the receiver.

Table 4.1: Main features differences between CSP technologies

CSP Tech	Operating Temperature (°C)	Ratio of Solar Concentration	Thermal Storage Suitability	Average Annual Efficiency	Land-Use (Occupancy)	Cost/kWh
PTC	20-400	15-45	Suitable	15%	Large	Medium Costs
LFR	50-400	10-40	Suitable	8-11%	Moderate	Low Costs
PD	120-1500	100-1000	Difficult	25-30%	Small	High Costs
SPT	300-1000	150-1500	Highly Suitable	17-35 %	Moderate	High Costs

Table 4.2: the pros and cons of each type of CSP technology

CSP Tech	Pros	Cons
PTC	- PTC is the most demonstrated, proven, and mature technology, and thus the most commercially used technology. - Ability to match high-temperature applications.	- Complex configuration - High precision required - Large land occupancy - PTC involves high thermal losses
LFR	- Ability to match high-temperature applications. - Low land occupancy compared with PTC to generate the same energy - Lower thermal losses than PTC - Simple and stable construction - Less affected by wind loads compared with PTC as a result of its construction stability	- Less efficient than PTC - Less commercially used than PTC
PD	- PD systems are distinguished by having high conversion efficiency. - High modularity. - PD System appropriate to decentralized power supply and outlying, stand-alone power applications. - PD systems are not constricted to flatlands.	- PD System has not been used on a large commercial scale, therefore performance, operating, and investment costs are not commercially demonstrated. - Poor ability of integration with utility grids. - Do not involve thermal storage system
SPT	- High efficiency of power generation due to the possibility of achieving temperature above 1000°C - The ability to retrofit gas turbines and combined power cycles	- High capital costs for investment. - High maintenance costs and requirements.

CHAPTER 5

EBSILON® Professional for Thermodynamic Cycles Design and Simulation

5.1 Preamble

In this chapter, EBSILON® Software is introduced as a design and simulation tool for the power plant processes. This software is adopted in this research due to its availability for graduate students and researchers, its specialization in thermodynamic processes simulation, well-established components library, the availability of inserting formulas and Kernel scripting, and proven use in scientific research for design, modeling, and optimization of thermal systems and retrofits. EBSILON provided a powerful tool for thermal engineers due to its powerful mathematical infrastructure, flexibility, and output proved reliability that made it an adopted choice for many studies around the world (Jingzhi, 2014, Li et al., 2015, Wołowicz et al., 2019, Świerzewski and Kalina, 2019). All necessary gathered data from previous chapters for hybridization between olive pomace as a biomass source and CSP technology that extracted solar energy and based on the main criteria of steam power plant that mentioned in chapter 3, the hybrid model investigation will be built by EBSILON® Software.

EBSILON® Professional is developed by STEAG Energy Services GmbH for more than 20 years. The first version was accomplished by Sofbid GmbH in 1990. After the merger of Sofbid with STEAG GmbH in 2006, EBSILON® Professional became one of the Important products of STEAG Systems Technologies product portfolio (STEAG-Energy, 2015).

5.2 Basic Concept and Structure of EBSILON® Software

EBSILON is the abbreviation for "Energy Balance and Simulation of the Load response of power generating or process controlling Network structures". EBSILON® Professional was developed for engineering thermodynamic simulation. It is a mass-energy balance calculation software for thermodynamic processes. Also, it includes other additional systems such as thermochemical processes. However, the main theme is thermodynamical simulation (Da Rocha, 2010, Swat, 2020).

In EBSILON®, the thermodynamic cycles and processes are established from many objects such as components (pump, valve…etc.), text boxes, lines, and graphical elements. water and steam tables, combustion calculation, and Properties of gases and gas mixtures are additionally integrated into the software database (Da Rocha, 2010, Swat, 2020). Figure 5.1 depicts a power plant configuration in EBSILON.

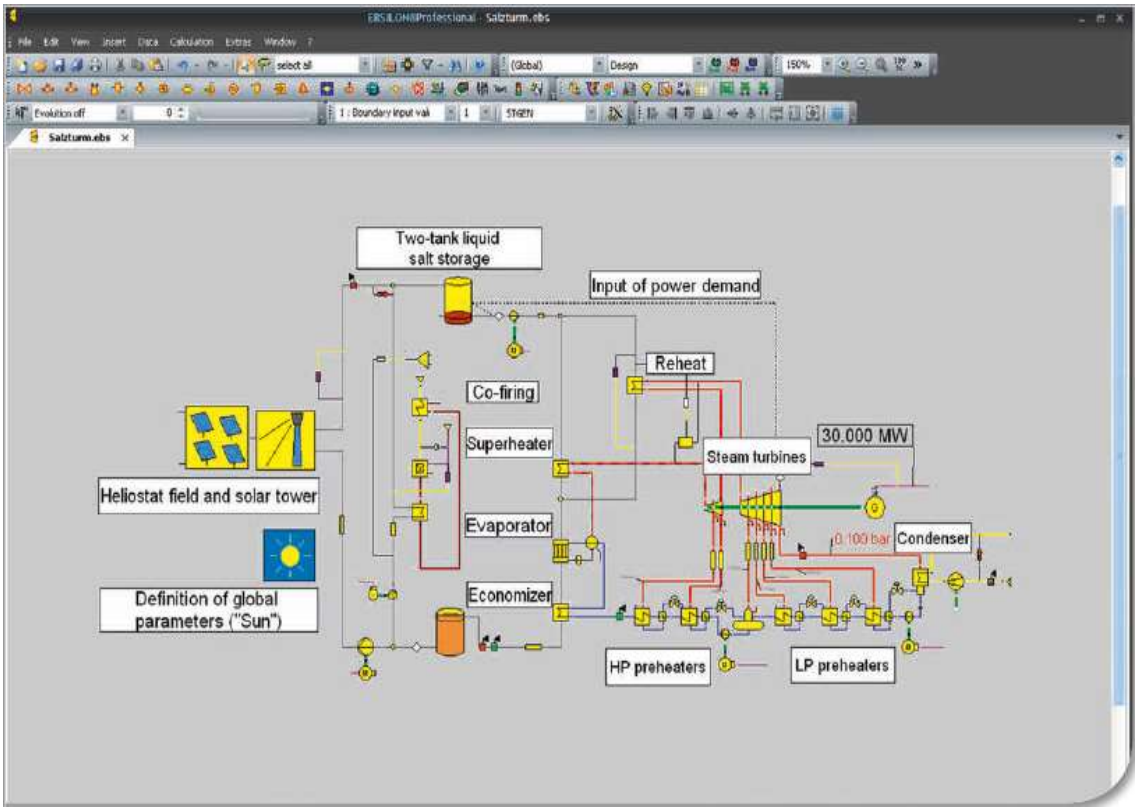

Figure 5.1: Power Plant on EBSILON (STEAG-Energy, 2015)

The structure of the software is based on:

- Physical and logical components are used in the design of the power plants.
  The physical components like steam generators, pumps, turbines, solar fields, steam generators, condensers, heat exchangers, cooling towers, etc.
  The logic components like controllers, efficiency meters, signal transformers, etc.

- Programmable components for design and simulate complicated power plants processes (Da Rocha, 2010, Swat, 2020).

In EBSILON, The simulation process is performed internally in two steps (Swat, 2020):

- First step: generation of mass and energy balance nonlinear system of equations from the inputs of the thermodynamic cycle.
- Second step: use the iteration method to solve the system of equations to compute the residual unknown variables and parameters.

Building the thermodynamic model is performed by adding the system blocks, such as turbines, pumps, heaters…etc. Each block contains a set of mathematical formulas that describe its behavior and response to the input values. These blocks are interconnected via lines representing either physical connections such as pipes and ducts, or logical connections that just transfer data and values from one block to another. For physical lines, the stream values and the media flowing within are determined and involved within the calculation process. EBSILON simulation process calculates the output results in their steady-state manner. There are some blocks that EBSILON can calculate their status during the transient response. However, thermodynamic power cycles are simulated and studied on their steady-state condition (Da Rocha, 2010, Swat, 2020).

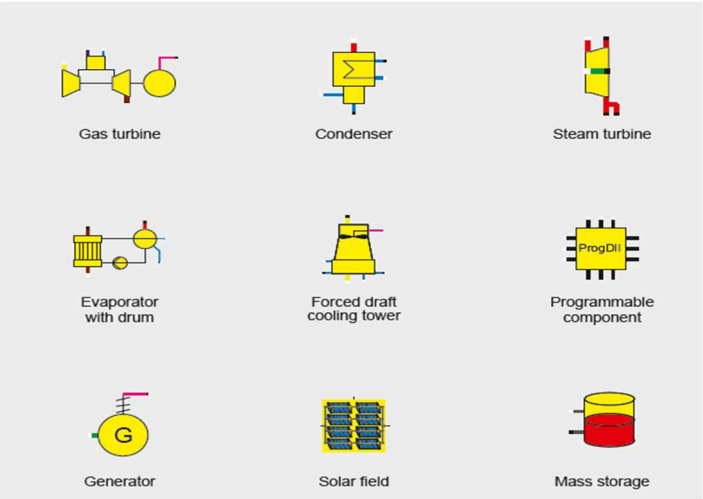

Figure 5.2: Example of Components in EBSILON (STEAG-Energy, 2015)

5.3 Time Series Calculation

In EBSILON, there is a time series calculation option for performing different several calculations under different conditions for an existing thermodynamic cycle diagram. The time series structure is illustrated in Figure 5.3 (Swat, 2020). The time series option enables the investigation of the change in the parameters of the thermodynamic power cycle during operation over a time interval. For instance, the thermodynamic power cycle could be studied against the changes in the ambient temperature during the day. By dividing the day into small time intervals and running the simulation process to obtain results for each time interval. This could be performed separately, which means that for each time step the values are irrelevant to the step before, or depending on it, or even integrating with it.

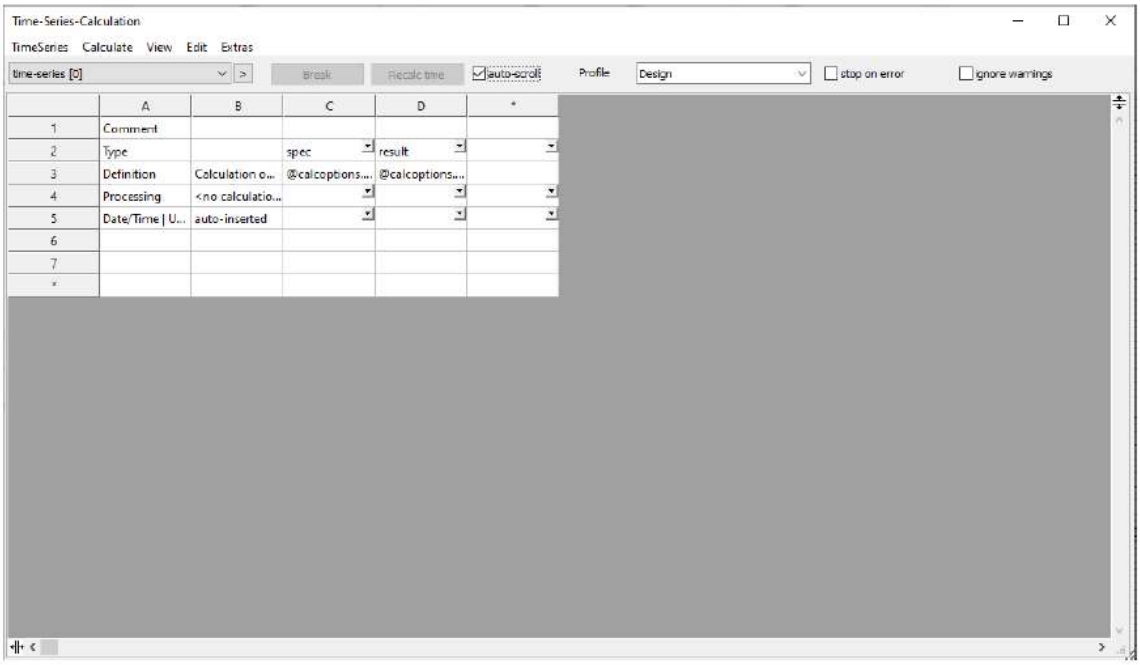

Figure 5.3: Time Series Structure in EBSILON (Reference 1)

5.4 Basic Strategy for Power Cycle Construction and Investigation by EBSILON® Software

The following are fundamental instructions that must be noticed when constructing a power plant diagram (Swat, 2020):

- The power plant diagram is implemented using the following: Physical and Logic Components (boiler, turbines, boilers, pumps, controllers, etc.), Text boxes, Lines and the boundary conditions on the lines, and Value crosses (used to show main variables and parameters such as temperature, enthalpy, mass flow rate, and pressure after each simulation).
- All inputs and boundary conditions are checked before each simulation
- Start the simulation.
- Simulation results: the results after the simulation are entered into the power plant diagram directly and appeared on the value crosses, if there are any errors and warnings there is a window for analysis of the warning and errors to amend and correct errors.

5.5 EBSILON® Simulation Modes

The several operation modes for simulation in EBSILON as the following (Swat, 2020):

- Design Mode: the power plant in this mode is constructed taking consideration of the design conditions (nominal conditions), all construction components have been accomplished under nominal operating conditions to simulate the cycle under the nominal load
- Partial Load Mode (off-design mode): this operation mode is used to simulate the performance of the power plants and cycles under various load situation conditions.
- Validation Mode: this operation mode is used to investigate the performance of already existing power plants to identify the prosaic points to enhance the quality of these power plants.

In this research, design mode will only be used for the design and build steam power plant by hybridization between CSP and Biomass as an energy source for the steam generation that drives the steam turbine for electricity generation. The plant cycle will be investigated under different conditions and simulation will be run for one year using the time series calculation option in hourly steady-state conditions.

CHAPTER 6

Hybrid CSP-Olive Pomace Proposed Physical Model and Analysis

6.1 Preamble

Up to this point, olive pomace status Palestine, steam power plant overview, CSP technologies, and simulation software EBSILON were introduced and explained. In this chapter, a proposed model is proposed to combine Olive pomace and CSP technology to power up a steam power plant. This proposed model will be studied and simulated under EBSILON environment.

The proposed models rely mainly on olive pomace, CSP is used to supplement the heat needs when solar radiation is available. The simulation will consider the circumstances and considerations in the Palestinian territories. The steam power plant will be considered subcritical since supercritical power plants are only feasible on a mega-scale. And the considered CSP technologies are the line focusing technologies, namely the Linear Fresnel Reflectors LFR and Parabolic Troughs. Stirling Dishes are not considered due to the irrelevancy to the scope, and Solar Power Tower is not also considered due to its extreme costs and sophisticated engineering requirements for erection and operation.

6.2 Hybrid Power Plant Site Selection Criteria

Potential location for installing CSP systems have to comply with certain requirements; This includes solar radiation requirements, land availability and use, land slope, water availability, infrastructure status, and meteorological conditions. the consideration also involves the requirements for olive pomace gathering and storage (Yasin, 2019b). The CSP power plants or CSP retrofits of hybrid plants erection locations needs to fulfill the following criteria:

1- DNI Amounts: CSP systems erection location should have a sufficient annual amount of DNI which should be no less than 2000 kW/m² to obtain attractive and reasonable levelized electricity prices. Figure 6.1 depicts the Direct Normal Irradiance (DNI) map of Palestine from Solar GIS which is a model that has high

accuracy database of DNI and other metrological information computed and updated daily from satellites (SolarGIS, 2020). As shown in Figure 6.1, all governorates in Palestine have annually adequate DNI amount that makes them appropriate for CSP applications.

2- Land: CSP systems need large flat areas with allowable slope area around 1-2% for Linear Fresnel and Parabolic Troughs. Otherwise, site preparations are needed. In Palestine, most areas are characterized to be mountainous except for Jericho and Gaza as also can be inferred from Figure 6.1. Jericho area is selected in this study.

3- Plant Cooling: The cooling of the power plant must be considered as a variable when selecting the power plant location. Although the cost of wet cooling is lower and more efficient, this choice is not valid in Palestine due to the scarcity of water in the West Bank. So, the dry cooling option is selected in this study.

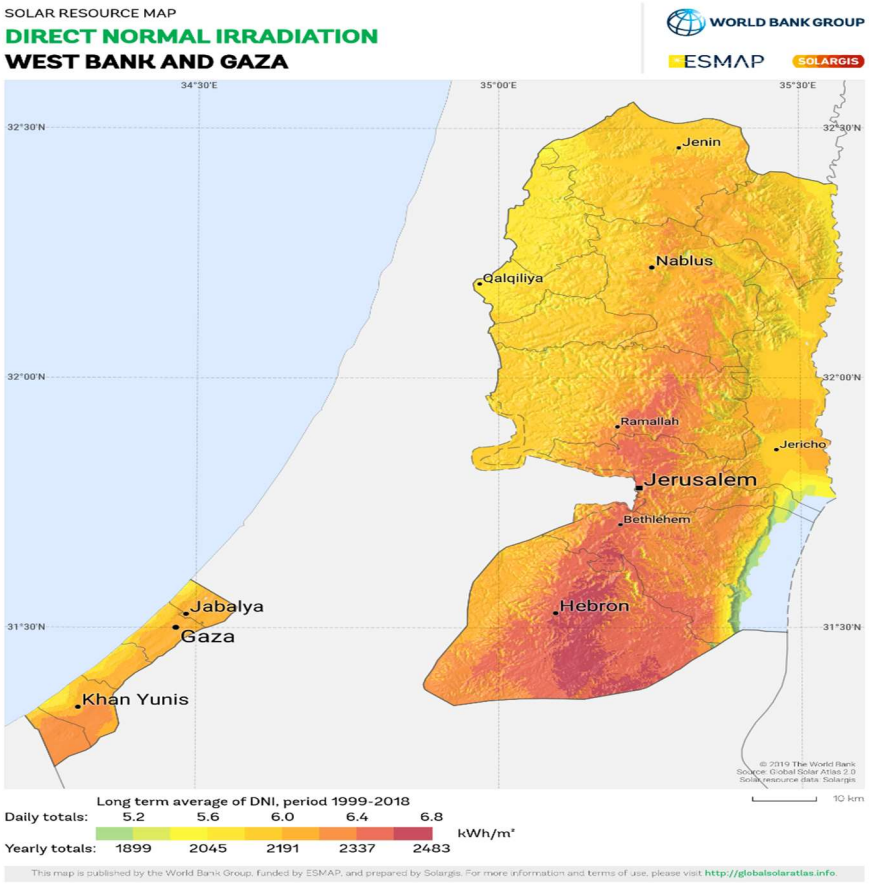

Figure 6.1: Direct Normal Irradiance (DNI) of Palestine from 1999-2018 (SolarGIS, 2020).

4- Logistic Considerations: The location must be selected so that the transportation of olive pomace from other governorates is valid. And have suitable roads for transporting power plant equipment. The availability of a utility grid to transport the generated power.

5- Wind: CSP construction generally is wind resistant. However, Palestine's wind profile shows low-speed winds in most areas. Figure 6.2 represents a wind speed map for Palestinian different governates (Yasin, 2019b).

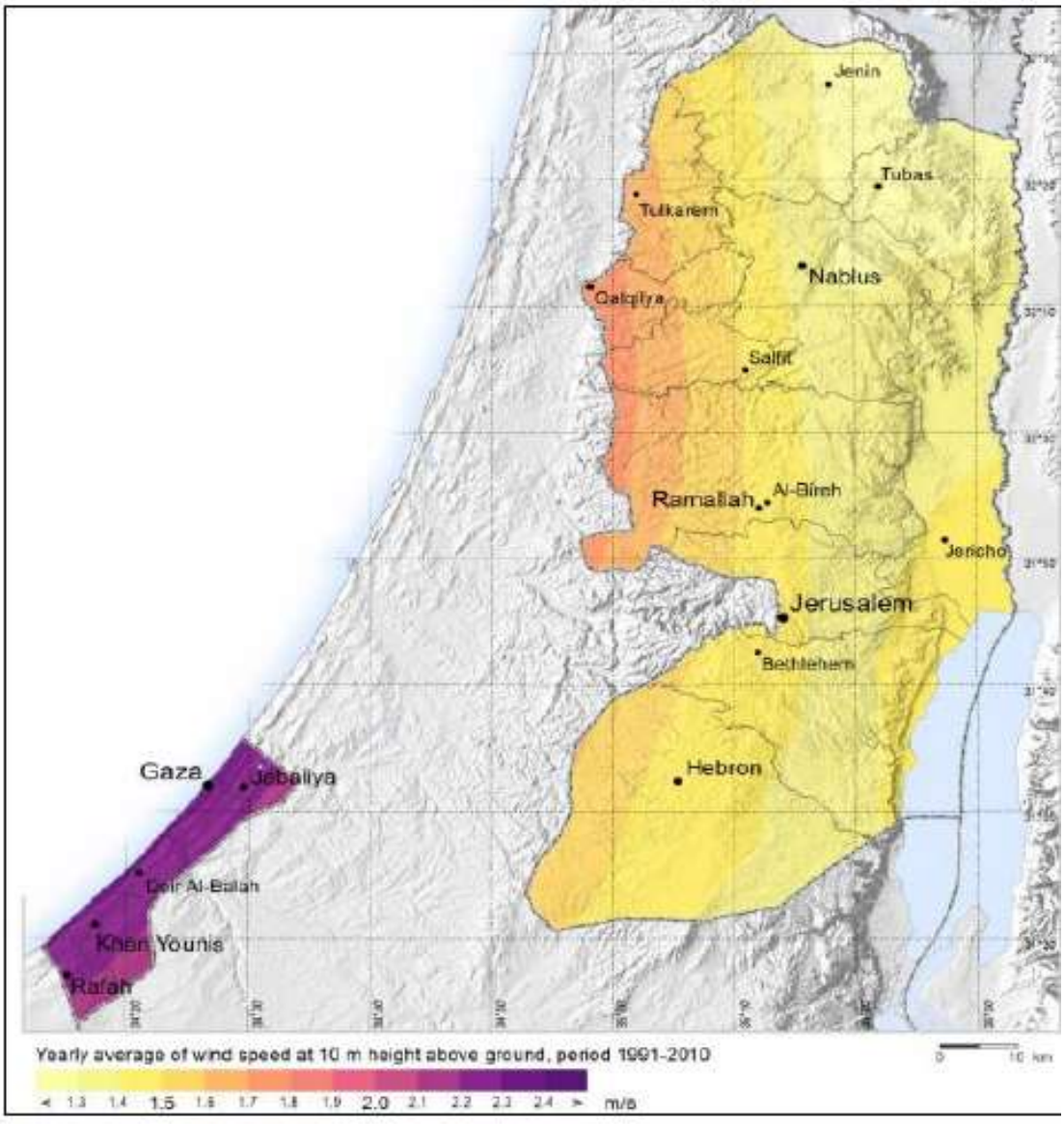

Figure 6.2: Direct Normal Irradiance (DNI) of Palestine from 1991-2010 (Yasin, 2019b)

in Jericho the wind speed average is around 1.5 m/s, Hebron not exceeding 2.4 m/s, Nablus around 1.76 m/s, Ramallah with 2.84 m/s, Gaza with 2.8 m/s. In the proposed location of this study in Jericho, wind speed is not a problem.

6- Ambient temperature: It affects solar field and power block efficencies. In the case of this study, hgih ambient temperatures is an advantage for reducing the thermal losses from the solar field but requires more area for heat transfer in the air-cooled condenser. However, the moderate to high ambient temperatures pays in favor of the power plant. Figure 6.3 depicts the average ambient temperature in different governates in Palestine.

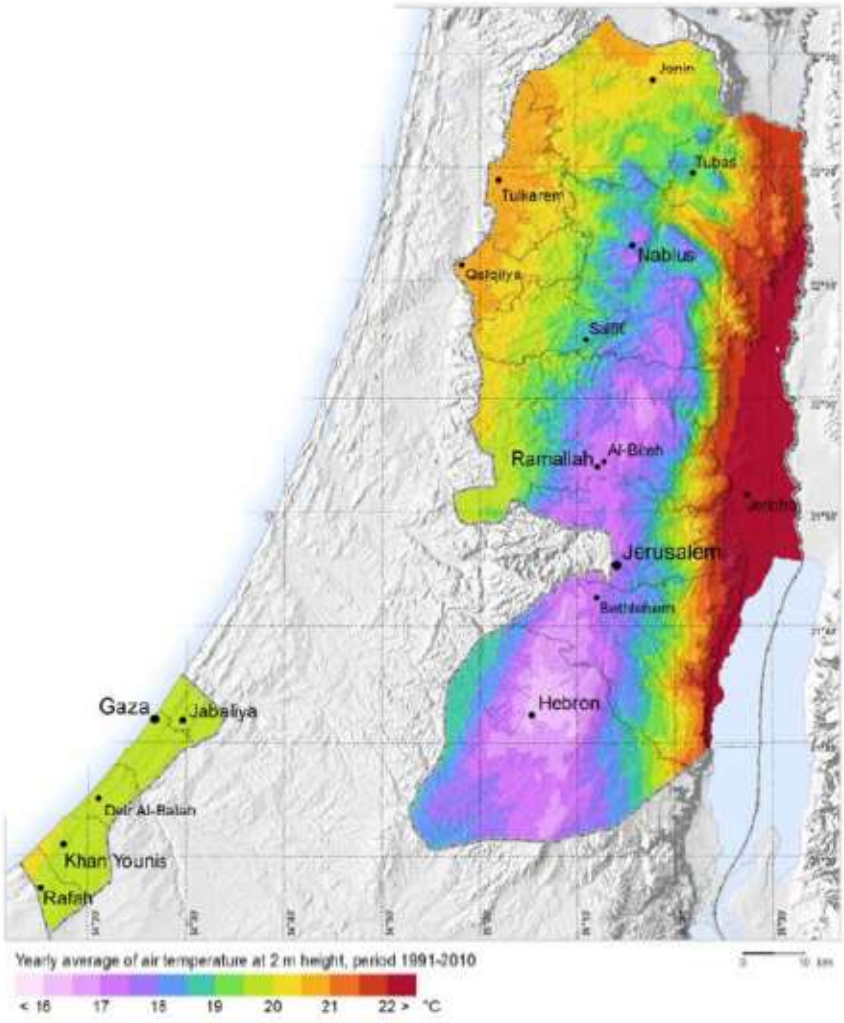

Figure 6.3: Yearly average Ambient Temperature in Palestine in Years (1991-2010)

Based on the above-mentioned criteria, Jericho is the best governorate for the implementation CSP-Biomass hybrid power plant. Gaza can be suitable for providing water for the water-cooled condenser but it is not considered for its low land availability and the political complication for transportation and gathering the olive pomace from other governates. Also, a study conducted by Draidi for investigating the feasibility of CSP technologies in Palestine resulted that Jericho is the best choice for applying CSP technologies (Draidi, 2016a). So, Jericho is selected in this study, location at 35.468 Longitude and 31.944 in Latitude.

6.3 Main Approach

1- Selecting a location in Jericho governorate that is suitable for the erection of all power plant components and thermal solar field suitable for both LFR and PT systems.
2- Estimating the power plant capacity based on the available olive pomace annual average quantities and solar field land capacity for linear Fresnel and Parabolic Trough
3- Selecting the basic thermal properties of the hybrid power plant, namely the live steam pressure and temperature and condenser pressure. These data will be selected according to the power plant equipment manufacturers.
4- Building and Optimizing the power block: Introducing 4 different Rankine cycle power blocks with optimized components to achieve the best efficiency. Then adopting one of them to be hybridized with the solar field.
5- Building the two solar field models based on Linear Fresnel and Parabolic Trough. And interface the solar field to the power block. Yielding two different hybrid power models, one is hybridized with LFR and the other with PT.
6- Identifying the operation strategy of the hybrid power plant.
7- Generating hourly steady-state analysis based on time series that provides all required inputs (DNI, wind speed, ambient temperature, sun location…etc.). simulating different parameters of the hybrid power plant. Showing mainly the olive pomace requirements and the generated heat from the solar field.

8- Repeating the simulation for 3 constant power output of the plant. On under the estimated capacity, on at the estimated capacity, and one above the estimated capacity. To check the annual consumed olive pomace if it in the average of the available yearly quantities in Palestine, if not re-adjust the power plant capacity to match the generated annual quantities of olive pomace.
9- Simulating the proposed hybrid models for Linear Fresnel and Parabolic Trough on 24 hours in the worst and best day of the year in average DNI. The best day is Oct 6th and the Worst is Jan 18th.
10- Comparing between the results from LF hybrid power plant models and PT hybrid power plant models
11- Calculating LCOE for the proposed LF hybrid power plant models and PT hybrid power plant models.
12- Discussing results, and inferring conclusions about the feasibility of the scope.

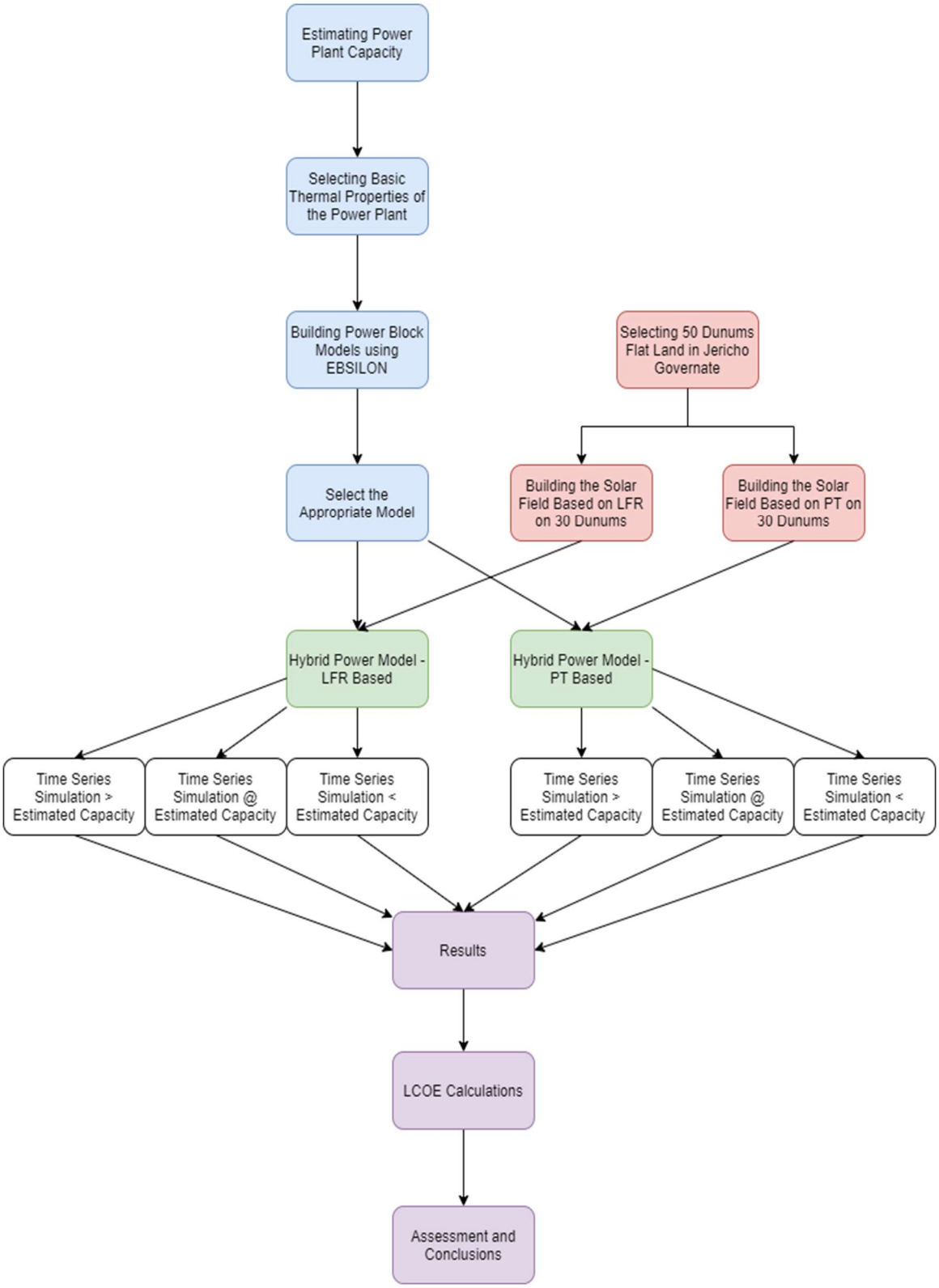

Figure 6.4: Approach Flowchart

6.4 Major Study Assumptions:

1- Olive pomace is dried and ready to be combusted. Treating, drying, and storage of the olive pomace is out of study scope.
2- Power plant shut downs and starts periods are not considered in the scope of this research
3- The calculation is based on quasi-steady-state conditions.
4- Solar field land was restricted to 30 dunums according to the real estate status in most of Palestine. According to a conducted investigation, the total power plant area can be assumed to be established over 50 dunums of flat terrain. To be reasonable and applicable from a real estate perspective.
5- Radiation losses are not included in the solar field and other power plant components.
6- A variant load power plant is not involved (part load calculation) because it does not coincide with one of the objectives of this research. Power plant capacity will be fixed throughout its annual operation.
7- Olive pomace is the main fuel to drive the power plant. Solar hybridization is to exploit the abundance of solar radiation to reduce the required amounts of olive pomace.
8- Control system is provided conceptually. No advanced control is applied.
9- A hybrid power plant is designed conceptually (a framework). Developed design with details is out of scope.
10- Kinetic and Potential energy in thermodynamic analysis for power block is neglected.

6.5 Estimated Power Plant Capacity

As a first step, it is essential to estimate the hybrid power plant capacity. To take this as a cornerstone to the following modeling and simulation processes. It starts from the facts related to the olive pomace and solar radiation in Palestine, added to the selected land location and size.

Regarding the olive pomace. The average Net Calorific Value NCV of olive pomace can be estimated from the average Gross Calorific Value GCV of it as measured in the laboratory. Considering the composition of olive pomace, NCV on a dry basis of dry samples according to the following formula (Tawarah and Rababah, 2013):

$$NCV = GCV - ((2442)\left(\frac{\%H}{100}\right)(9.01) + (92.7)(\%S) + (42.6)(\%N)) \tag{6.1}$$

$NCV = 15.7\ MJ/kg$ (estimated value from olive pomace composition)

Rankine cycle efficiency (η_{th}) can be roughly considered around 30%, So:

$$\text{The Power Plant Capaciy} = \text{Total Heat Input} * \text{Power Plant Efficiency} \tag{6.2}$$

And:

$$\text{Total Heat Input} = \text{Heat from Olive Pomace} + \text{Heat from CSP} \tag{6.3}$$

The Q symbol it will be used for any energy gained or transferred per second.

$$\text{The Overall Thermal Input} = Q_{in,Olive\ Pomace} + Q_{in,CSP} \tag{6.4}$$

$$\text{The Estimated Capacity of The Power Plant} = \left(Q_{in,Olive\ Pomace} + Q_{in.CSP}\right) * \eta_{th} \tag{6.5}$$

$$The\ Annual\ Estimated\ Thermal\ Input\ from\ Olive\ Pomace = Average\ Amount\ Olive\ Pomace * NCV\ of\ Olive\ Pomace \quad (6.6)$$

The average annual generated amount of olive pomace is 40,000 tons. So:

$$The\ Estimated\ Thermal\ input\ from\ olive\ pomace\ yearly = 40\ X\ 10^6\ (kg) X\ 15.7\ \left(\frac{MJ}{kg}\right) = 628 * 10^6$$

Then, the total heat input from olive pomace could be calculated as:

$$Q_{in,Olive\ pomace} = \frac{(628\ X\ 10^6\ (MJ/year)}{(8760\ X\ 3600)}$$

$$Q_{in,Olive\ pomace} = 19.9\ MW$$

For solar field thermal input, the average annual optical efficiency of Parabolic Trough PT collector around 60% and 40% for Linear Fresnel LF (Kincaid et al., 2018), the annual DNI in the selected site is 2198 kWh/m², the annual hours of available DNI about 4000 hours (SolarGIS, 2020), the net area for PT solar field is 9810 m² and the net area of LF solar field is 17296 m², considering a 30 dunums used for installing solar field:

$$The\ Thermal\ Input\ Estimated\ from\ a\ PT\ Solar\ Field = \frac{(\sum DNI\ \left(\frac{kwh}{m^2}\right)\ Yearly * Average\ Optical\ Efficiency * Net\ Area\ of\ solar\ collector(m^2)}{(\sum Hours\ of\ DNI\ per\ Year)} \quad (6.7)$$

$$Q_{in,\ PT\ Solar\ Field} = \frac{2198\ \left(\frac{kwh}{m^2.year}\right) X\ 60\%\ X\ 9810\ (m^2)}{(4000)}$$

$$Q_{in,\ PT\ Solar\ Field} = 3.2\ MW$$

$$The\ thermal\ input\ estimated\ from\ LF\ Solar\ Field$$
$$= \frac{(\sum DNI\left(\frac{kwh}{m^2}\right)\ Yearly * Average\ Optical\ Efficiency * Net\ Area\ of\ Solar\ Collector(m^2)}{(\sum Hours\ of\ DNI\ per\ Year)} \quad (6.8)$$

$$Q_{in\ ,LF\ Solar\ Field} = \frac{2198\ \left(\frac{kwh}{m^2.year}\right) X\ 40\%\ X\ 17296\ (m^2)}{(4000)}$$

$$Q_{in\ ,LF\ Solar\ Field} = 3.8\ MW$$

The Estimated Output Capacity of Hybrid Power Plant Based on PT Solar Field $=$ $\left(Q_{in,Olive\ Pomace} * 30\%\right) + (Q_{in,\ PT\ Solar\ Field} * 30\%)$

The Estimated Output Capacity of Hybrid Power Plant Based on PT Solar Field $=$ $(19.9\ \text{MW} * 30\%) + (3.2\ \text{MW} * 30\%)$

The Estimated Output Capacity of Hybrid Power Plant Based on PT Solar Field $=$ $(5.97\ \text{MW}) + (0.96\ \text{MW})$

The Estimated output capacity of hybrid power plant based on PT solar field $=$ **6.93 *MW***

The Estimated Output Capacity of Hybrid Power Plant Based on PT Solar Field $=$ $\left(Q_{in,Olive\ Pomace} * 30\%\right) + (Q_{in,\ LF\ Solar\ Field} * 30\%)$

The Estimated Output Capacity of Hybrid Power Plant Based on PT Solar Field $=$ $(19.9\ \text{MW} * 30\%) + (3.8\ \text{MW} * 30\%)$

The Estimated Output Capacity of Hybrid Power Plant Based on PT Solar Field $=$ $(5.97\ \text{MW}) + (1.14\ \text{MW})$

The Estimated Output Capacity of Hybrid Power Plant Based on PT Solar Field $=$ **7.11 *MW***

This estimation based on the Rankine cycle efficiency of 30% not involves any thermal losses from the solar field and does not include the net efficiency of the power plant and its variation, combustion efficiency of 100%. The three capacities will be chosen to study the hybrid power plant around the estimated capacities for PT and LF, the three selected capacities are 6 MW, 7 MW, and 8 MW.

6.6 Hybrid Power Plant Modeling

After drawing the main outlines of the power plant criteria, Now, the hybrid power plant model can be introduced based on the estimated capacity from the annual available olive pomace quantities, the amounts of DNI, and the considered land area required to erect the solar field and the rest of the plant facilities and equipment.

6.6.1 Power Block Modeling

The main parameters of the Rankine power block are live steam pressure, live steam temperature, and condensing pressure. Accordingly, the turbine used in the cycle should be able to generate the required capacity -namely 6 to 8 MW- at the selected values of live steam state and condensing state. It is worthy to mention that the plant will consider both reheat and regenerative heating to obtain an improved efficiency.

The steam power plant design needs the following: determination of the live steam temperature and pressure that enters the steam turbine and the condenser pressure and all other variables in the power plant are determined related to these 3 variables that must be chosen to create high thermal efficiency, and any improvements to the efficiency after that is based on the concepts that mentioned in Chapter 3 by utilizing regeneration and reheat process, it’s worth noting that the mass flow rate of the steam that enters the turbine determines the capacity of the power plant.

From a thermodynamic perspective, it is better to increase the live steam temperature as much as could be achieved to increase the theoretical Carnot efficiency of the plant, thus the actual cycle efficiency is increased. But on the other hand, increasing the live steam temperature increases the boiler and turbine costs since high-temperature-resistant materials should be considered in manufacturing. However, an optimized choice is to refer to the turbine manufacturer to obtain sufficient info about the turbines, so that a proper

choice is made. Referring to technical data published by the power industry manufacturer Siemens, it provides turbines with capacities up to 45 MW that operates on live steam up to 550 ºC (Siemens, 2021). So, to proceed in the modeling process of the power block and establish the components design parameters, live steam temperature will be selected to be 550 ºC, live steam pressure to be 60 bar at such selected power capacity for best technical and economic considerations (Servert and San Miguel, 2011). And condensing pressure 0.25 bar, as it is providing a safe threshold for obtaining acceptable efficiency for the model without compromising the turbine health with any moisture generation.

The modeling process is done using EBSILON. Each component of the hybrid plant will be introduced and all its parameters will be adjusted within EBSILON. In such a way that all power plant components are compatible with each other and instance simulation results in zero errors.

- Steam Generator:

The steam generator selected for the model is considered with reheat. The steam generator pressure is considered at the live steam pressure selected for the power plant which is 60 bar. And live steam temperature of 550ºC.

In EBSILON, the steam generator is inserted as two separate components: The boiler and the combustion chamber. The boiler heat exchanger is connected with the combustion chamber with a logic line that transfers the produced heat from the combustion chamber as an input to the boiler heat exchanger. Figure 6.5 depicts the boiler module in EBSILON.

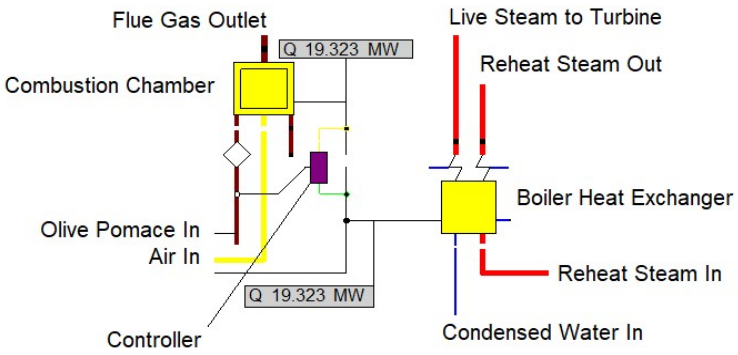

Figure 6.5: Complete Boiler Model with Mass Feed Controller.

In the boiler model, a controller is inserted to control the feeding of olive pomace into the combustion chamber, so that the boiler produces live steam at the setpoint temperature. Boiler adds the heat input from the combustion chamber into the working fluid according to the following formula:

$$Q_{Boiler} = M_{Live} * \left(H_{live,out} - H_{water,in}\right) + M_{Reheat} * \left(H_{Rehea\ ,out} - H_{Reheat,in}\right) \quad (6.9)$$

Where Q_{Boiler} is the same provided from the combustion chamber. Radiation losses from the boiler are neglected. In EBSILON Q symbol is used for any energy gained or transferred per second. Also M_{Live} is the mass flow rate of live steam, M_{Reheat} is the mass flow rate of steam that enters the reheat line, $H_{live,out}$ is the enthalpy at the live steam outlet line in the boiler, $H_{live,in}$ is the enthalpy at the live steam inlet line in the boiler, $H_{Reheat,out}$ is the enthalpy at the reheat steam outlet line in the boiler, $H_{Reheat,in}$ is the enthalpy at the reheat steam inlet line in the boiler.

In the combustion chamber module, the combustion parameters regarding the olive pomace are inserted. When using olive pomace as a fuel, the excess air ratio should be according to studies carried out on olive pomace is 1.35 (λ=1.35) that performs best combustion efficiency about 98% (Topal et al., 2003). Olive pomace composition is inserted into the model for proper combustion calculations. Flue gas temperature is adjusted to 200 ºC (Atimtay and Varol, 2009, Power, 2019). The heating value in the model is inserted according to the average GCV of tested samples in the laboratory 17.095 MJ/kg. Combustion chamber energy balance formula:

$$M_{air.in}H_{air} + M_{Fuel.in}H_{Fuel} + M_{Fuel.in}\ NCV = Q_{Boiler} + M_{fluegas}\ H_{fluegas} + M_{As}\ \ H_{As} \quad (6.10)$$

Where M symbol is used for the mass flow rate, H symbol is used for the enthalpy.

- Steam Turbine

The turbine is divided into high pressure and low-pressure turbine. Including both reheat and steam bleed lines regenerative process to improve efficiency. Figure 6.6 represents the turbine assembly in this study power block model.

In EBSILON any extraction (bleed or reheat) is implemented using multiple turbine components through the expansion process of steam before entering the condenser. Also in each stage, both reheat and a bleed pressure equal to the stage output pressure which is determined according to the design requirements in EBSILON using the general input value component.

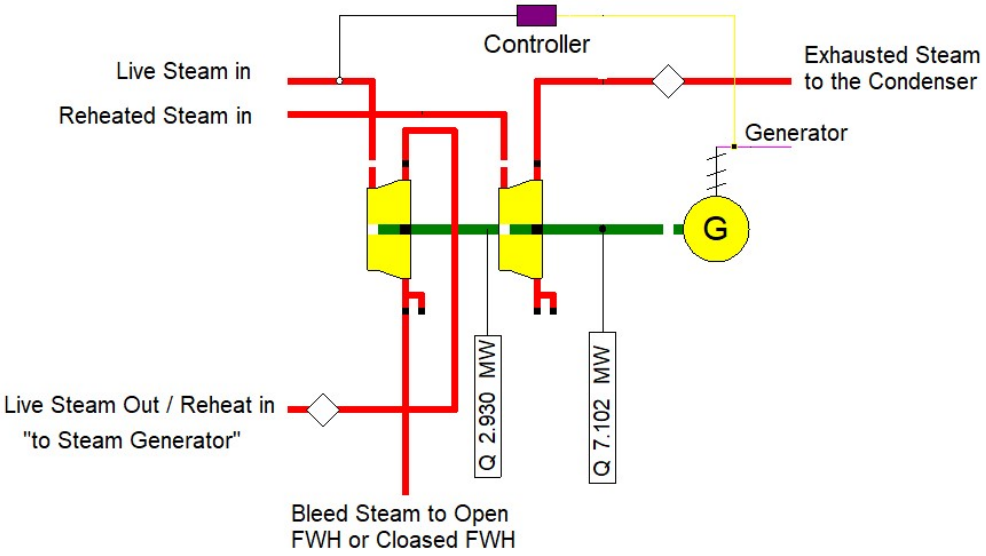

Figure 6.6: Multistage Turbine Model in EBSILON.

The energy generated on shaft per second (shaft power) $Q_{Turbine-shaf\ \ (ideal)}$ is calculated for an ideal turbine of isentropic efficiency of 100% as:

$$Q_{Turbne-shaft\ (ideal)} = M_1\ (H_1 - H_2)\ \eta_{mech} \tag{6.11}$$

Where M_1 inlet mass flow rate, H_1 is the enthalpy at the inlet, and H_2 is the enthalpy at the outlet in case of isentropic efficiency of 100%, and η_{mech} is the mechanical shaft efficiency.

By using the isentropic efficiency η_{is} the energy generated on shaft per second $Q_{Turbine-shaft}$ will be:

$$Q_{Turbine-shaft} = Q_{Turbine-shaf\ (ideal)} * \eta_{is} \tag{6.12}$$

The effect of isentropic efficiency appears on the value of enthalpy at the turbine outlet, the enthalpy of the outlet is higher than H_2 that mentioned in equation (6.11) for the ideal case. The isentropic efficiency η_{is} of 90% (Jingzhi, 2014) is the default isentropic efficiency that will be used for steam turbines.

- Pumps and Compressors

For all fans, pumps, and compressors, the isentropic efficiency is given as 85% for turbo machinery and motor parts. So that the overall efficiency η_{all} is around 70%. Their contribution to the power block is minor generally.

Power input to drive a fan, pump or compressor is given by:

$$Q = M\ (\Delta H)/\eta_{all} \tag{6.13}$$

Where:

- Q: Electrical power input
- M: Fluid mass flowrate
- ΔH: The change of the enthalpy between the inlet and the outlet
- η_{all}: The overall efficiency of the equipment.

Overall efficiency η_{all}=

Isentropic efficiency η_{is} * Mechanical Shaft Efficiency η_{mech} * Motor Efficiency η_{motor}

(6.14)

Shaft mechanical efficiency is considered 99.8%. figure 6.7 represents fans and compressors as displayed in EBSIOLN.

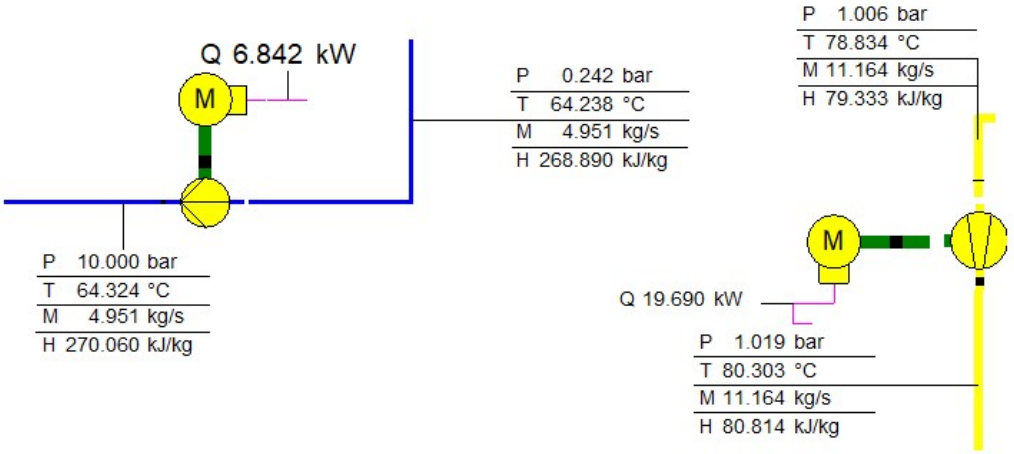

Figure 6.7: Pump and Compressors Components in EBSILON

- Air Cooled Condenser

The condenser in the proposed power block is selected as an air-cooled condenser. Since in Palestine the surface water is almost absent. Generally, the use of water for cooling the plant condenser either by water cooling or even using water as makeup for cooling tower, both are not applicable due to the scarcity of water resources. So, the selected condenser for the proposed plan in this study is the air-cooled condenser.

The air-cooled condenser is composed of A-shaped heat exchange bays, steam flows from the top and condenses down while air is flowing through the aluminum finned copper heat coil. Figure 6.8 depicts the air-cooled component in the proposed power block model.

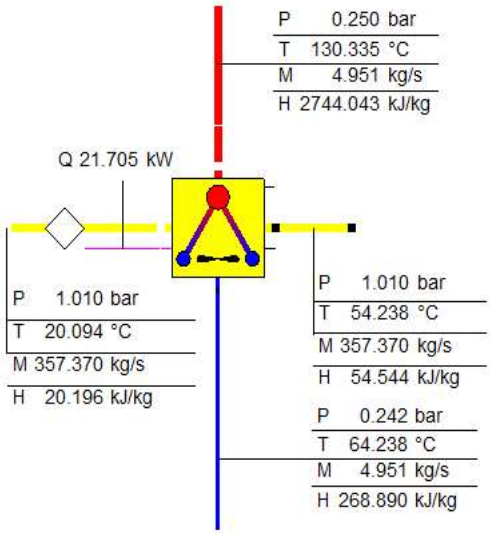

Figure 6.8: Air Cooled Condenser Component in EBSILON

In this component. Either the number of bays must be inserted and the specifications must be adjusted, this method is adopted when all the criteria of the bays are provided via a vendor, or to give the boundary conditions (inlet and outlet specs of the working fluid and ambient air inlet) and EBSILON will be used to provided standard specifications of the air-cooled condenser according to ASME PTC 30.1-2007 'Air-cooled Steam Condensers' and VGB-R 131 Me 'Acceptance Test Measurements and Operation Monitoring of Air-Cooled Condensers under Vacuum' (ASME, 2007).

Since airflow through the condenser is managed via forced axial fans, which are usually speed controlled to maintain the required heat rejection rate against variant ambient parameters. To calculate the shaft power of the fan and subsequently the electrical motor power, air-side pressure drop must be known. Efficiencies of the fan and electrical motors are provided. table 6.1 specifies the parameters per bay as ASME standard for the air-cooled condenser.

Table 6.1: Air-cooled condenser single-bay specification according to ASME

Specification	Value	Unit
Nominal Active Area per Bay	1065.96	M^2
Nominal Air Flow per bay	35.74	kg/s
Nominal pressure drops through air side	50	Pa
Min Allowable Overall Heat transfer coefficient (U)	50	$W/m^2 K$
Electric Motor Nominal Efficiency	98	%
Fan Overall Nominal Efficiency	70	%

- Deaerator (Open Feed Water Heater FWH)

Deaerator is an open feed water heater collecting the bleed steam from turbines and the condensate from the air-cooled condenser. Regenerating energy within the power block. Figure 6.10 shows the deaerator component in the proposed power block.

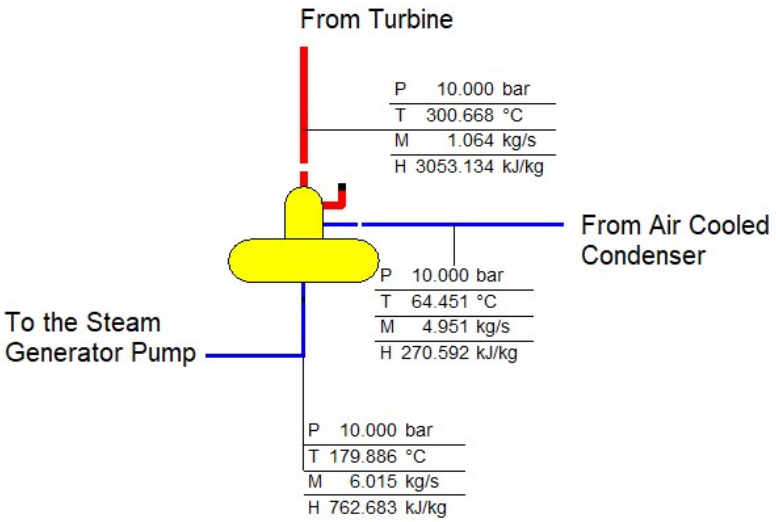

Figure 6.9: Deaerator Component as Displayed in EBSILON

This component simply complies with the mass and energy balance to calculate the outlet state of the working fluid. The exit deaerator ensures the complete mixing and the homogeneity of the leaving working fluid.

6.6.2 Proposed Power Blocks

Using EBSILON, four power block models were developed using all the mentioned criteria and restrictions. Each of the power blocks was tuned to maximize its thermal efficiency to the maximum so that it can be reliable in further assessment calculations. Each model is utilizing reheat. The first two models (Model I and Model II) utilize regeneration via open FWH only at different steam bleed pressures, the other two models (Model III and Model IV) utilize regeneration via closed and open feed water heaters at different steam bleed pressures.

Model I

This model configuration defines the reheat and bleed pressures at the same value (11 Bar). Bleed and reheat steam pressure was changed through the available range so that maximum efficiency is achieved. Figure 6.10 represents the model configuration.

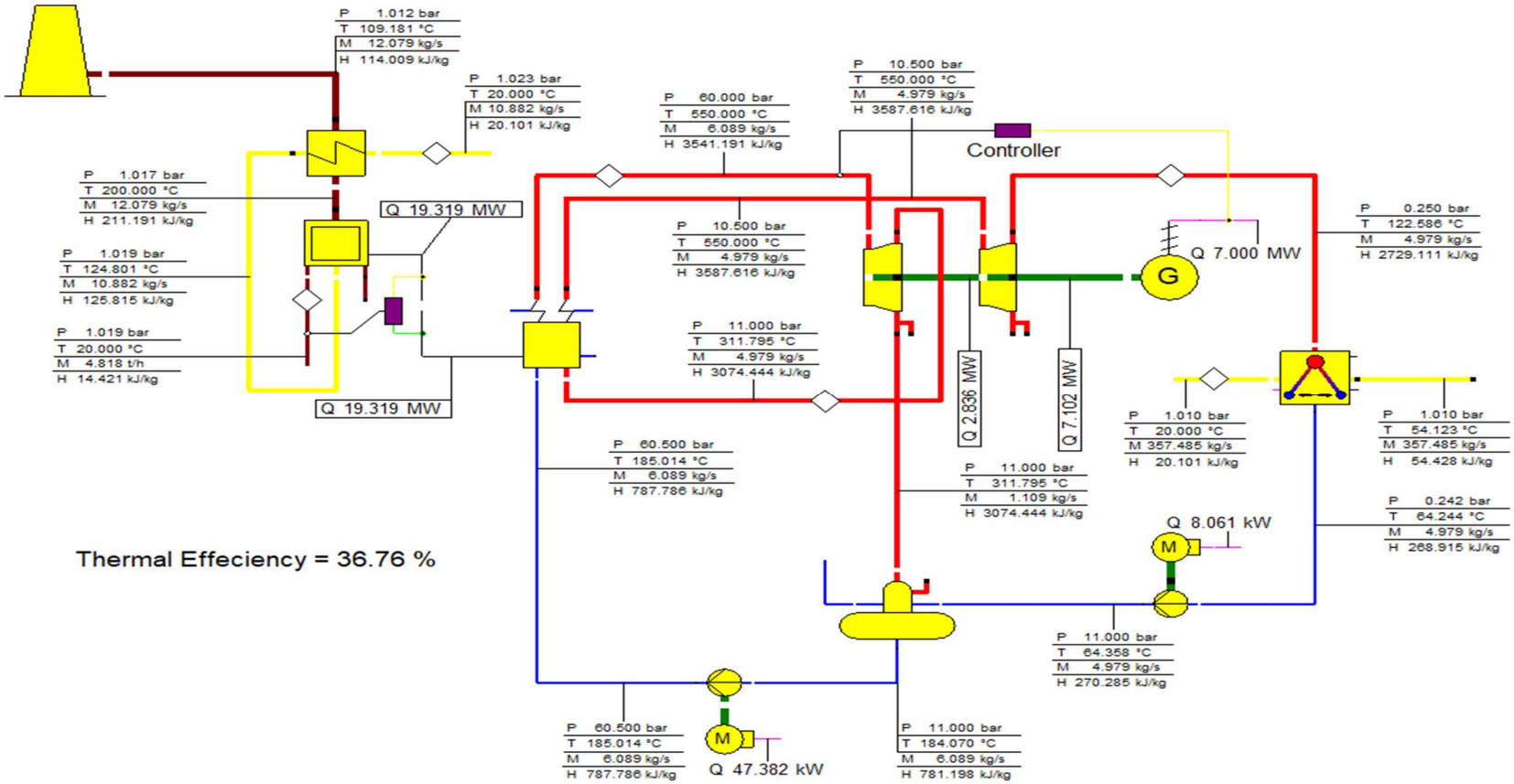

Figure 6.10: Power Block Model I Configuration in EBSIOLN

Model II

This model configuration defines the reheat and bleed pressures at different values. Bleed steam pressure was changed through the available range so that maximum efficiency is achieved. Figure 6.11 represents the model configuration.

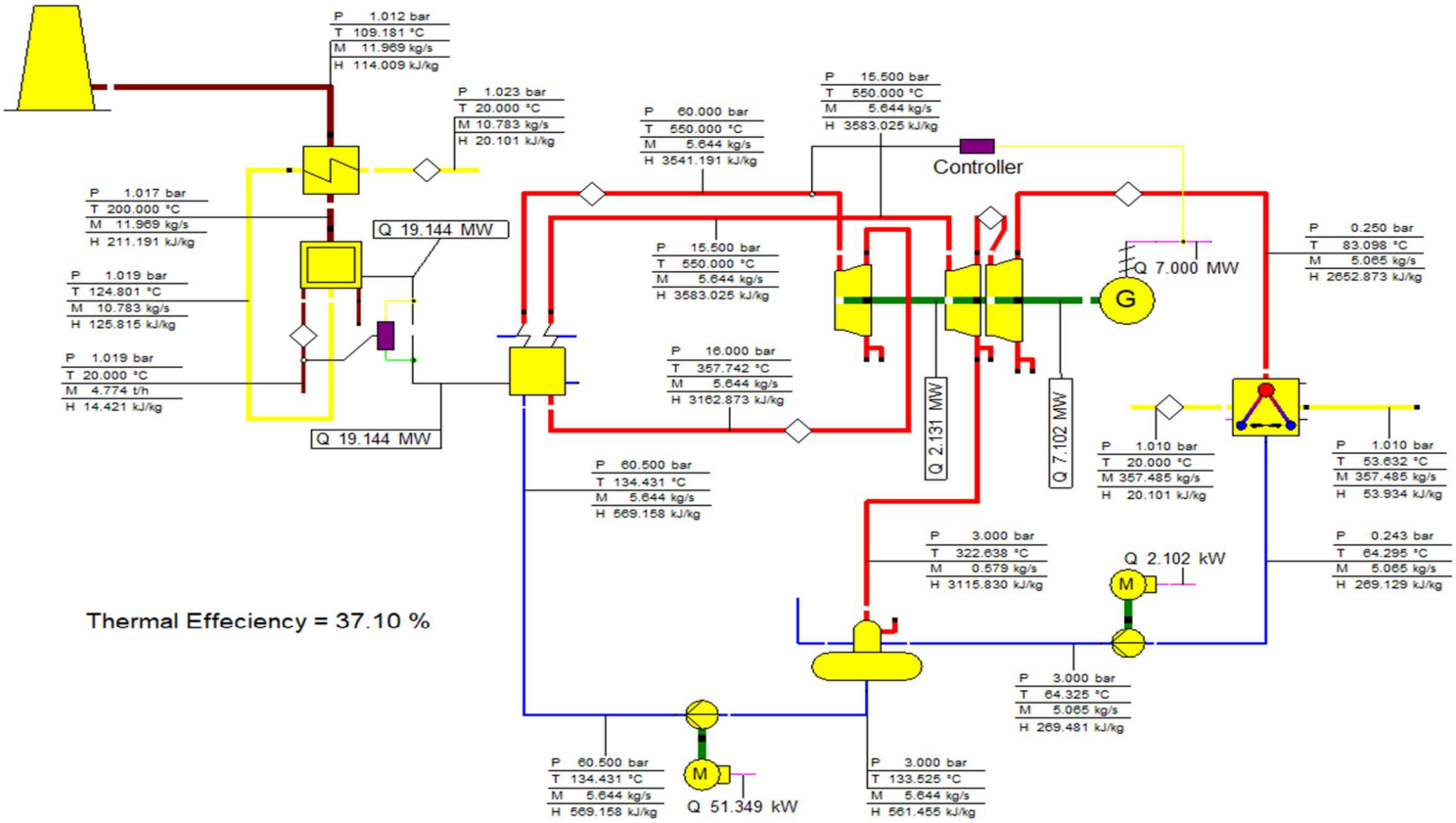

Figure 6.11: Power Block Model II Configuration in EBSIOLN

Model III

This model configuration utilizes both closed and open FWHs. And defines the reheat and bleed pressures at different values. Both reheat and bleed steam pressures were changed through the available range so that maximum efficiency is achieved. Figure 6.12 represents the model configuration.

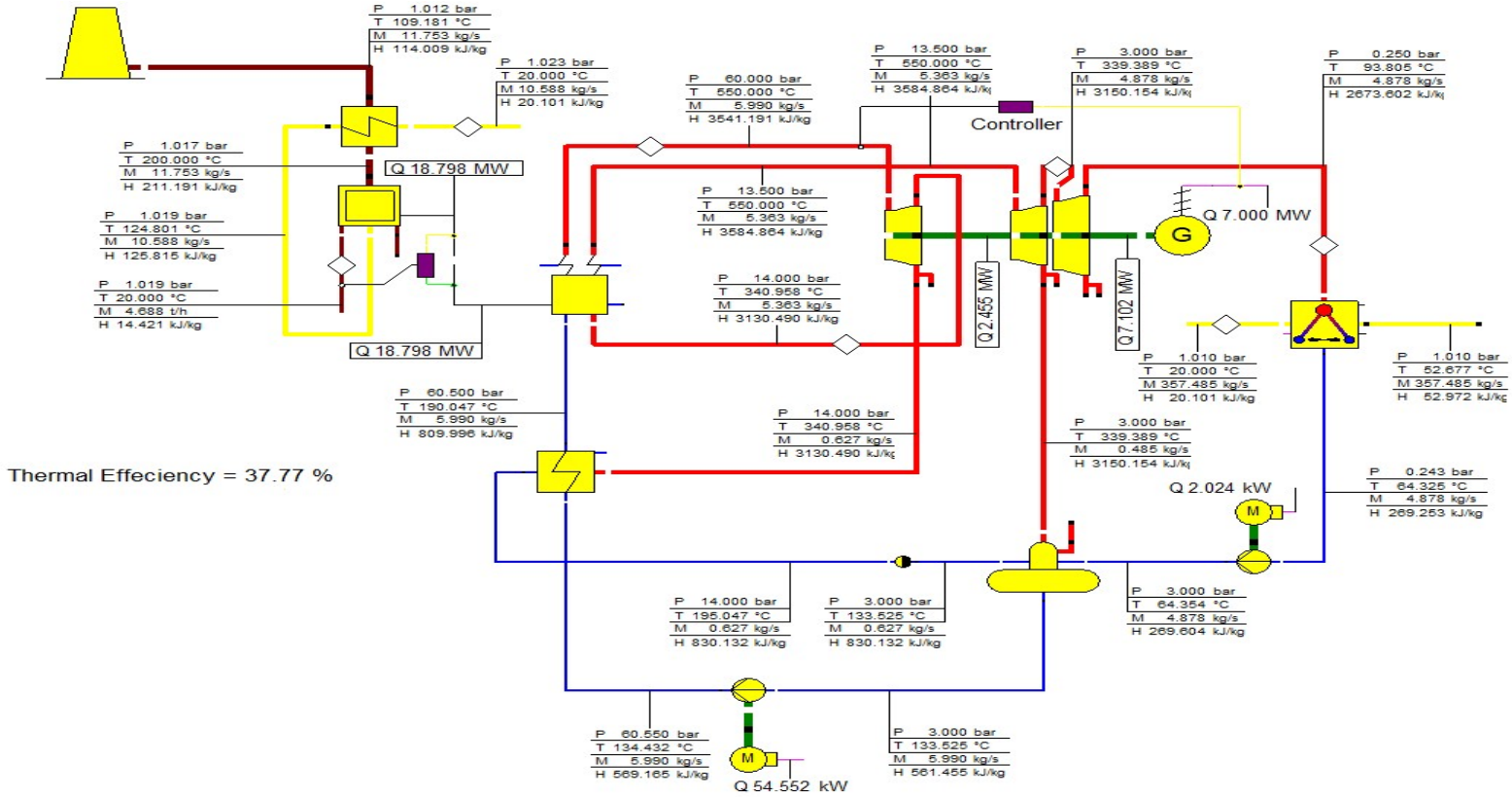

Figure 6.12: Power Block Model III Configuration in EBSIOLN

Model IV

This model resembles model III but with alteration of the closed FWH location. Figure 6.13 represents the model configuration.

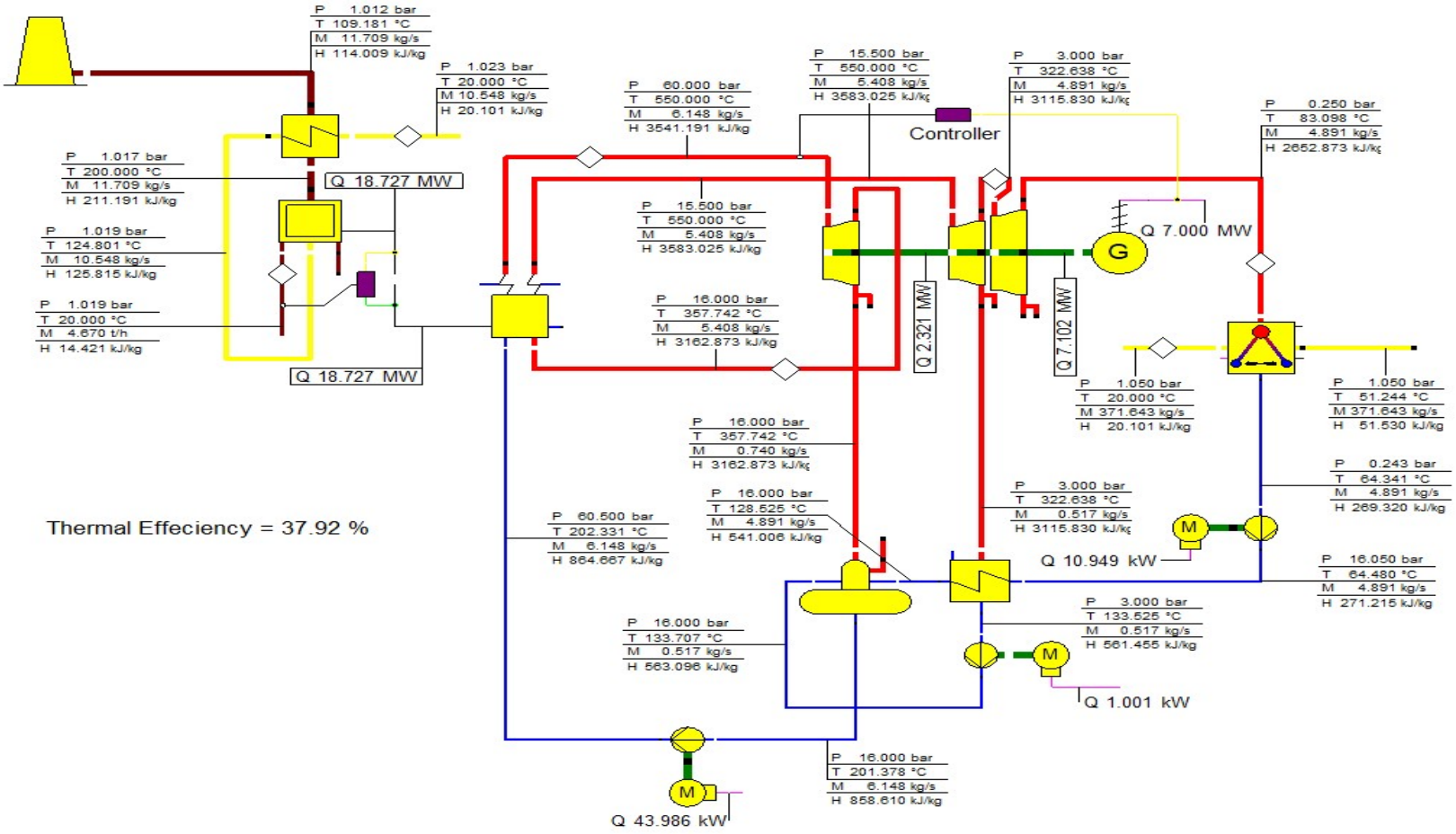

Figure 6.13: Power block model I configuration in EBSIOLN

Summary of Power Blocks and Selection

After building these different models for the power block component, and optimizing their working parameters to achieve the best available thermal efficiency, it is vital at this point to adopt a configuration to hybridize it with a CSP source. Table 6.2 represents the efficiencies of these different proposed power blocks.

Table 6.2: Summary of power blocks main specs

Power Block No.	Thermal Efficiency %	Using of Reheat	Utilizing Open FWH	Utilizing Closed FWH
Power Block I	36.75	Yes	Yes	No
Power Block II	37.10	Yes	Yes	No
Power Block III	37.70	Yes	Yes	Yes
Power Block IV	37.92	Yes	Yes	Yes

As it is shown in Table 6.2. the more regenerative utilized more improvement in the efficiency is obtained. The difference between the lowest power block and the highest power block model is 1.17%. Taking into consideration that the overall estimated capacity is quite small, there is no serious need to increase the efficiency by adding expensive components such as closed FWH since it will pay back in long times and often needs high-cost large tube bundles. In this study, model I will be chosen to proceed for the following reasons:

- Acceptable thermal efficiency
- Lowest in erection costs (Whitfoot, 2018)
- Simplest in configuration.

6.6.3 Solar Field Modeling

Solar field modeling in this study is based on a candidate selected location in Jericho that fulfills the major criteria of plenty of sunshine and the flat terrain. As mentioned before, Palestine features mountainous terrains and has no extended flat areas in most districts. The solar field will be considered on a rectangular area of 30,000 m^2 (200m*150m) for this study purposes. Thus, the simulation can provide a closer estimation that is viable in real circumstances for application purposes.

The solar field will be built using linear Fresnel reflector and parabolic trough technologies. Generating two different solar field models based on each technology. each model will be later hybridized with the selected power block. Resulting in two-hybrid power plant models that will be used for simulation and generating results.

The design of the solar field will be built based on the maximum average DNI, which occurs on 10th June of the year based on the recorded data (SolarGIS, 2020) for the selected site to evaluate the max thermal power that can yield from the solar field. Also, to choose the best hybridization method with the biomass-powered power block.

It is worthy to mention that thermal storage is not considered in this solar field, since the energy storage concept is for overcoming the fluctuation in radiation availability and extending the power block service time. These reasons don't exist in the case of this study since the biomass is available and stacked for the continuous operation of the plant regardless of the sun availability, and the power block is assumed to run 24 hours 7 days a week, so no need to consider the thermal storage option in the design of the solar field.

Solar Angles and Optical Efficiency Modifiers

Solar line focusing reflectors tracks the sun on just one axis. Either parabolic troughs or linear fresnel reflectors, both track the sun from sunshine to sunset by rotating the reflecting mirrors around their longitudinal axis. However, not all of the DNI is captured in any single-axis solar tracking system. So, modifiers should be applied to the collector's standard optical efficiency (which is the gained heat divided by the incident solar power) to determine the generated solar power at any time of the day. To do this, some solar angles should be introduced. Figure 6.15 represents a schematic depicting solar angles for a solar reflector, and Table 6.3 identifies and explains each angle.

Regarding the collector azimuth orientation, line focusing reflectors are either installed considering their longitudinal axis (receiver axis) east to west or north to south. When installed in North-South orientation, there will be shading losses in the morning and evening times due to the shading of reflectors on each other. When they are installed in East-West orientation, there will be spillage of sun beams out of the receiver location. However, in this study, the orientation is taken to be North-South orientation.

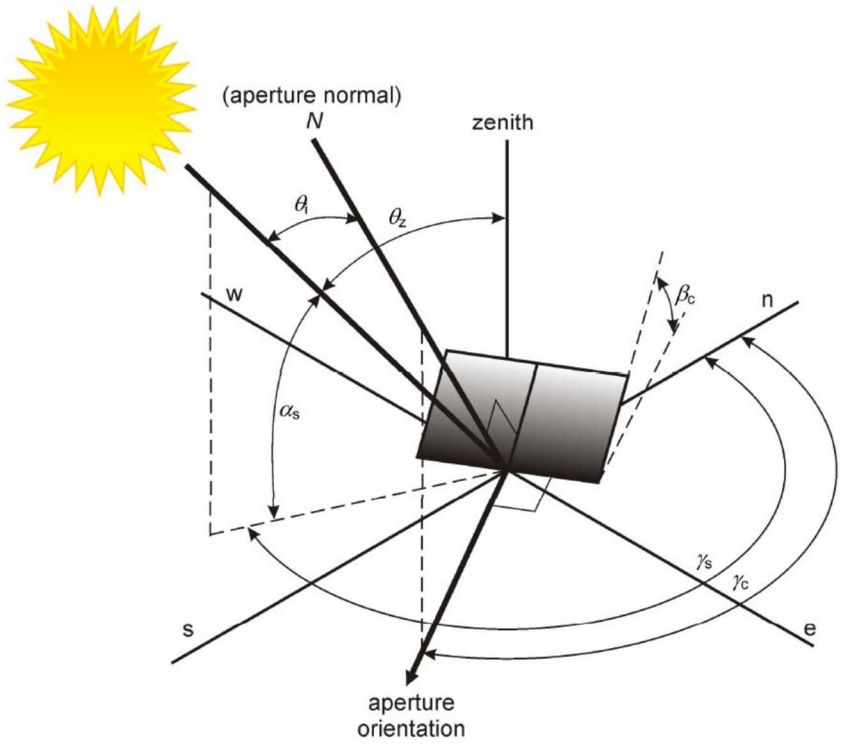

Figure 6.14: Solar angles for a solar reflector

Table 6.3: Solar angles for a solar reflector.

Solar Azimuth	γ_s	The angle between the North and the solar position projected on the horizontal plane
Solar Elevation	α_s	Vertical angle between straight line to the sun and horizontal plane
Zenith Angle	θ_z	The Angle between the sun beam and the zenith
Collector Azimuth	γ_c	The angle between North and aperture orientation
Collector Axis Tilt	β_c	The inclination of the collector surface from the horizontal plane
Incident Angle	θ_i	The angle between the normal to the projected aperture area and the sun beam. In EBSILON it is introduced as RPHIIINC

The standard optical efficiency of a solar collector is taken under the following circumstances:

- The mirrors are ideally clean
- The mirrors are free of shade
- Incident angle equals zero

For a parabolic trough collector. Figure 6.15 depicts the sun and collector angles related to its thermal performance. The Incident Angle Modifier IAM is simply the component of the sun beam in the direction of the normal to the aperture area. So, at any time of the day,

the sun path should be identified. Then, considering the angles of the collector, this modifier could be calculated.

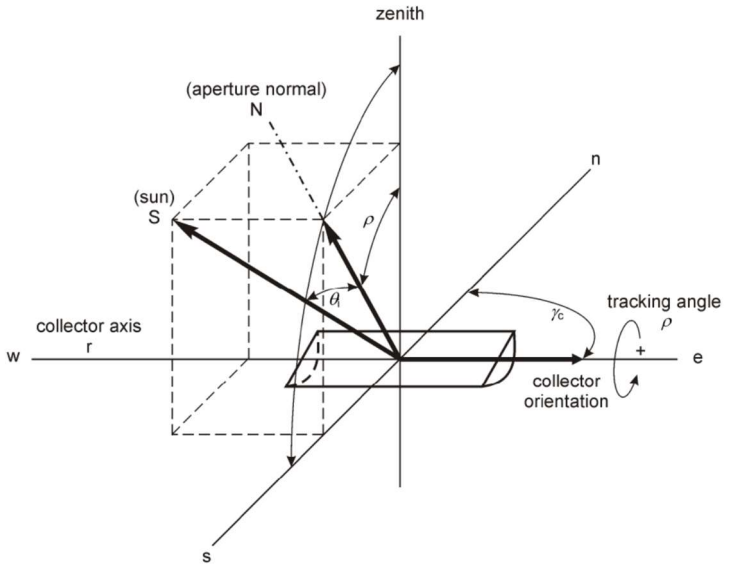

Figure 6.15: Line focusing collector's angles

For the LFR, the IAM is calculated taking into consideration the sun location, the transversal angle, and the longitudinal angle. Figure 6.45 shows the solar angles related to the LFR. The components of the sun beam should be analyzed against both angles to calculate the IAM of the LFR.

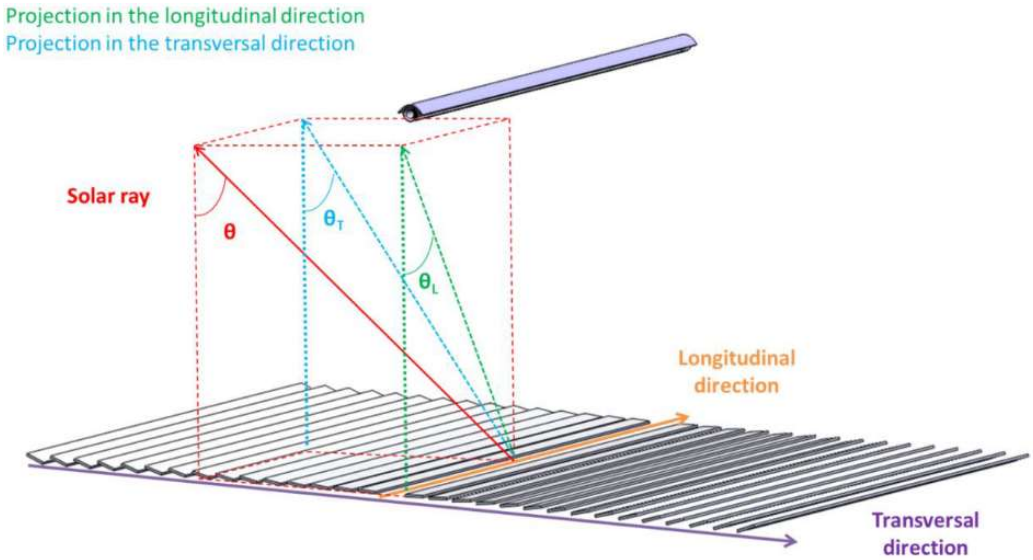

Figure 6.16: LFR solar angles. Incident, transversal, and lonigitudinal angles. In EBSILON, the transversal angle is introduced as RPHIITRAN

All of these parameters that affect the performance of the selected LFR and PT have been taken into consideration. In EBSILON, the sun component formulates the sun path every time in the year through the whole simulation process. Identifying continuously the sun angles, besides it counts for the ambient temperature, which is also a parameter that is needed to calculate the heat loss from solar collectors. At the same time, the solar reflector components also take the required data about the sun location and the ambient temperature from the sun component simultaneously.

Linear Fresnel Solar Field

The selected LFR model for linear fresnel solar field is manufactured by Industrial Solar Gmbh (Formerly MIRROXX) model LF-11 (IndustrialSolar, 2020a). All the data involved has been considered when building the solar field components in EBSILON. Figure 6.315 represents a schematic and dimensions of the collector.

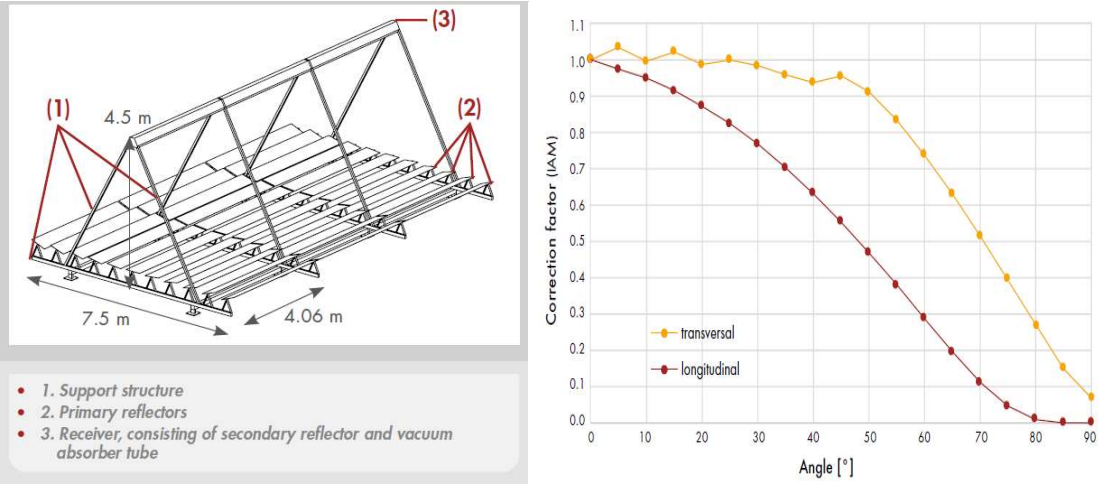

Figure 6.17: LF-11 Linear Fresnel reflector and IAM data, By Industrial Solar (IndustrialSolar, 2020a)

Table 6.4: General Specification of LFR LF-11 module

Module width	7.5 m
Module length	4.06 m
Gross area of Module	30.45 m²
Height of absorber above mirrors (Focal length)	4.5 m
Maximum operational wind speed	100 km/hour (27.8 m/s)
Absorber inner diameter	6.56 cm
Peak optical efficiency (for Sun in Zenith)	0.686
Aperture surface Area of module	23 m²

LFR component in EBSILON is defined using the parameters extracted from the technical data sheet provided by the manufacturer. And taking into consideration all the modifiers and heat loss components. The LFR component is linked to the Sun component in EBSILON so that it takes all its ambient and solar inputs accordingly. Figure 6.19 represents the LFR and Sun components in EBSILON.

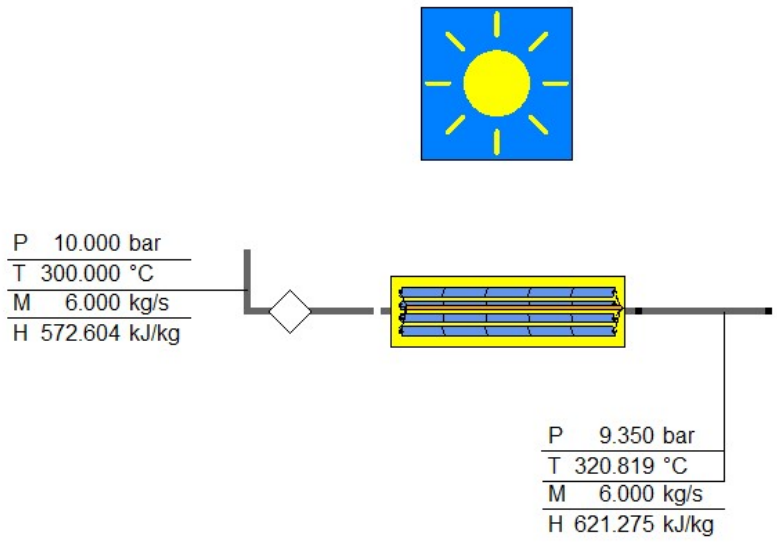

Figure 6.18: Linear Fresnel Collector and Sun Component as in EBSILON

The array design of the linear fresnel should comply with the manufacturer's instructions (IndustrialSolar, 2020b). Accordingly, the parameters were set in EBSILON. Row spacing in the linear fresnel must be 3 meters at least between two parallel zero-spaced LFR strings. The maximum number of LFR modules in series is 80 modules. By applying these instructions. The field is composed of 16 sets of series-linked collectors of LFRs and with 47 LFR modules in series with a total length of 190.82 m. Figure 6.24 shows the design of the LFR solar field in the considered 200m*150m flat land.

The pressure drops along with the solar absorber 0.5 bar for 150 m length on the internal diameter of 6.5 cm inner diameter, the length of each collector is 190.82 m (47 m X 4.06 m), and the pressure drop along each collector 0.65 bar. Table 6.5 illustrates the design data about the solar field. Table 6.5 shows the solar field design data for LFR

Table 6.5: Solar Field Design Data of LFR

Collector length	190.82 m
Number of modules in series of each collector	47 modules
Number of parallel collectors in the solar field	16 collectors
Collector gross width	7.5 m
Collector aperture net width	5.665 m
Net Area of each collector	1,081 m²
Net area of the solar field	17,296 m²
Pressure drops in each collector	0.65 bar
Orientation	North-South
Mirror cleanliness	100%
Incident angle Modifier (IAM) (correction factor)	As detailed in Figure 6.17
HTF	Therminol VP-1

For energy balance between the DNI and the thermal energy gained by the HTF the following equation is used for each collector

The thermal energy input into the HTF (QEFF) is given by:

$$\mathrm{QEFF} = M_{HTF} X\ (H2 - H1) \tag{6.15}$$

Where M_{HTF} is the mass flow rate in kg/s of the HTF inside the collector, and H1, and H2 is the enthalpy of HTF at the inlet and the enthalpy of HTF at the collector outlet respectively in kJ/kg.

QEFF is a function of solar thermal input QSOLAR and the thermal losses QLOSS along with each collector:

$$\mathrm{QEFF} = \mathrm{QSOLAR} - \mathrm{QLOSS} \tag{6.16}$$

$$\mathrm{QSOLAR} = \mathrm{DNI\ X\ ANET\ X\ FOPT\ 0\ X\ \ IAM\ \ X\ ETASHAD\ X\ ETACLEAN\ X\ ETAENDL} \tag{6.17}$$

Table 6.6: The variables of solar equation

DNI	Direct Normal Irradiance
ANET	Net aperture area of the collector
FOPT 0	Peak optical efficiency (for Sun in Zenith = 0.686 for LF-11)
IAM (KIA factor as used in EBSILON)	Incident angle Modifier correction factor
ETASHAD	Factor to include shading losses
ETACLEAN	Factor to correct for actual mirror cleanliness (considered 100%)
ETAENDL	Factor to correct end loss effects determined from the model

"FOPT 0" represent the collector optical efficiency under the following conditions: incident angle of 0º, clean collector mirrors, without shading and thermal heat losses.

The IAM factor (described in EBSILON in another abbreviation KIA factor) is used for solar radiation incident angle losses. In Linear Fresnel collector IAM is determined from two modifiers factors: longitudinal incident angle modifier and transversal incident angle modifier as the following equation:

$$IAM = IAM\ (RPHIINC)\ X\ IAM\ (RPHITRAN) \tag{6.18}$$

The term $RPHIINC$ is used in EBSILON for incident angle (longitudinal), and the term $RPHITRAN$ is used for transversal angle. From Figure 6.18, incident angle modifier all the correction factors for incident longitudinal angle and transversal angle are adjusted in each collector of the solar field for simulation using the characteristic line tables inside the LFR component as shown in Figure 6.20 and Figure 6.21.

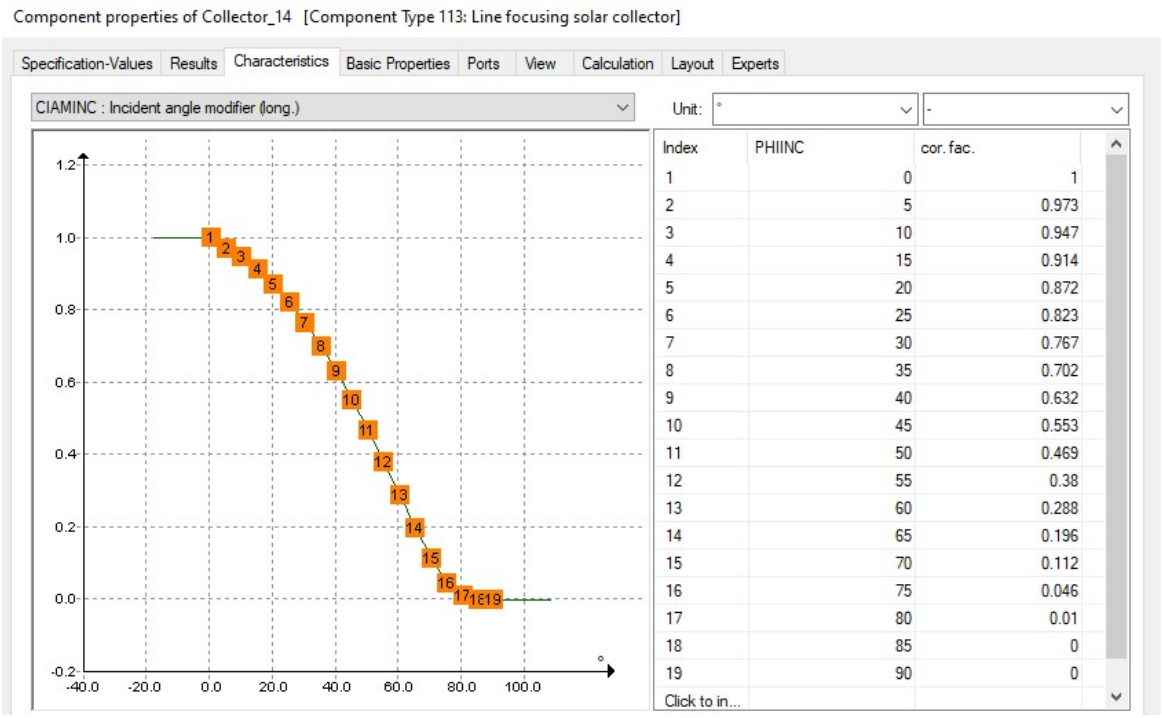

Figure 6.20: Linear Fresnel Collector Incident Angle Modifier Table in EBSILON

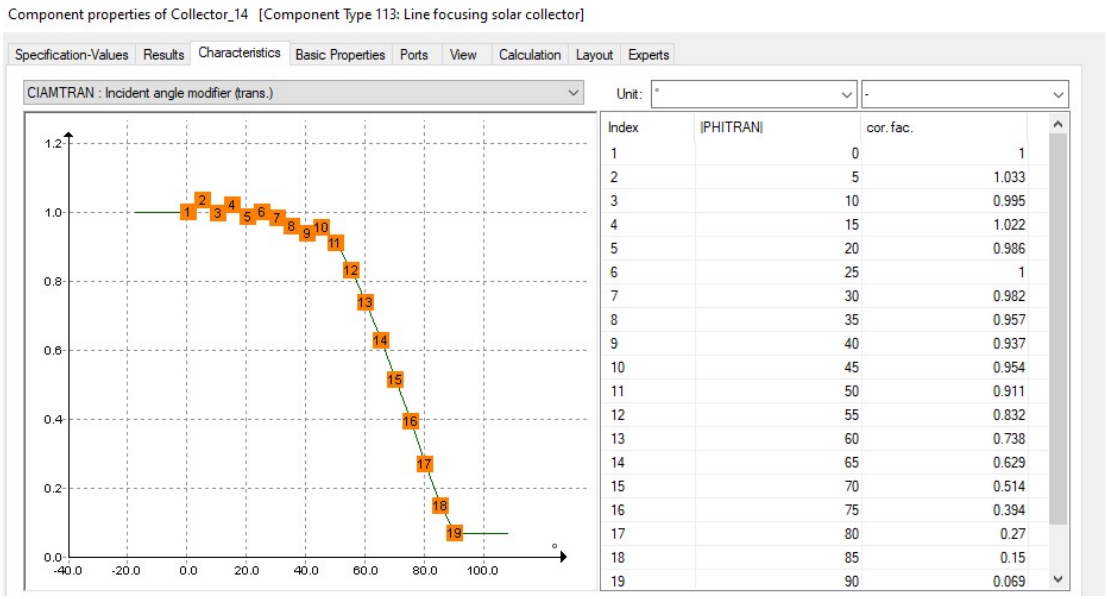

Figure 6.21: Linear Fresnel Collector Incident Angle Modifier (Transversal Angle) Table in EBSILON

ETASHAD effect occurs when the sun is near the horizon, and thus the collectors shade each other. ETASHAD is a function of ROWDIST which is the distance between parallel collectors.

$$ETASHAD = 1 - \min[1, \max\ 0, [1 - \left(\text{ROWDIST X } \frac{Cosine\ (\text{RPHITRAN})}{Gross\ Collector\ Width}\right)]\ ]$$

(6.19)

ETAENDL effect is very small and negligible and not included for Linear Fresnel and for Parabolic Trough

The thermal losses QLOSS of the collector are calculated in EBSILON on the length-specific heat loss q_{LOSS} by:

$$\text{QLOSS} = \ q_{LOSS}\ X\ collector\ length$$

(6.20)

$$q_{LOSS\ (LF-1\ )} = a_1\ (T_{HTF} - T_{amb}) + a_4\ (T_{HTF} - T_{amb})^4$$

(6.21)

$T_{HTF} - T_{amb}$ is the temperature difference between HTF temperature and ambient air temperature (T_{HTF}: HTF temperature, T_{amb} is the absorber ambient temperature), a_1 and a_2 are the thermal losses coefficients, and $q_{LOSS\ (LF-11)}$ is the thermal heat losses for Linear Fresnel LF-11.

This equation is defined in EBSILON software by, to evaluate the thermal losses during the simulation process we need to enter the thermal coefficients for LFR model LF-11

The thermal losses coefficients achieved from the data sheet of LF-11 named as u1 and u4, u1 = 0.032913 in W/ (m² K) and u4 = $1.4838\ X\ 10^{-9}$ W/ (m² K⁴). the formula for thermal losses in EBSILON software is based on collector length and the coefficients u1and u4 is based on the collector net aperture area, we multiply u1 and u4 by net collector width to match between u1 and u4 and EBSILON coefficients a_1 and a_2

$$a_1 = 0.032913\ X\ 5.665 = 0.18645\ \text{W/m K}$$

$$a_2 = 1.4838\ X\ 10^{-9}\ X\ 5.665 = 8.4057\ X\ 10^{-9}\ \text{W/m K}$$

Parabolic Trough Solar Field

The selected PT module for the Parabolic Trough solar field is manufactured by Eurotrough Solar Gmbh model Eurotough 2012 (ET-SCAL). Same as LFR. The PT component is also linked to the Sun component in EBSILON so that it takes all its ambient and solar inputs accordingly. All data was plugged into EBSILLON and manufacturers' instructions were followed in designing the solar field. Figure 65 shows the PT solar field layout. It comprises 12 parallel-connected lines of PTs, each is 150 m in length. Row distances are 17.3 m (3 times the aperture width) (Schenk et al., 2012). Figure 6.22 and Table 6.7 represent Eurotrough PT collector's parameters.

Collector type	SKAL-ET
Aperture width/length	5.8 m/150 m
Net aperture area collector	817.5 m
Number of collectors per loop	4
Focal length	1.71 m
Row distance (center to center)	3 × aperture width = 17.3 m
Peak optical efficiency (related to net aperture area)	78%

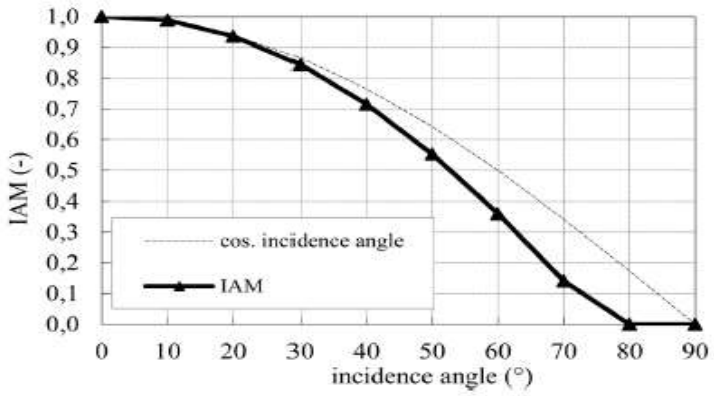

Figure 6.22: Eurotrough PT Collector Parameters

Table 6.7: General Specification of Eurotrough PT

Collector width	5.8 m
Collector length	150 m
Gross area of the collector	870 m²
Height of absorber above mirrors (Focal length)	1.71 m
Absorber inner diameter	6.54cm
Peak optical efficiency (for Sun in Zenith)	0.78
Aperture surface Area of collector	817.5 m²

For Energy analysis of PT all the equation used in LFR is used for the PTC Except the IAM Incident angle Modifier correction and q_{LOSS} equation.

IAM is just a function of incident angle

$$IAM = IAM\ (RPHIINC)$$

(6.22)

IAM correction factor from Figure 6.22 (Datasheet of PT) is defined in PTC in EBSILON through characteristic line in PT component as shown in Figure 6.23.

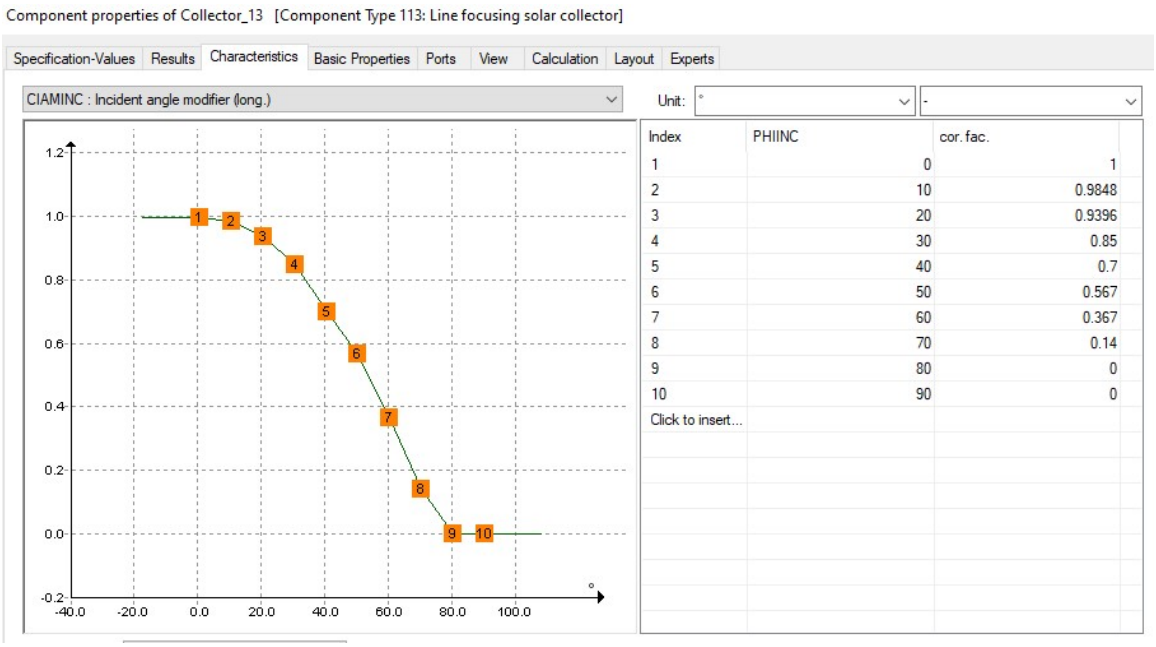

Figure 6.23: Parabolic Trough Collector Incident Angle Modifier Table in EBSILON

The thermal losses equation of PTC as following:

$$q_{LOSS}\ (\ PTC) = a_0 + a_1\ (T_{HTF} - T_{amb}) + c_2 (T_{HTF})^2 + \ c_3\ (T_{HTF})^3 + \ d_1\ DNI\ (\frac{\text{FOPT}}{\text{FOPT 0}})\ \ (T_{HTF})$$

(6.23)

Where:

$$\text{FOPT} = \text{IAM}\ \ \text{X ETASHAD}$$

(6.24)

FOPT is the optical efficiency of the collector. The thermal losses coefficients a_0, a_1, c_2, c_3, and d_1 in previous equation is achieved from Experimental testing of the thermal losses of vacuum receiver PTC collector (Burkholder and Kutscher, 2009) as follows: a_0 = 4.05 W/m, a_1 = 0.247 W/m K, c_2 = - 0.00146 W/m^{o}C^{2}, c_3 = $5.65e\ X\ 10^{-6}$ W/m^{o}C^{3}, and d_1 = $7.62\ X\ 10^{-8}$ m / ^{o}C.

Table 6.8: Solar Field Design Data of Eurotrough PTC

Collector length	150 m
Number of parallel collectors in the solar field	12 collectors
Distance between parallel collectors	17.3 m
Net Aperture Area of each collector	817.5m²
Net area of the solar field	9,810 m²
Pressure drops in each collector	0.5 bar
Orientation	East-West
Mirror cleanliness	100%
Incident angle Modifier (IAM) (correction factor)	As detailed in Figure 6.23
HTF	Therminol VP-1

Solar Fields Layouts

Figures 6.24 and 6.25 represents a schematic layout of both LFR and PT solar fields

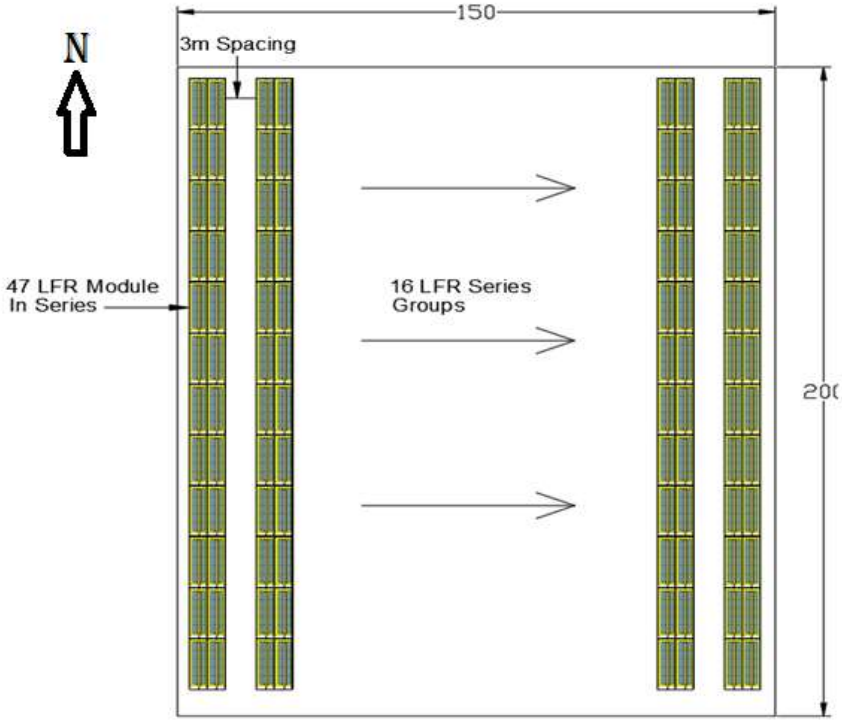

Figure 6.24: LFR Solar Field Design based on a 30,000 m² Flat Land

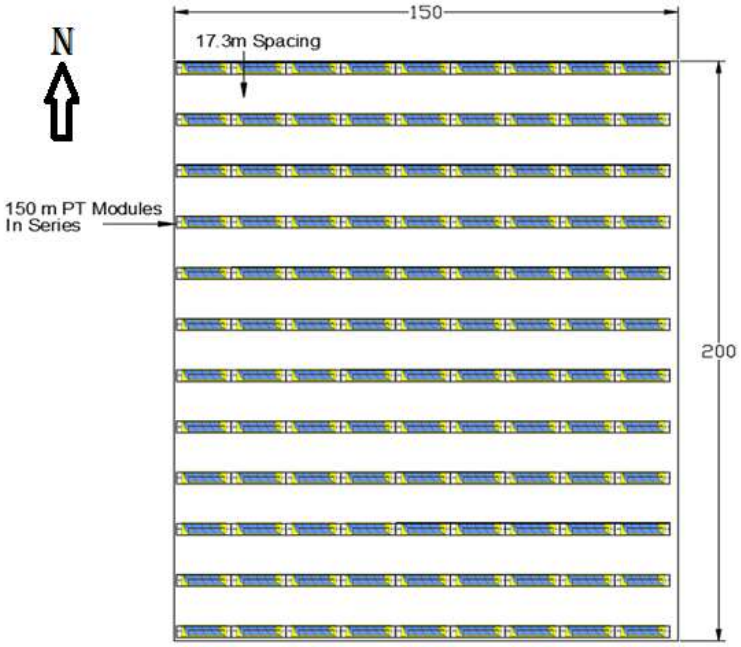

Figure 6.25: PT Solar Field Design Based on a 30,000 m2 Flat Land

Heat Transfer Fluid for Solar Field

The Heat Transfer Fluid HTF used in the solar field is Therminol VP-1 (SOLUTIA, 2020). This HTF works in-between temperature 12 ºC to 400 ºC. and well-known as an HTF in thermal CSP application.

6.6.4 Hybridization CSP into the Power Block

Hybridization for the CSP technology in the power plants comes in two main forms (Soares, 2018):

- Power boosting mode: in this mode, the CSP is used to boost the output power of the power plant in the daytime. In this mode, the fuel consumption needed for the scheduled power generation quantities is not affected by the CSP retrofit. The mission of the CSP hybridization is to boost the productivity of the power plant.
- Fuel-saving mode: as the name suggests, the hybridization of the CSP is meant to save a portion of the fuel needed to operate the power plant.

Figure 6.26 depicts a schematic diagram that explains the differences.

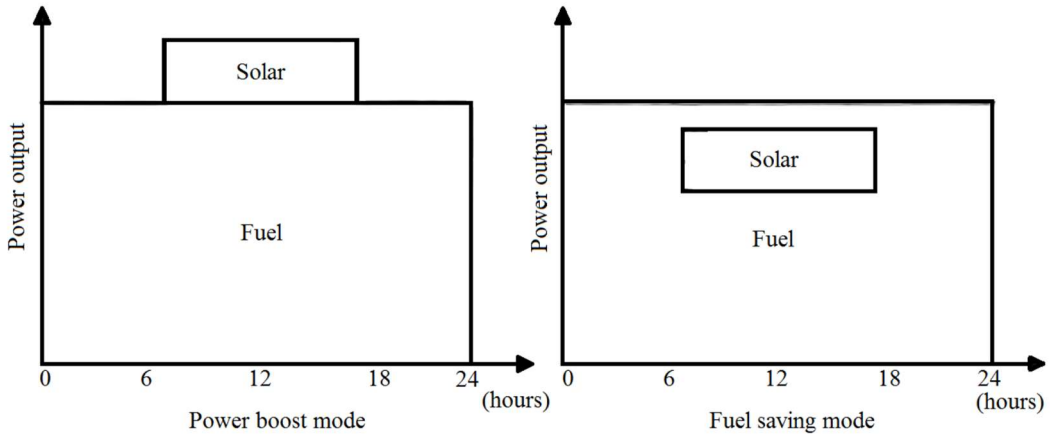

Figure 6.26: Power boosting and fuel-saving modes in hybridization

In the case of this study. The considered power plant capacity is constant. So that the hybridization will be in fuel save mode all the time.

After solar fields are designed and modeled in EBSILON according to their technical specifications and the recommendation of the system manufacturers. The solar field

output can be simulated with high accuracy. To determine the way of interfacing the solar field to the power block. Two main information must be determined:

- The required heat input to the power block to generate 7 MW of electricity
- The heat output of the solar field is based on the best day of the year.

Based on the weather data (SolarGIS, 2020). The maximum average DNI occurs on June 10th around 12:00 PM, The maximum available DNI is 868 W/m2. Based on that, the thermal power output of the solar fields is calculated via EBSILON. Table 6.9 introduces each solar field's maximum thermal power output.

Table 6.9: Solar Thermal Power Output for LFR and PT solar fields based on best DNI

Field	Thermal Power Output (MW)
LFR Field	9.62
PT Field	6.40

These values in the table represent the maximum thermal power input that can be achieved in the year. By comparing these values to the required heat input to generate 7 MW, which is 19.319 MW as depicted in Figure 6.10 (model I). This shows that the CSP alone is incapable of fulfilling the required heat input to generate 7 MW. Thus, the solar field should be connected to the power block steam generator in series, to inject the collected thermal power from the sun into the working fluid, preheating it before entering the steam generator. Consequently, the consumed olive pomace to run the steam generator is reduced (fuel-saving mode).

The connection of the solar field to the power block demands certain requirements that should be considered:

1- The mechanism of solar field connection to the power block: the mechanism is by using oil to water (HTF to WF) shell and tube heat exchanger located just before the steam generator. Thus, heat is transferred effectively. Figure 6.27 introduces the combination as modeled in EBSILON.

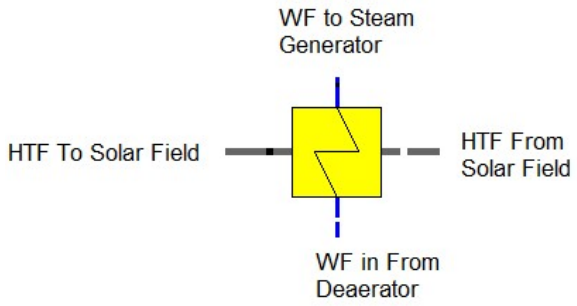

Figure 6.27: Oil to Water Shell and Tube Heat Exchanger in EBSILON

- The operational temperature range in WF and HTF: to obtain efficient heat transfer between the WF and the HTF, the temperature difference should be maintained until both fluids exit the heat exchanger. By looking at the WF of the power block, the temperature of the WF flowing out of the deaerator is 185 ºC. and the maximum temperature of the WF that could be reached is 276 ºC (the saturation temperature at 60 bar) before it turns into superheated steam. Consequently, the temperature of the HTF leaving the heat exchanger is considered to be fixed and maintained at 300 ºC all the time, and the inlet temperature of the HTF depends on DNI and collector's circumstances. The inlet temperature of the WF is fixed as 185 ºC, and the exit temperature is calculated according to the other temperatures.

The heat exchanger has 4 terminals. Two will be for passing the working fluid, and the others for the HTF. Where three out of four temperatures are known ($T_{HTF\ out}$=300 ºC, $T_{HTF\ in} = T_{HTF\ out} + \Delta T_{\text{from Solar Field}}$, $T_{WF\ in}$ = 185 ºC). the WF outlet conditions can be determined. The main equations describing the heat exchanger energy balance in Figure 6.28 can be written in the following:

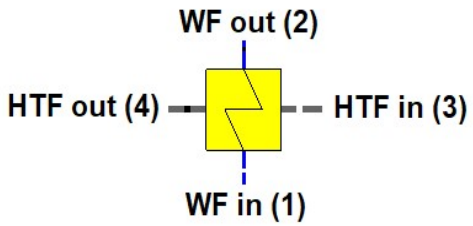

Figure 6.28 Heat Exchanger Main Inlets and Outlets

$$Q_{gained\ by\ WF} = Q_{Given\ by\ HTF} \tag{6.25}$$

$$Q_{gained\ by\ WF} = U * A * LMTD = (M_2H_2 - M_1H_1) \tag{6.26}$$

$$Q_{Given\ by\ HTF} = U * A * LMTD = (M_3H_3 - M_4H_4) \tag{6.27}$$

Where:

U: The overall heat transfer coefficient (W/m^2 K)

A: The heat exchange area (m^2)

M: Mass flowrate (kg/sec)

H: Enthalpy (kJ/kg)

LMTD: the logarithmic mean temperature difference, which is calculated by

$$LMTD = \frac{\Delta T_{inlets} - \Delta T_{outlets}}{\ln(\Delta T_{inlets} / \Delta T_{outlets})} \tag{6.28}$$

Where ΔT_{inlets} is the temperature difference between WF and HTF entering the heat exchanger, and ΔT_{oulets} is the temperature difference between WF and HTF leaving the heat exchanger.

Based on all introduced information. Figures 6.29 and 6.30 show the complete hybrid power plant model configuration based on both LFR and PT solar fields.

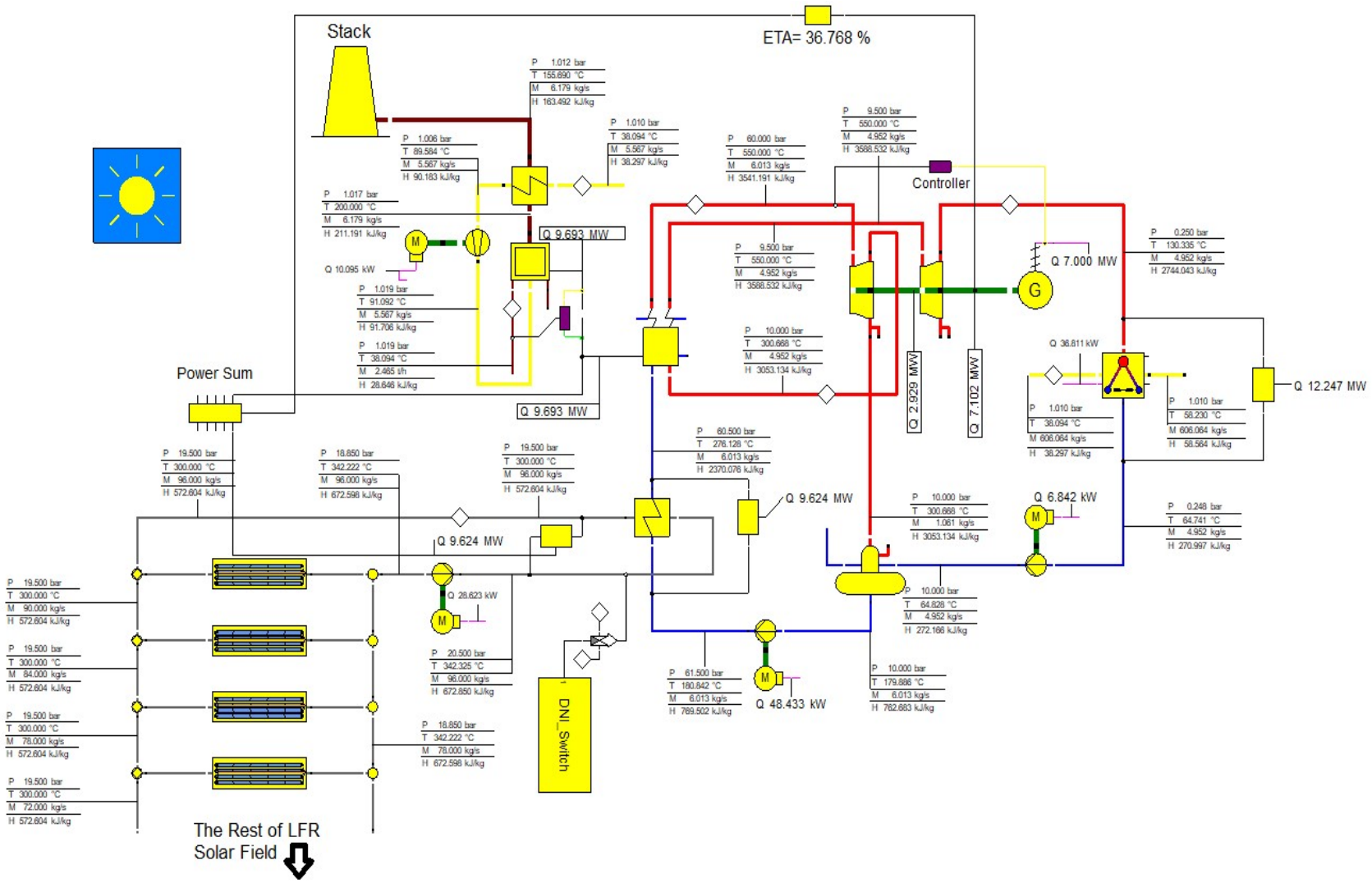

Figure 6.29: Hybrid Olive Pomace-CSP (LFR) Power Plant Model Configuration

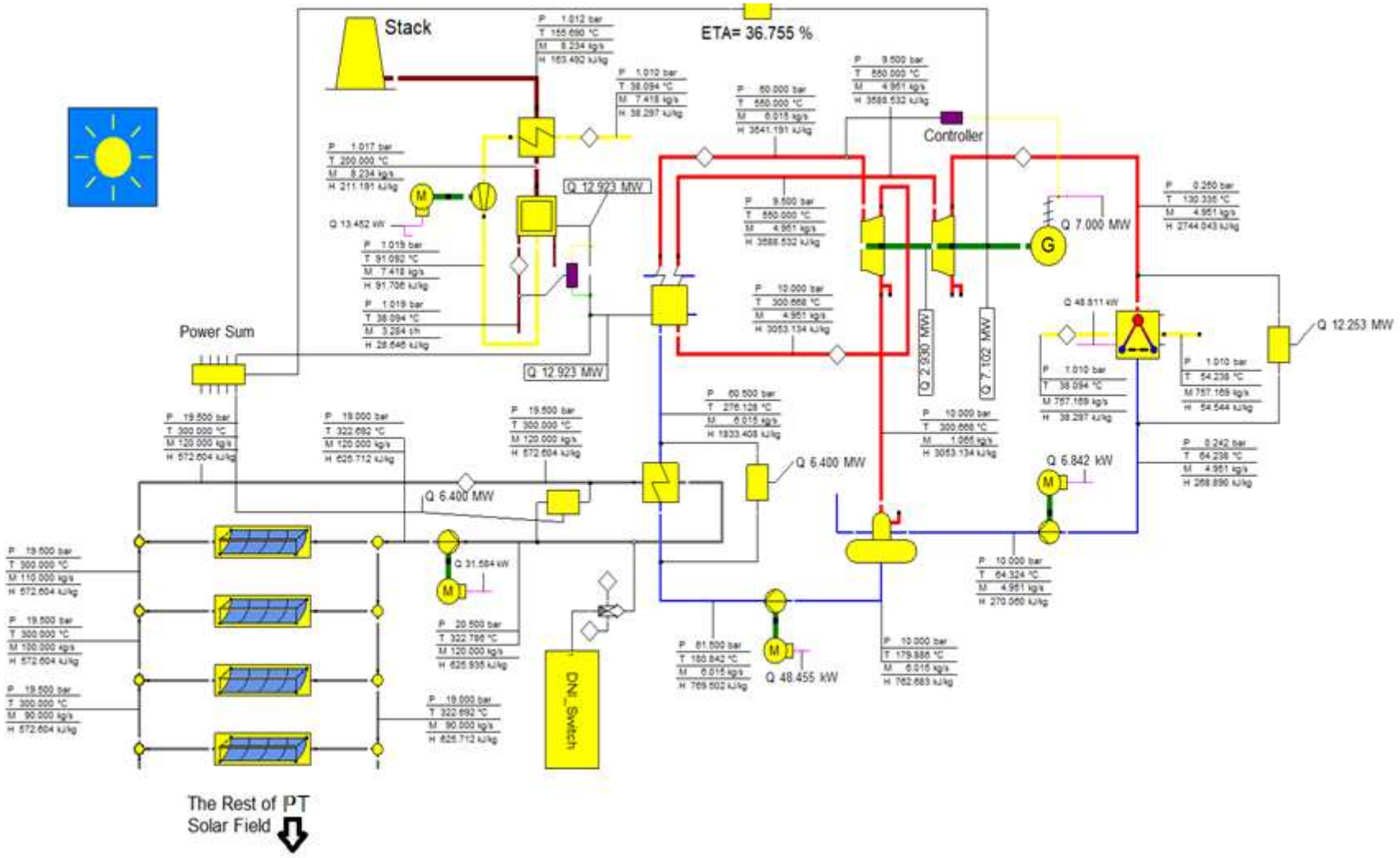

Figure 6.30: Hybrid olive pomace-CSP (PT) power plant model configuration

6.6.5 Scope of Operation and Controllers

The model includes some essential controllers to control and ensure the proper performance of the power plant. Following are the controllers:

- Power generation capacity controller: this controller ensures the fixed power generation capacity regardless and changes in the plant parameters. The controller commands more or less mass flowrate of live steam to achieve the desired set point of generation capacity. Figure 6.31 shows this controller as displayed in EBSILON

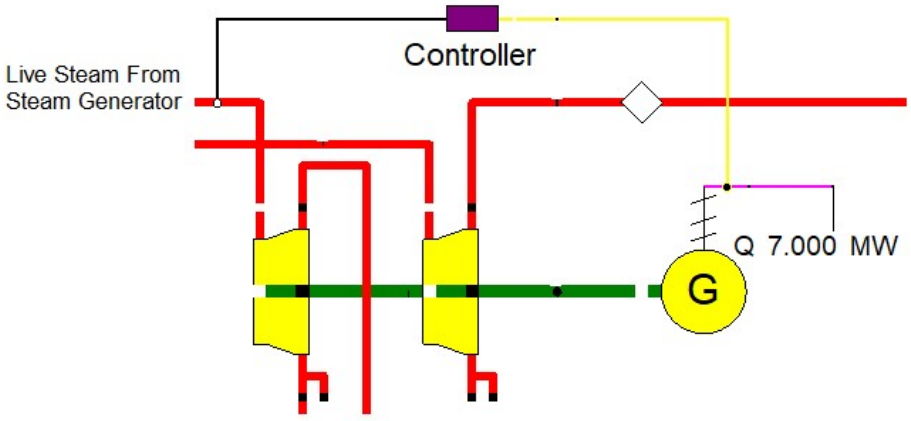

Figure 6.31: Power Generation Capacity Controller

- Olive pomace feeding controller: It controls the mass feeding rate of the olive pomace to the combustion chamber. In such a way that the heat input required to generate the desired live steam temperature is achieved. Figure 6.32 shows this controller as displayed in EBSILON

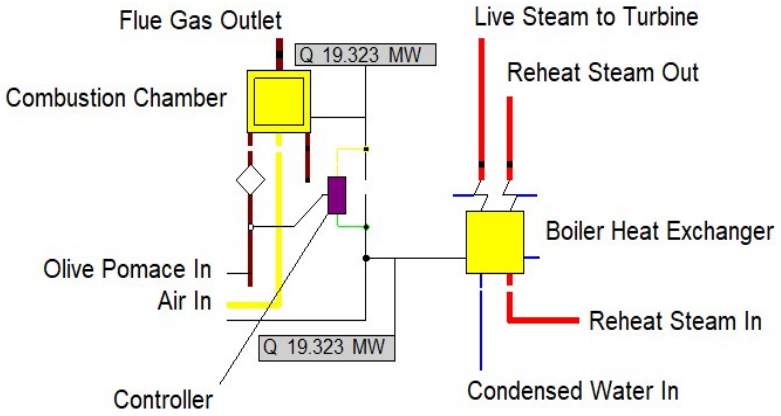

Figure 6.32: Olive Pomace Feeding Controller

- DNI switch Assembly: This controller is designed to switch the solar field heating system on whenever:

  - DNI is available and heat is generated from the reflectors.
  - The amount of heat generated is more than the thermal losses of the system.

  The DNI switch is a macro-object built inside the EBSILON to perform a specific function. In the developed models, the DNI switch simulates one string of solar reflectors. And a decision is made to either operate the system (generating HTF mas flow) or not (set HTF mass flow rate to 0.0). Figure 6.33 shows this controller as displayed in EBSILON

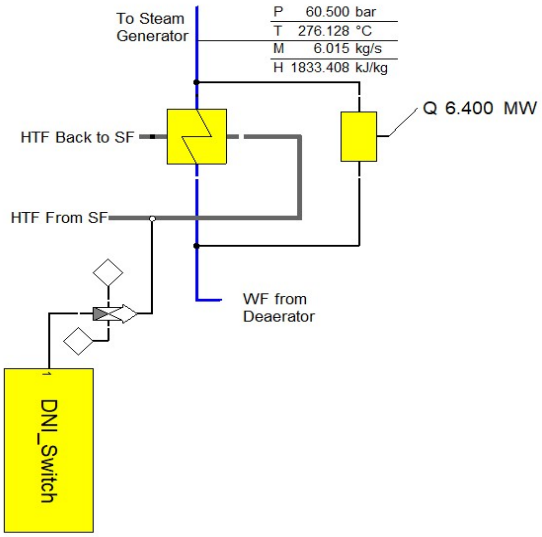

Figure 6.33: DNI Switch Controller of The Solar Field Operation

At this point, the power plant model development is done, Table 6.10 introduces a summary for all technical data and involved parameters.

The component in Figure 6.34 in EBSILON is used to identify some Design conditions epically olive pomace composition and heating value also is used to identify the HTF Therminol VP-1 conditions and specifications.

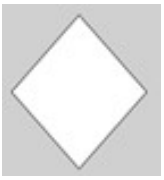

Figure 6.34: General Input Value/Start Value Component in EBSILON

Table 6.10: Technical Data for Power Block

Fuel	Olive Pomace	GCV	17.095 MJ/ kg
		NCV (as calculated by EBSILON under Boiler pressure of 60 bar)	16.484 MJ /kg
	Fuel Temperature	T_{fuel}	$T_{fuel} = T_{amb}$
	Composition	Elemental (C)	0.4842
		Elemental (H)	0.0596
		Elemental (O)	0.3409
		Elemental (N)	0.0097
		Ash	0.1056
Fresh air	Air Pressure	P_{air}	1 bar
	Air Temperature	T_{amb}	Variable
Combustion Chamber	Combustion Efficiency	$\eta_{combustion}$	98 %
	Excess Air Ratio	λ	1.35
	Exhaust gas outlet and slag temperature	$T_{flue\ gas}$	200 ºC
Boiler	Live steam Pressure	P_{live}	60 bar
	Live Steam Temperature	T_{live}	550 ºC
	Pressure Drop	ΔP	0.5 bar
Steam Turbine	Isentropic Efficiency	η_{is}	90 %
	Mechanical Shaft Efficiency	η_{mech}	99.8 %

	Reheat and Bleed Pressure	$P_{reheat-bleed}$	11 bar
Air Cooled Condenser	Overall Heat Transfer coefficient per Bay	U	50 W/m² K
	Pressure Drop in Air side	ΔP_{air}	50 Pa
	Condenser Pressure	$P_{condenser}$	0.25 bar (25 k pa)
Generator	Generator Efficiency	η_G	98%
Open FWH (Deaerator)	Pressure	$P_{Deaerator}$	11 bar
	Pressure Drop	$\Delta P_{Deaerator}$	0 bar
Pumps	Isentropic Efficiency	η_{is}	85 %
	Mechanical shaft Efficiency	η_{mec}	99.8 %
	Motors Efficiency	η_{motor}	85 %
Condenser fans	Overall Efficiency	η_{All}	70%

In the following chapter, the developed models will be used to simulate the power generation based on olive pomace and CSP throughout. So that results could be obtained for discussion and conclusions.

CHAPTER 7

Simulation Results and Economic Analysis

7.1 Preamble

After the hybrid power blocks are modeled via EBSILON using all the related information to all equipment and operation circumstances. In this chapter, the models are used for simulating the operation of the plant. So that generated information can be used to assess the outcomes.

The simulation will be based on the LFR and PT hybrid olive pomace-CSP models developed in the previous chapter. For each model, the annual DNI data and annual ambient temperature profile will be set and the power generation process for 12 months will be run based on a 1-hour timestep.

7.2 Power Block Results

Figure 7.1 depicts the T-s of the adopted power block in the previous chapter (Model I). this figure results from the given for each component of the power block.

- Power Plant T-s Diagrams

Figure 7.1 depicts the T-s of the adopted power block in the previous chapter (Model I). this figure results from the given for each component of the power block. The figure shows the real expansion processes in turbines and the pressure drops in heat transfer components.

- Boiler Efficiency

The boiler efficiency at this point can be determined using the following formula:

$$\eta_{Boiler} = \frac{Q_{WF} + Q_{Air\ Preheater}}{M_{olive\ Pomace} * NCV_{Olive\ Pomace}} \quad (7.1)$$

Where:

- Q_{WF}: The transferred power to the working fluid via the boiler

- $Q_{\text{Air Preheater}}$: The transferred power to the air entering the combustion chamber
- $M_{\text{olive Pomace}}$: The mass flowrate of the olive pomace into the combustion chamber
- $NCV_{\text{olive Pomace}}$: The net calorific value of olive pomace.

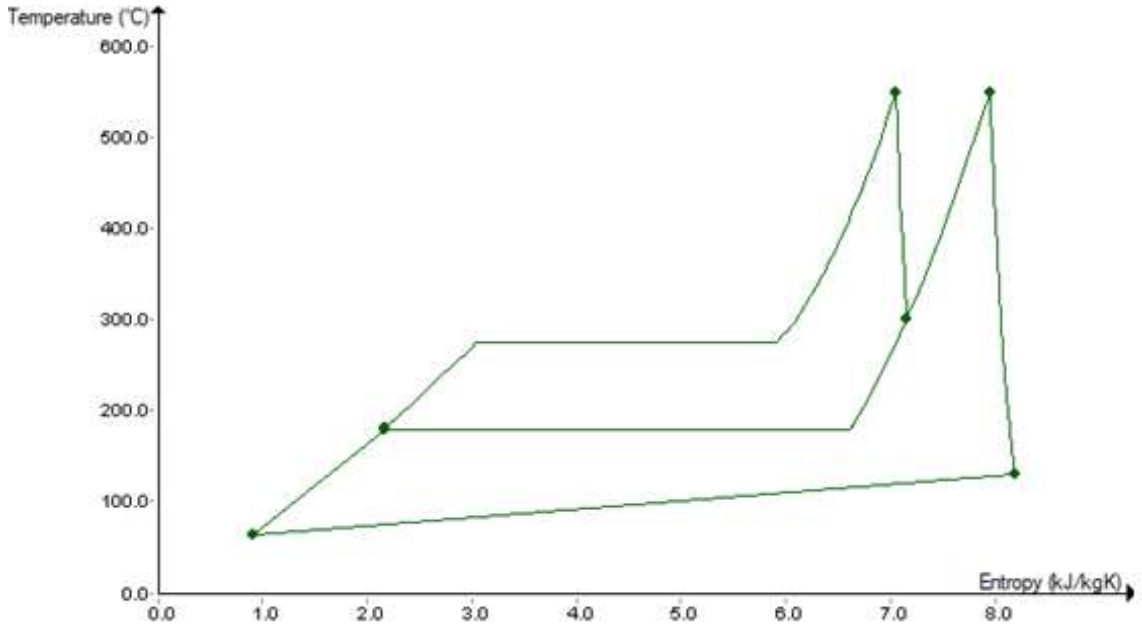

Figure 7.1: T-s Diagram of the adopted power block (Model I)

The calculated boiler efficiency at 20 ºC is 89.49 %, Figure 7.2 represents the relation between the ambient temperature and the boiler efficiency. The boiler efficiency increases as the ambient temperature decreases due to the excessive regenerative performance in the combustion chamber preheater.

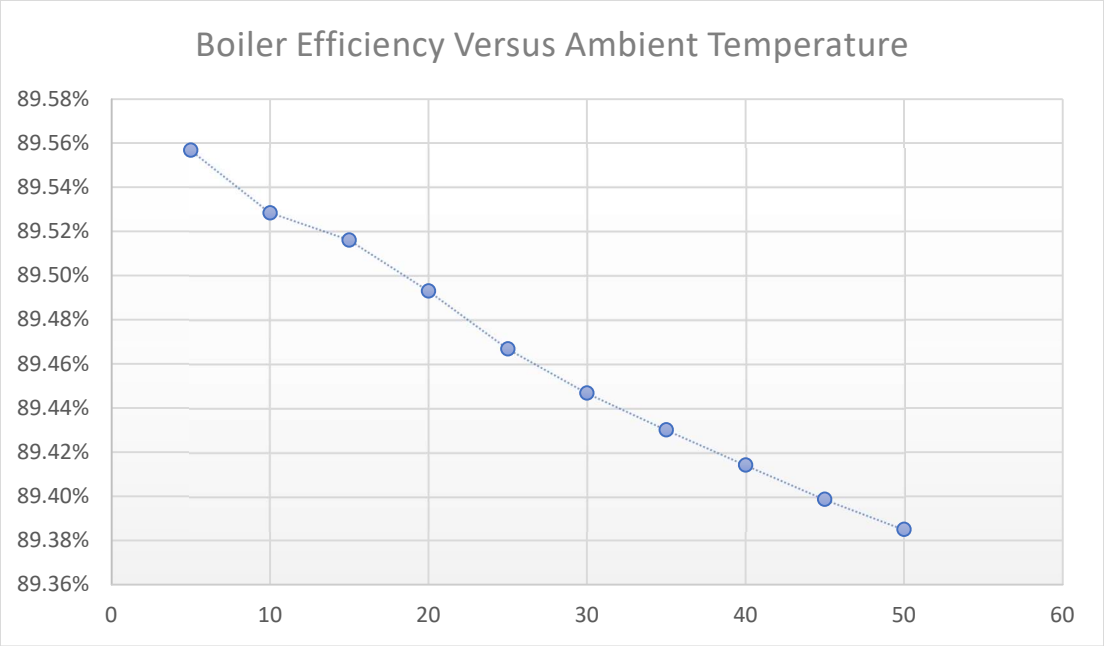

Figure 7.2: Boiler efficiency vas ambient temperature

- Power block Carnot Efficiency

Power cycle Carnot efficiency formula is:

$$\eta_{th,carnot} = 1 - \frac{T_L}{T_H} \tag{7.2}$$

Where:

- T_L: Low-temperature side of the cycle (in Kelvin)
- T_H: High-temperature side of the cycle (in Kelvin)

Accordingly, $\eta_{th,carnot}$ = 59 %.

7.3 Annual Simulation Results

Simulation of the hybrid power models was carried out through an entire year of operation. Changing all the parameters related to the operation such as ambient temperature, DNI, and sun path. Resulting in the following results:

- Olive Pomace Annual Consumption

Table 7.1 shows the required amounts of olive pomace annually. The simulation was run for 3 capacities: 6, 7, and 8 MW which is around the estimated capacity, for both LFR and PT solar fields:

Table 7.1: Olive pomace required amounts for annual operation

Power Plant Capacity	8 MW		7 MW		6 MW	
Solar Field Type	LFR	PT	LFR	PT	LFR	PT
Olive Pomace (Ton)	45,784.6	46,193.6	39,613.8	40,021.7	33,441.8	33,848.7

As shown in Table 7.1, the consumed amount of olive pomace increases when production power increases since the solar field area is fixed and does not increase accordingly. Figures 7.3, 7.4, 7.5, and 7.6 show the profile of olive pomace consumption in June and January, which are the best and worse in terms of the DNI amounts. All the generated figures will rely on the 7 MW capacity model that satisfies the olive pomace consumption compatible with the annual average amount of olive pomace in Palestine unless otherwise is stated.

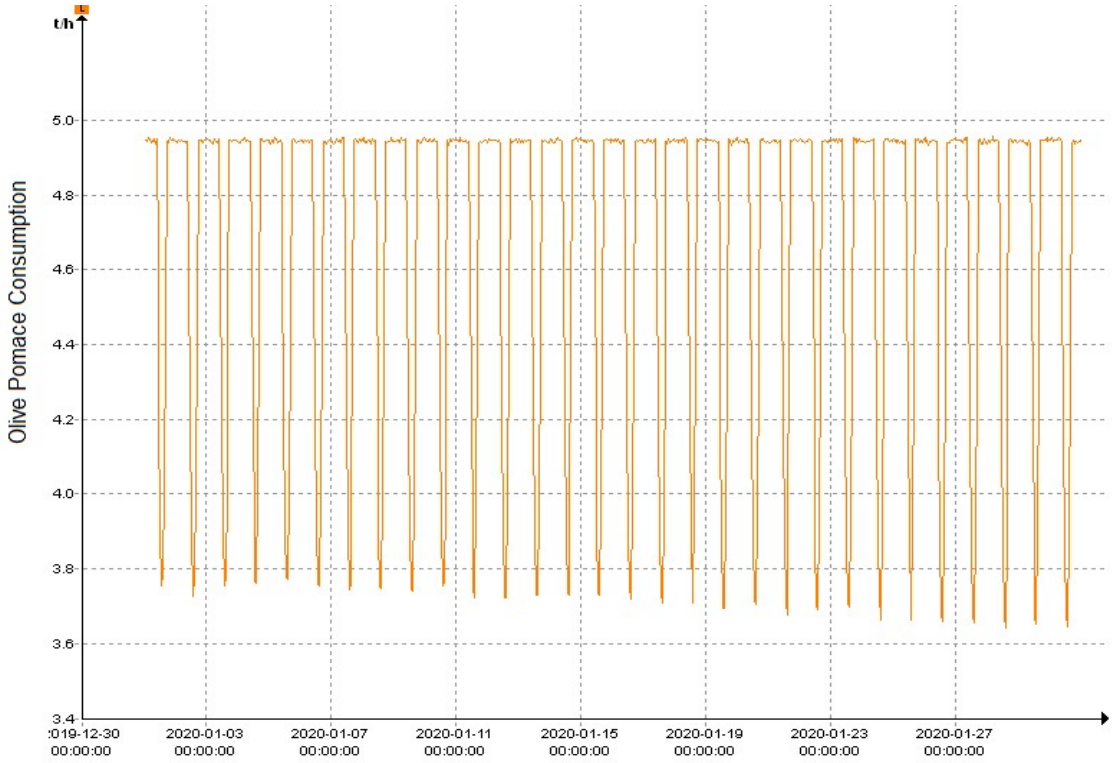

Figure 7.3: LFR hybrid model Olive Pomace Consumption Rate profile in January

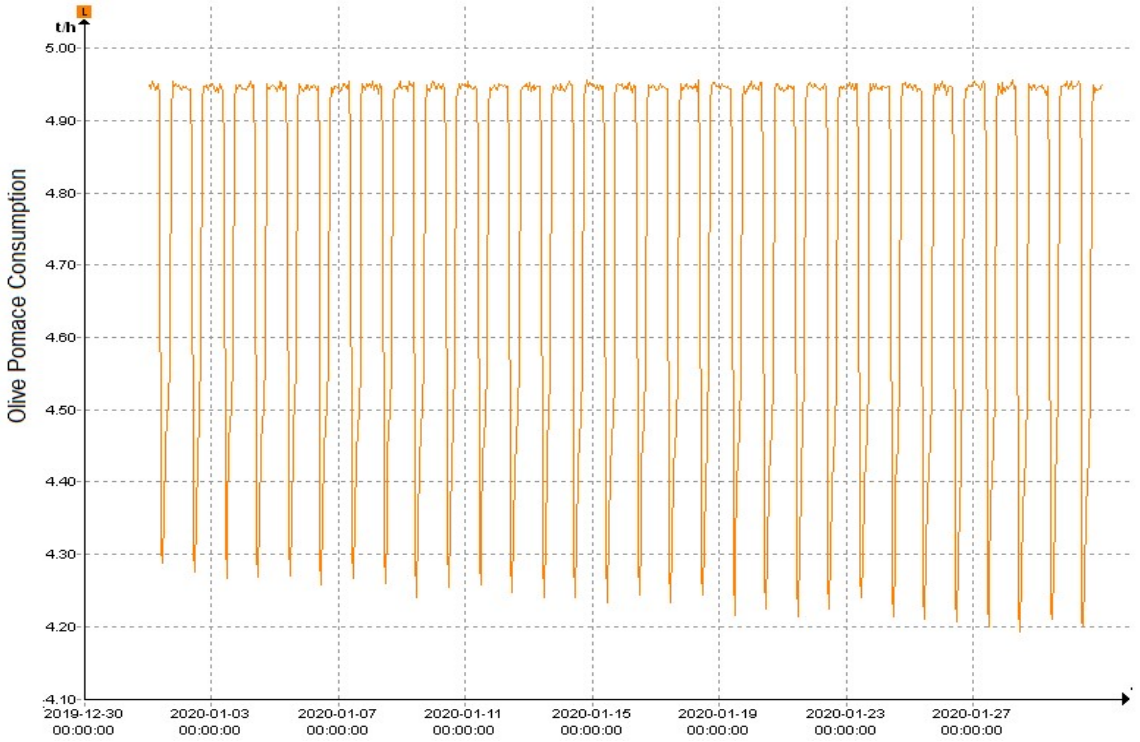

Figure 7.4: PT hybrid model Olive Pomace Consumption Rate profile in January

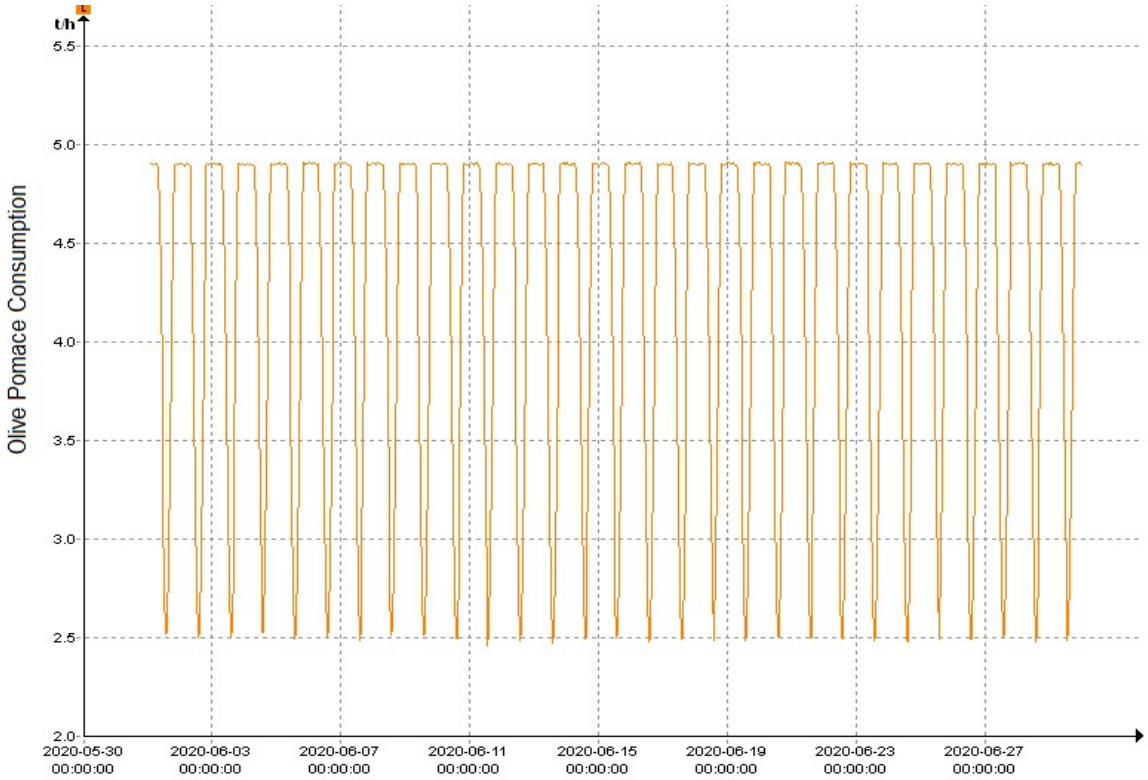

Figure 7.5: LFR hybrid model Olive Pomace Consumption Rate profile in June

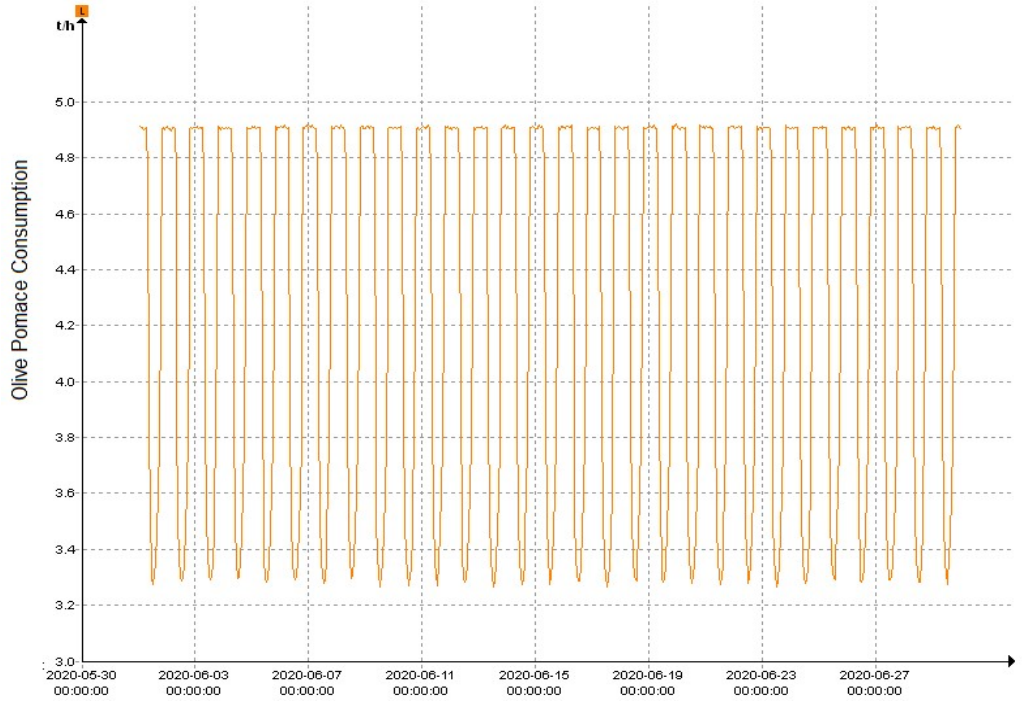

Figure 7.6: PT hybrid model Olive Pomace Consumption Rate profile in June

By looking at Figures 7.3 to 7.6, the olive pomace consumption rate oscillates according to the available DNI. Olive pomace consumption rate in January is higher than in June due to lower DNI rates in January.

- Boiler Expended Power (Energy Generated by Biomass Boiler per time)

Base on the annual simulation, Table 7.2 represents the annual boiler-generated energy to drive the power plant.

Table 7.2: Annual boiler expended energy

Power Plant Capacity	8 MW		7 MW		6 MW	
Solar Field Type	LFR	PT	LFR	PT	LFR	PT
Boiler Expended Energy (MWh)	179,615.1	181,218.9	155,372.1	156,971.1	131,129.0	132,723.4

Table 7.2 shows that the required expended energy for both LFR and PT hybrid models is so close, the LFR requires less boiler expended energy. Figures 7.7, 8, 9, and 10 show the profile of the boiler's expended power in June and January, which are the best and worse in terms of the DNI amounts.

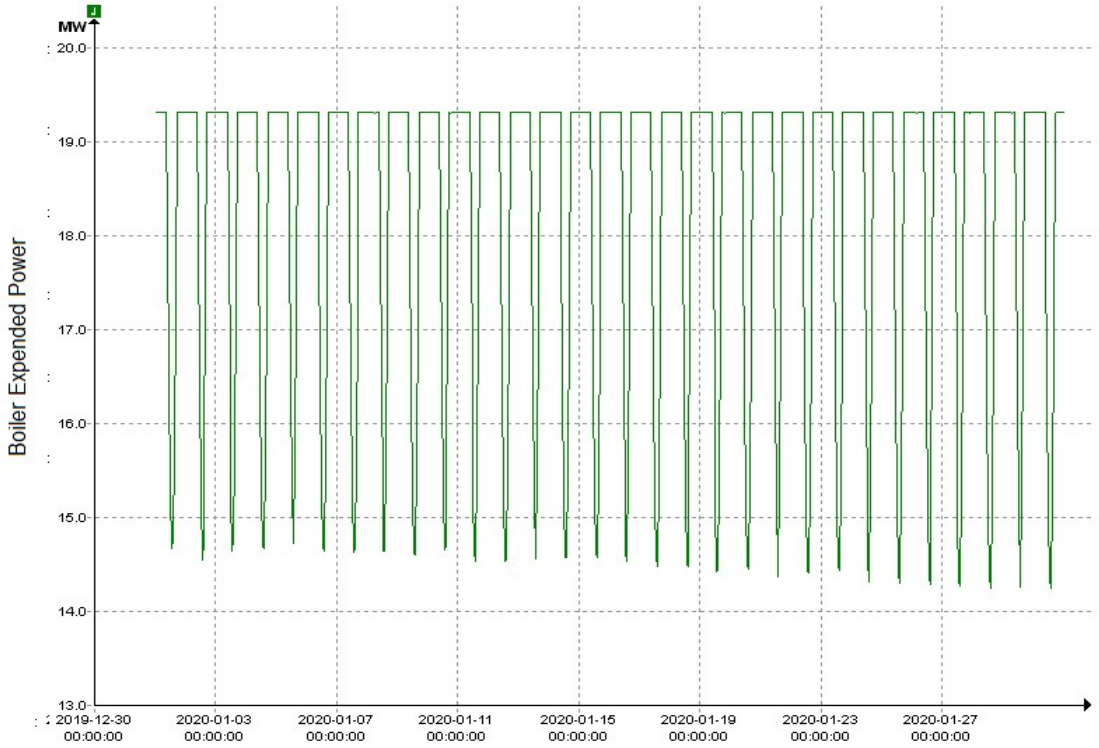

Figure 7.7: LFR hybrid model boiler expended power profile in January

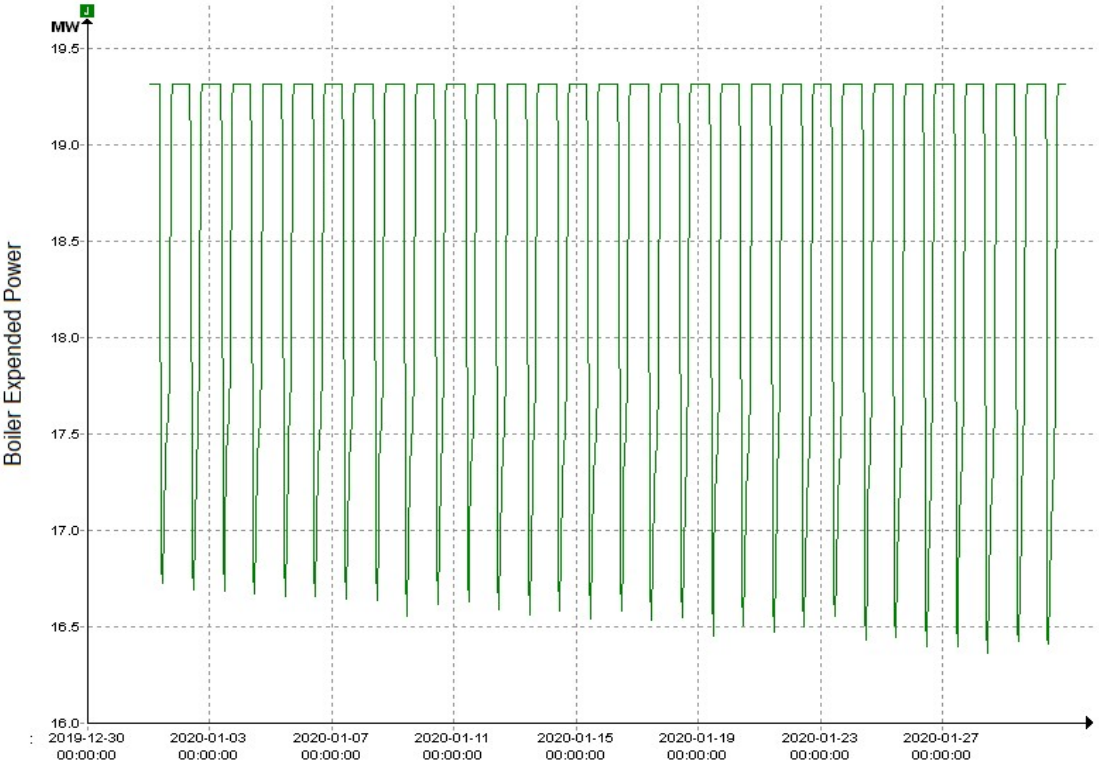

Figure 7.8: PT hybrid model boiler expended power profile in January

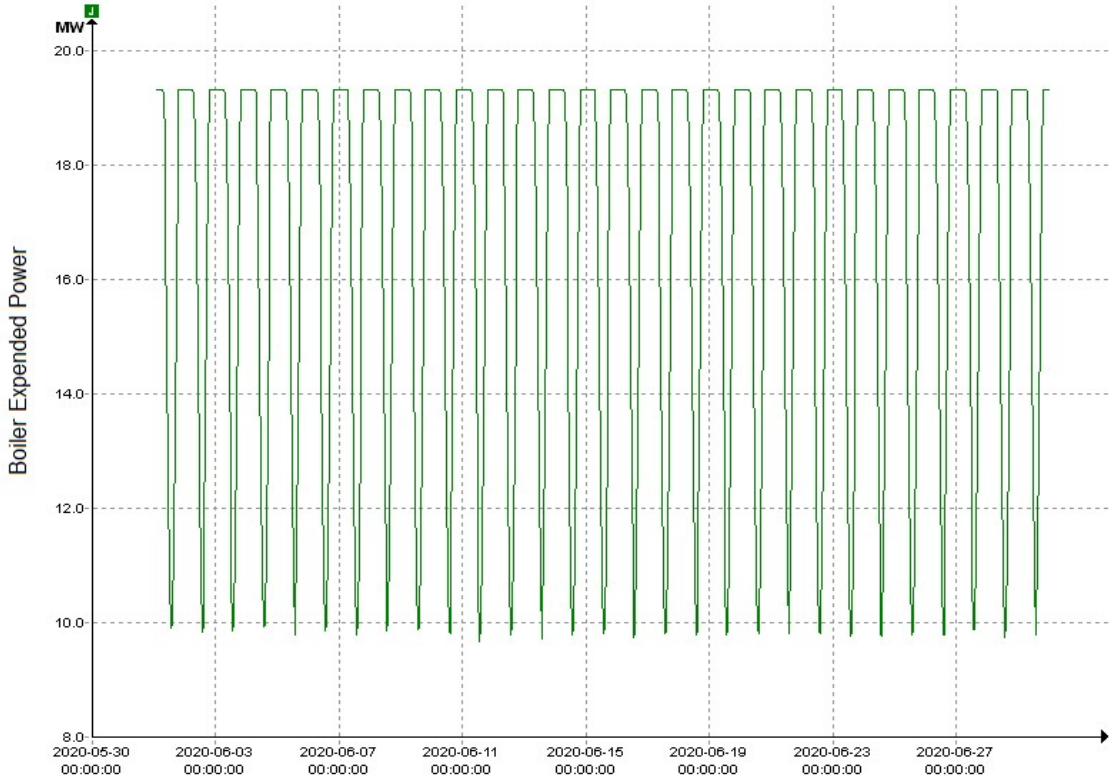

Figure 7.9: LFR hybrid model boiler expended power profile in June

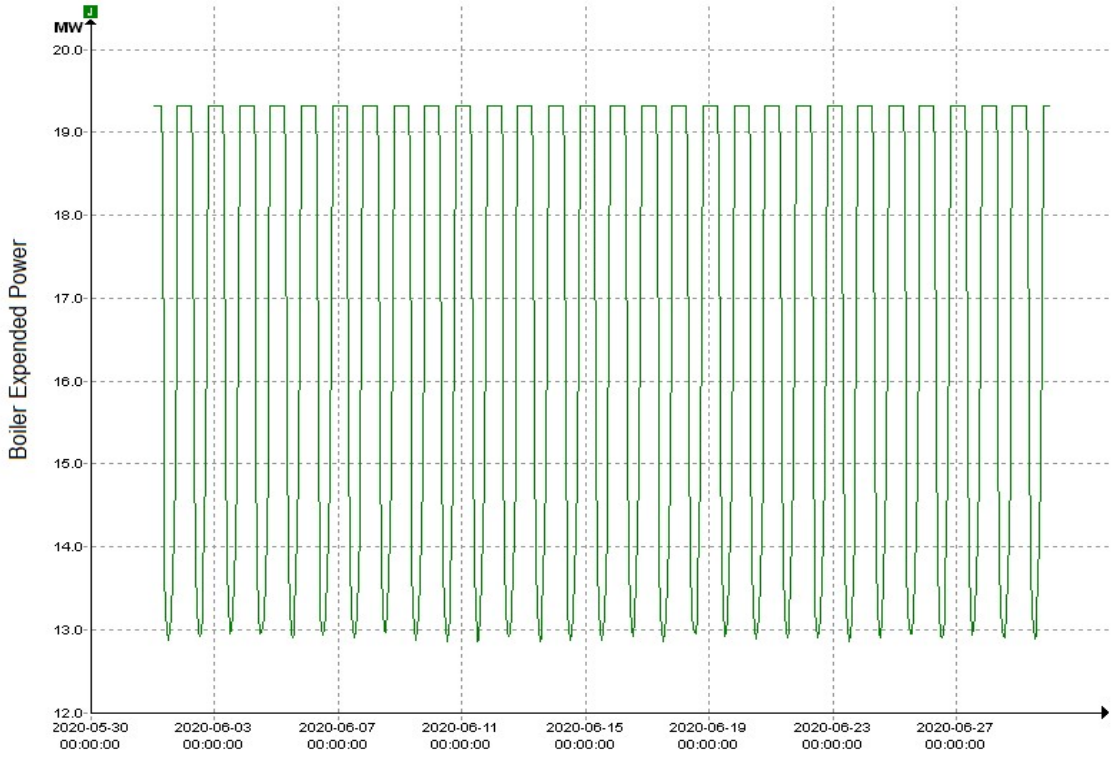

Figure 7.10: PT hybrid model boiler expended power profile in June

- Solar Energy Yield

Table 7.3 shows the summary of the solar energy yield for both LFR and PT solar fields (the solar energy generated by solar fields is the same for all capacities).

Table 7.3: Solar energy annual yield summary for all capacities, equipped with LFR or PT solar fields

Solar Field Type	LFR	PT
Net Solar Energy Yield Q_{EFF} (MWh)	14,325.6	12,762.8

Table 7.3 shows that LFR solar field exceeds in terms of net solar yielded energy. That despite LFR is lower than PT in optical efficiency, but it has the advantage of more allowable area occupation (less unoccupied area). Figures 7.11, 12, 13, and 14 show the profile of generated solar power in June and January, which are the best and worse in terms of the DNI amounts.

Figure 7.11: LFR hybrid model generated solar power (QEFF) profile in January

Figure 7.12: PT hybrid model generated solar power (QEFF) profile in January

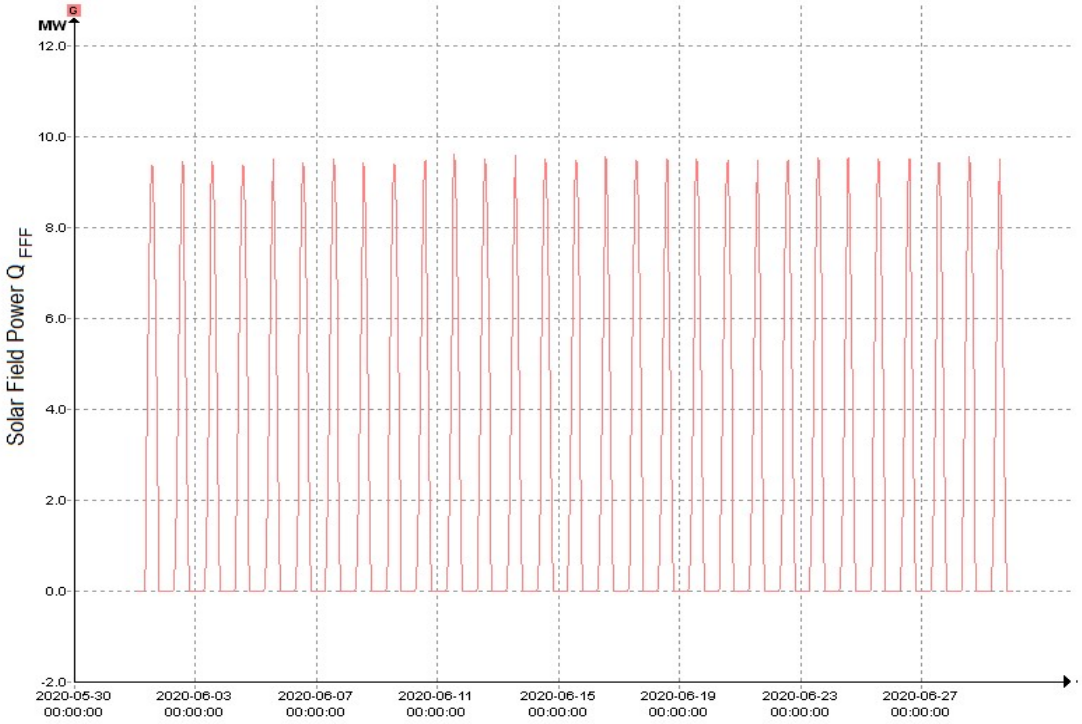

Figure 7.13: LFR hybrid model generated solar power (QEFF) profile in June

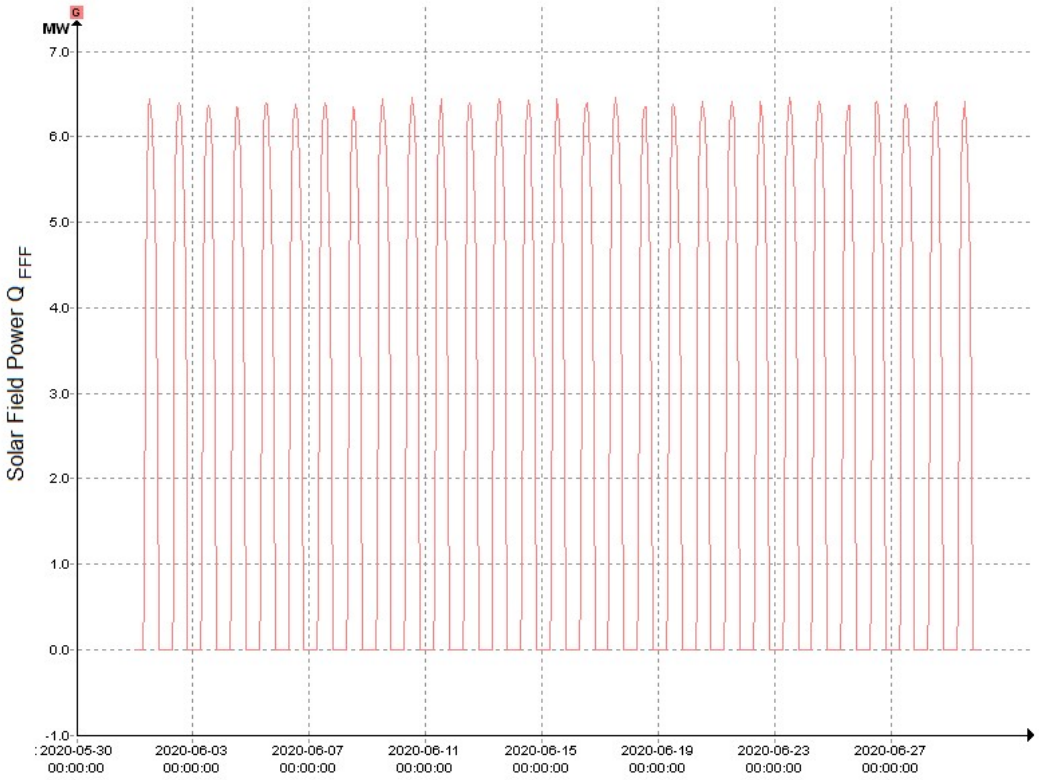

Figure 7.14: PT hybrid model generated solar power (QEFF) profile in June

- HTF Operational Temperature Range

HTF operational temperature range was tuned for not exceeding 400 ºC (the max of the Therminol VP-1) and not less than 300 ºC to maintain proper heat transfer on the oil to the water heat exchanger. Figures 7.15 and 16 introduce the HTF temperature swinging over time.

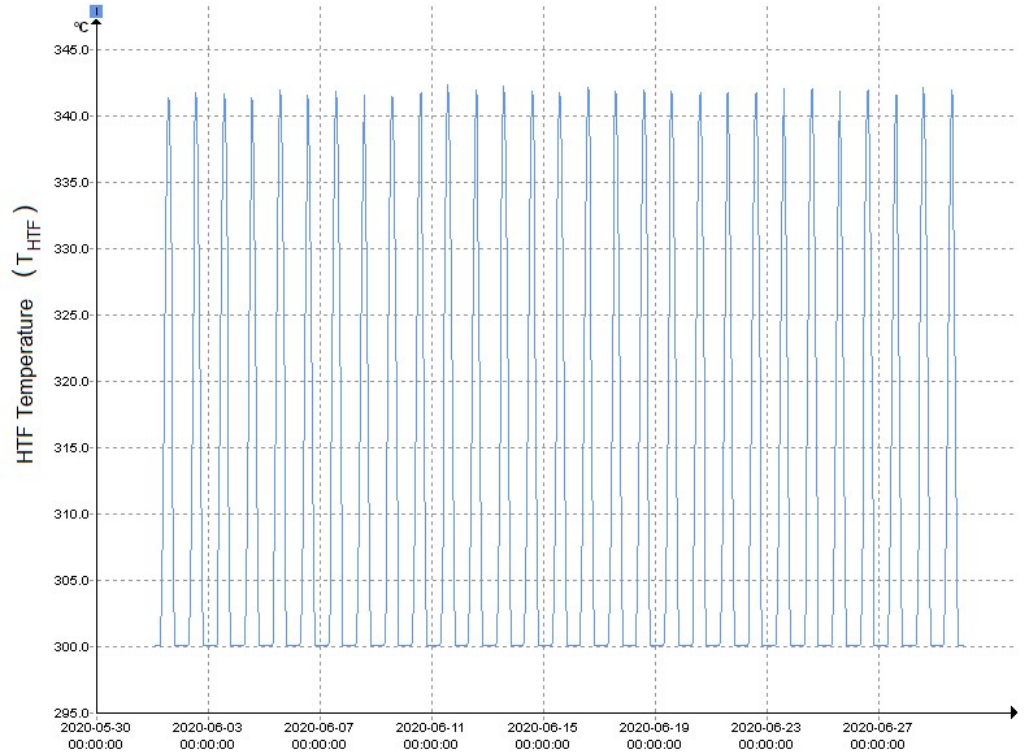

Figure 7.15: LFR hybrid model HTF (T_{HTF}) profile in June

Each solar field has its design HTF flowrate. This flowrate depends on the manufacturer's solar field design instruction and product specifications.

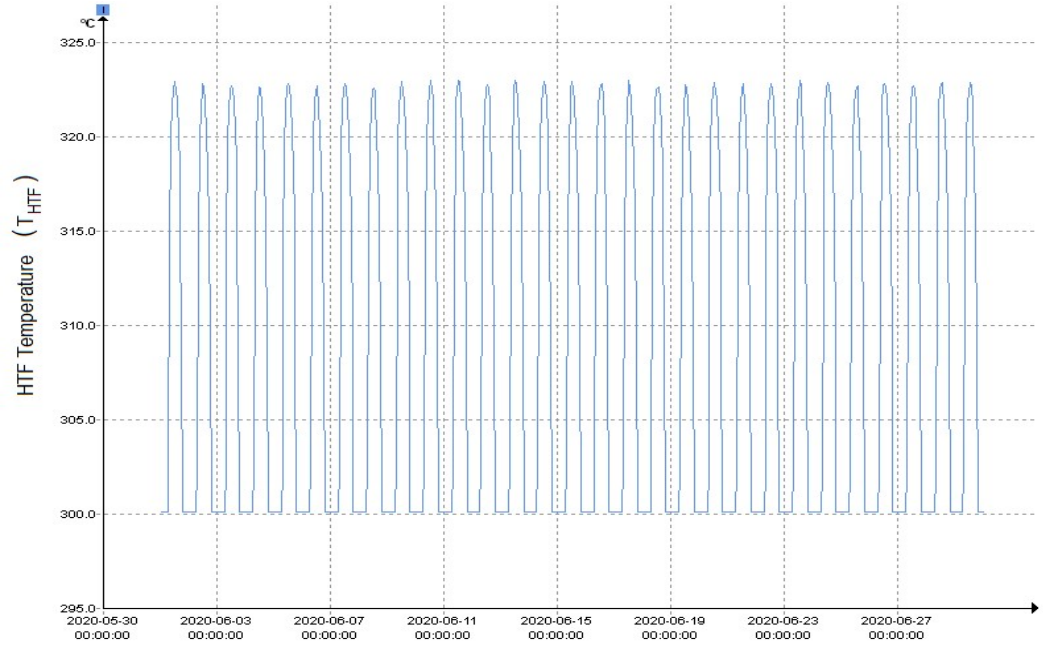

Figure 7.16: PT hybrid model HTF (T_{HTF}) profile in June

- Thermal Power Input Shares

According to the annual simulation, Table 7.4 introduces the thermal input shares to the power plant.

Table 7.4: Thermal input shares to the power plant.

Power Plant Capacity	8 MW		7 MW		6 MW	
Solar Field Type	LFR	PT	LFR	PT	LFR	PT
Boiler Share (%)	92.61%	93.42%	91.56%	92.48%	90.15%	91.23%
Solar Field Share (%)	7.39%	6.58%	8.44%	7.52%	9.85%	8.77%

Choosing lower electricity generation capacity leads to more solar energy share in the total heat input since less olive pomace will be needed at the same generated thermal power from the solar system.

- 24 hours simulation for highest DNI day (June 10th)

Plant performance was investigated taking June 10th, which is the highest DNI day in the year, and Jan 18th, which is the lowest DNI day in the year, as a case study to represent the essential data regarding the power plant. Figures 7.17 to 7.26 show different power plant and solar field characteristics as in these days.

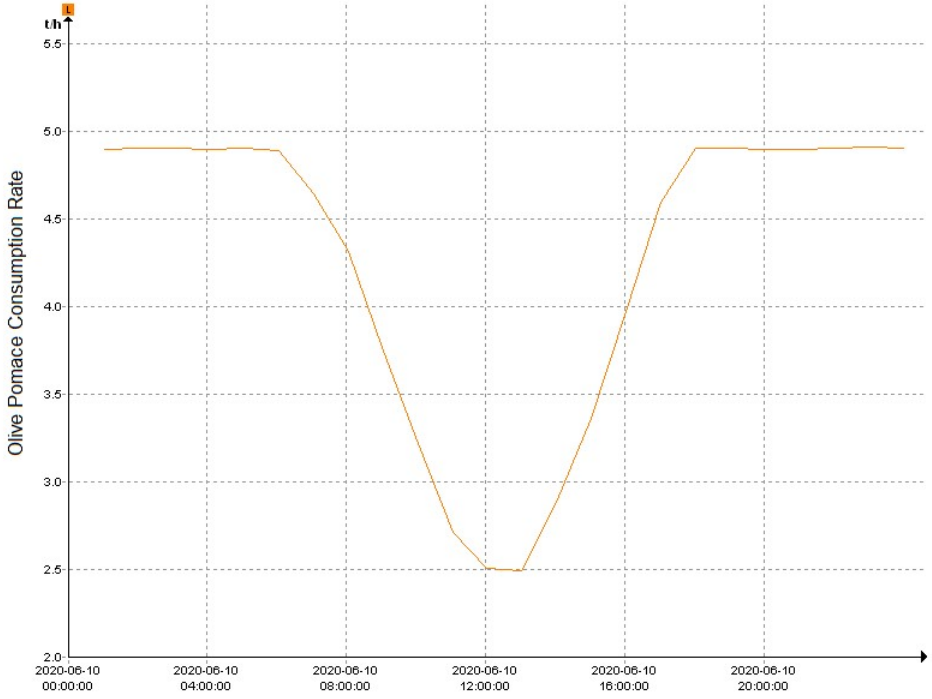

Figure 7.17: LFR hybrid model olive pomace consumption rate on June 10th

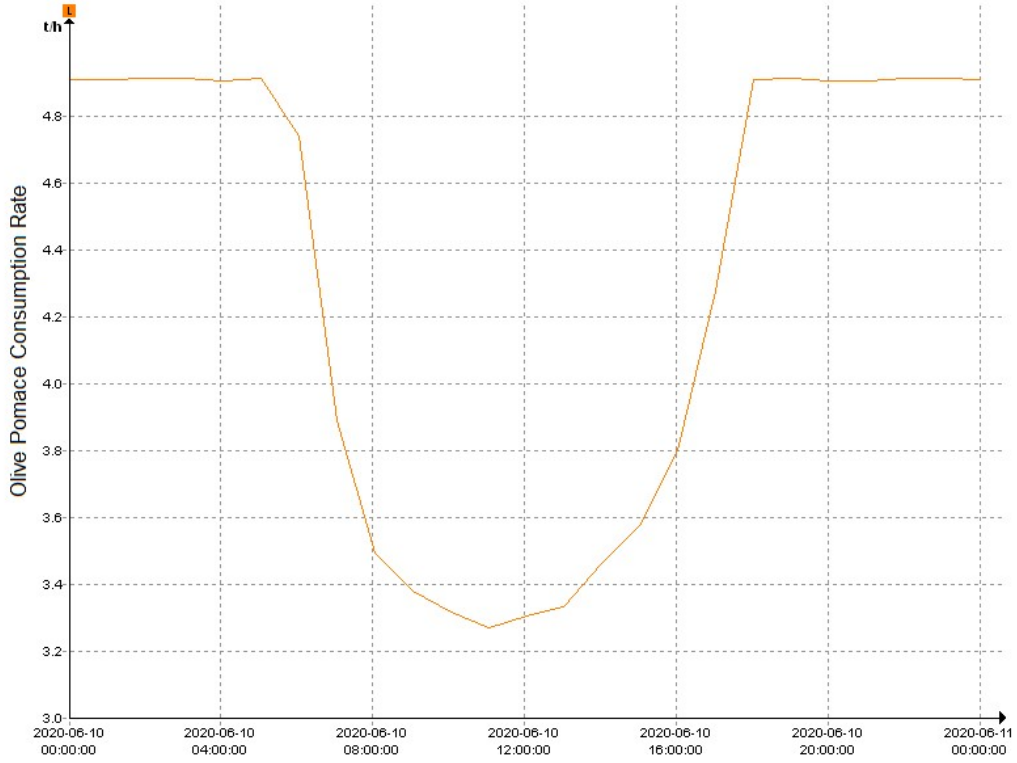

Figure 7.18: PT hybrid model olive pomace consumption rate on June 10th

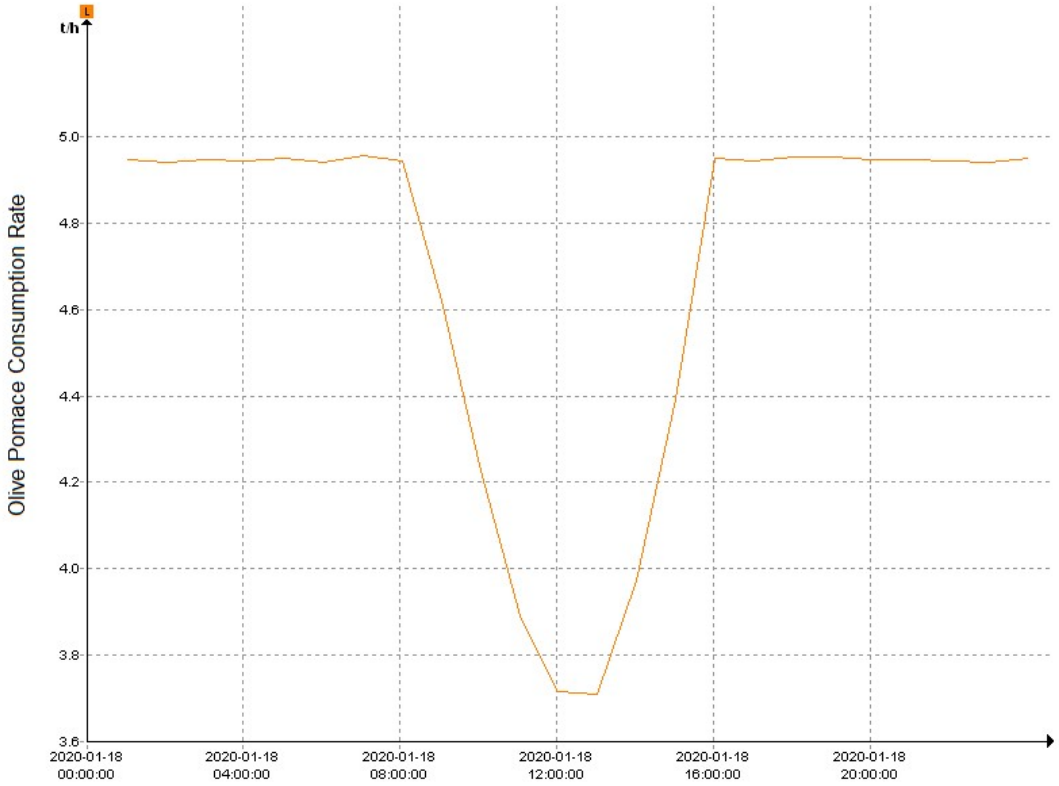

Figure 7.19: LFR hybrid model olive pomace consumption rate on Jan 18th

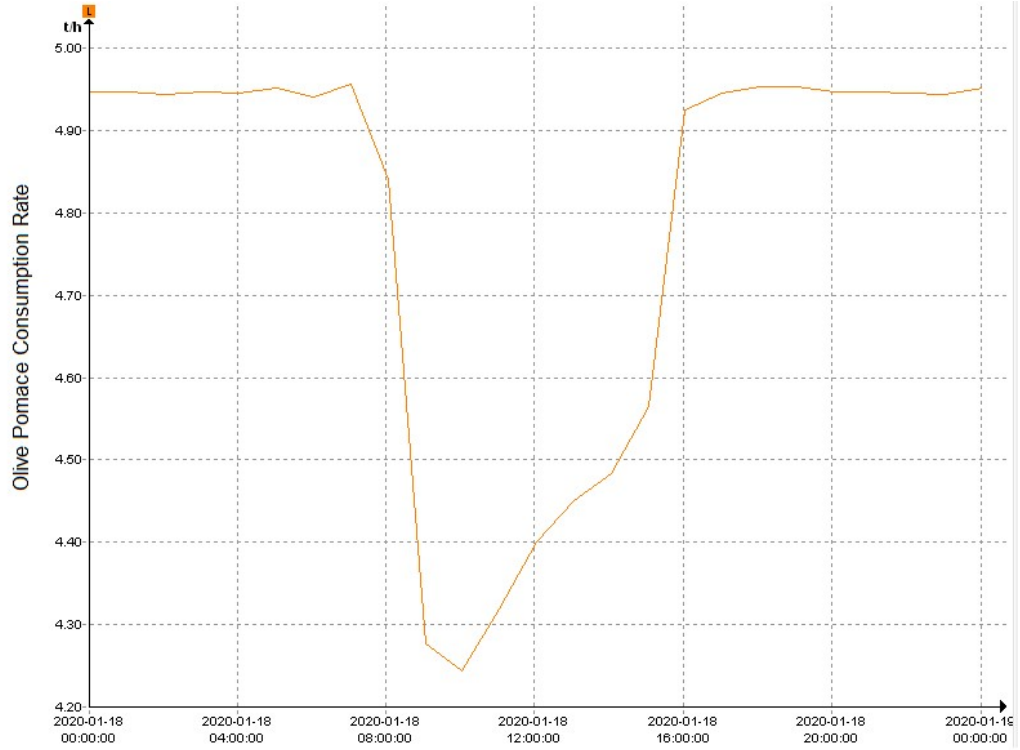

Figure 7.20: PT hybrid model olive pomace consumption rate on Jan 18th

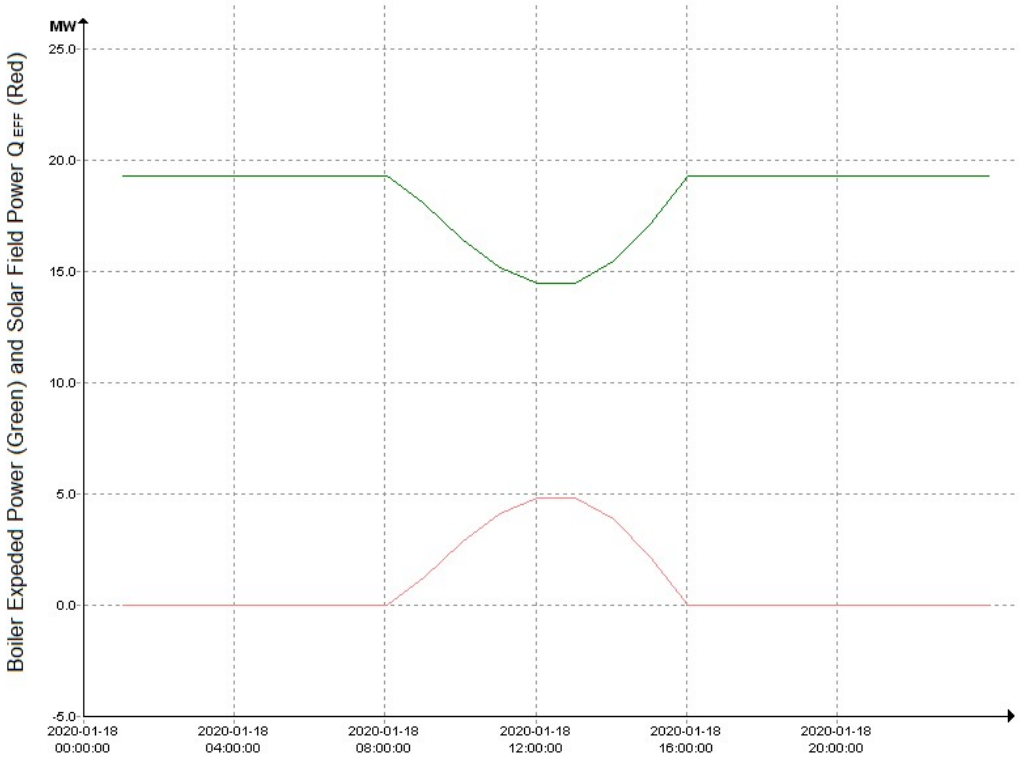

Figure 7.21: LFR hybrid model boiler expended heat and solar field heat on Jan 18th

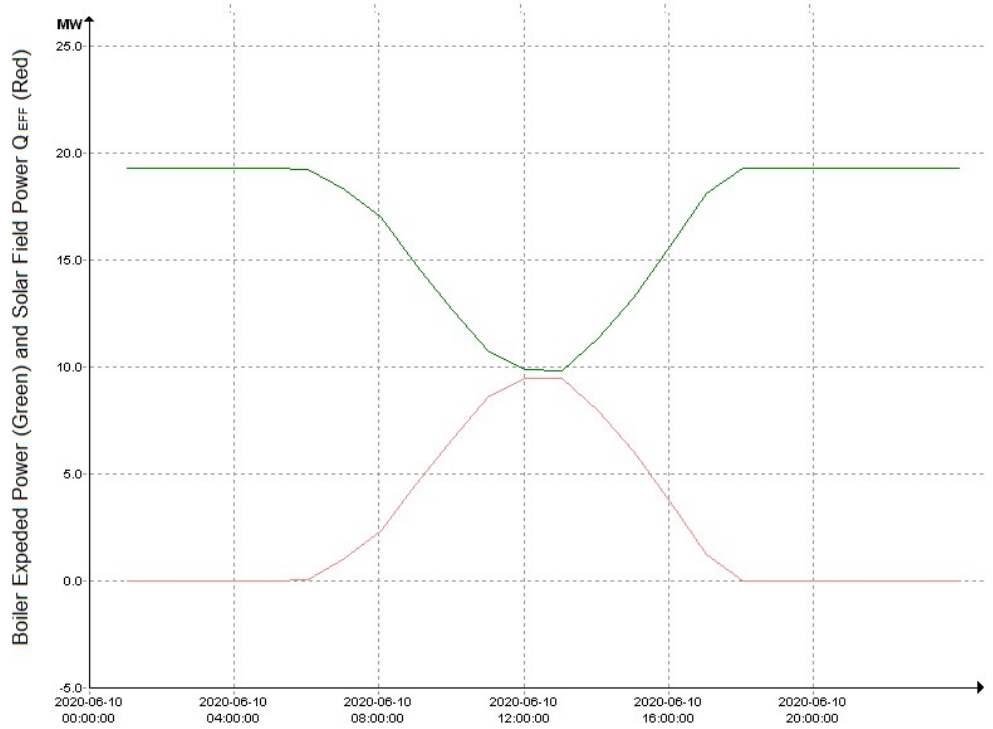

Figure 7.22: LFR hybrid model boiler expended heat and solar field heat on June 10th

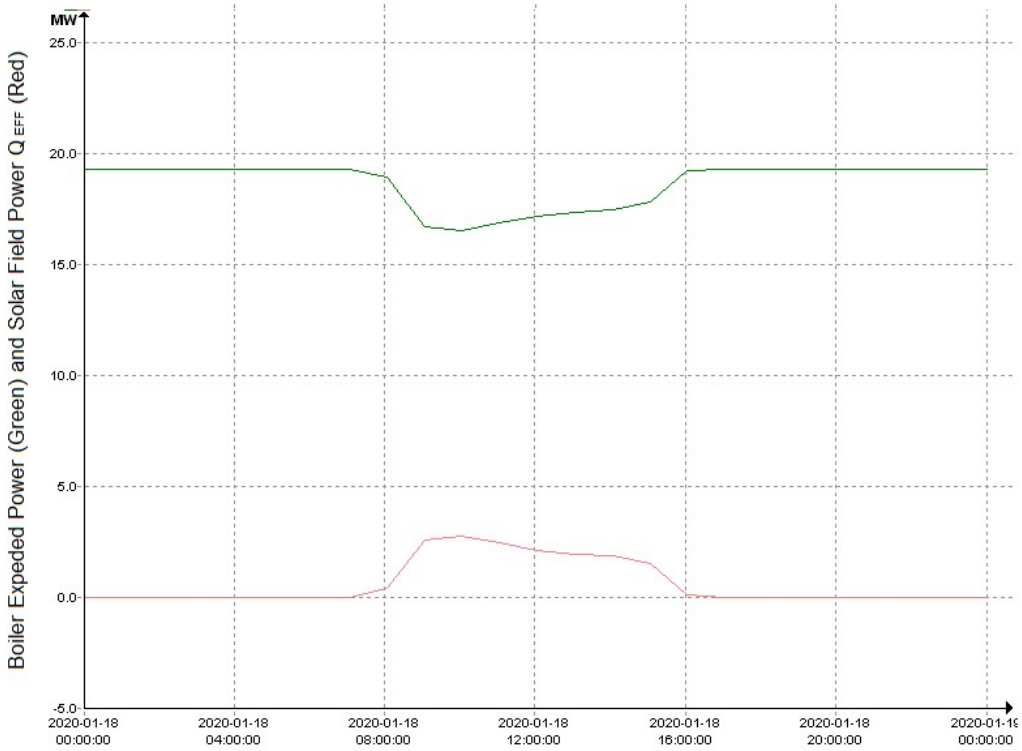

Figure 7.23: PT hybrid model boiler expended heat and solar field heat on Jan 18th

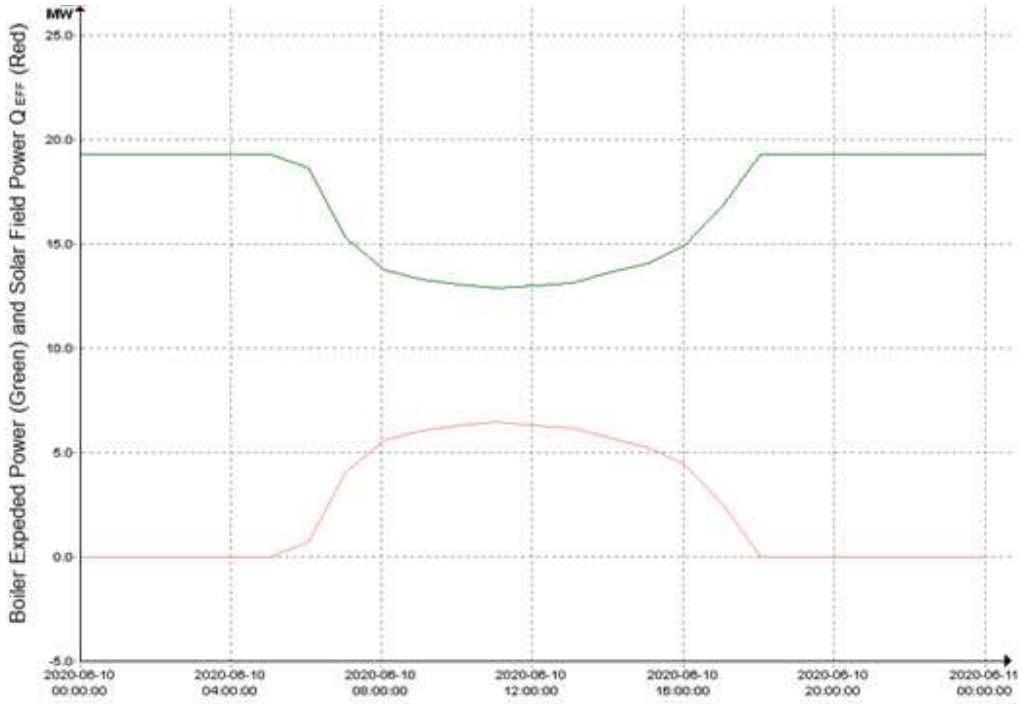

Figure 7.24: PT hybrid model boiler expended heat and solar field heat on June 10th

Table 7.5 shows the thermal Shares based on the best DNI on Jun 10th.

Power Plant Capacity	7 MW	
Solar Field Type	LFR	PT
Boiler Contribution (%)	87.32%	87.18%
Solar Field Contribution (%)	12.67%	12.82%

HTF temperature rise is also monitored so that it does not exceed the maximum allowable temperature which is 400 ºC. Figures 7.25 and 7.26 represent the HTF temperature on June 10th.

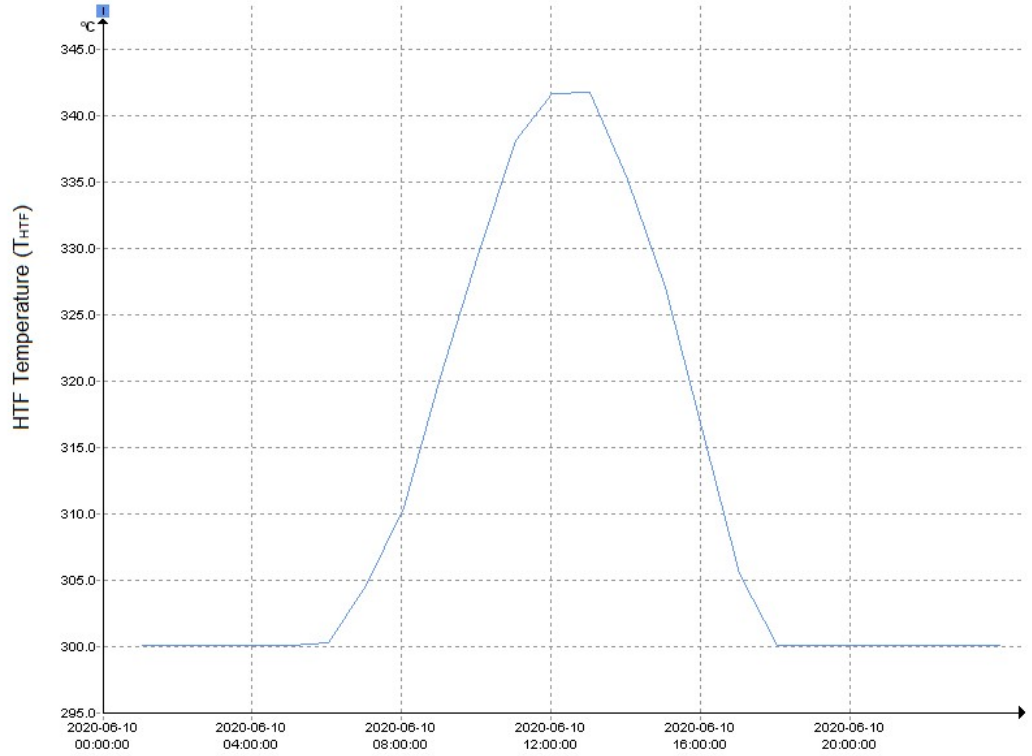

Figure 7.25: LFR hybrid model HTF Temperature on June 10th.

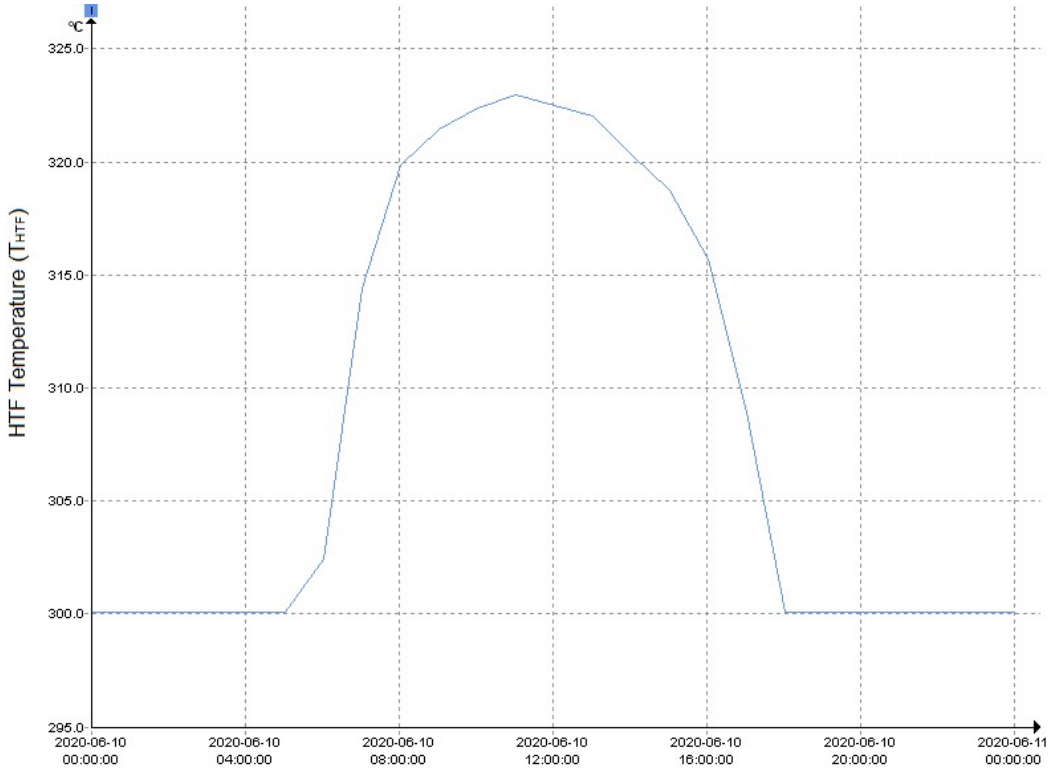

Figure 7.26: PT hybrid model HTF Temperature on June 10th.

PT solar field has the advantage of fast heating response when the DNI is available. That's because LFR suffers the transversal losses whereas the PT does not have this problem. As shown in Figures 7.25 and 7.26. they show a superior thermal performance of PT over LFR in heating response to the DNI availability.

- Solar Field Efficiency on the highest DNI day (June 10th)

Solar Field Thermal efficiency can be determined using the following formula:

$$\eta_{th,solar\ field} = \frac{Q_{EFF}}{DNI * A_{net}} \tag{7.3}$$

Where:

- A_{net}: a total of the aperture area of solar reflectors or concentrators

For LFR solar field, the field is composed of 752 LFR modules. Each aperture area is 23 m^2, giving an A_{net} of 17,296 m^2. And for PT solar field, consists of 12 PT each one aperture area is 817.5 m^2, with a total A_{net} of 9810 m^2.

Using the max DNI on June 10th. Simulation shows that the LFR field provides a heating capacity of 8.064 MW, and the PT field provides 6.467 MW of heating capacity. Yielding 57.5% solar field thermal efficiency for the LFR solar field, and 75.8% for the PT solar field thermal efficiency at the same given DNI 869.36 W/m^2. This demonstrates the superior performance of the PT over LFR in terms of the solar field efficiency on the same land size (relative to the less net area). Table 7.6 summarizes the solar field efficiency calculations.

Table 7.6: Solar field values for both LFR and PT solar fields at DNI=869.36 W/m^2

	LFR Solar Field	PT Solar Field
DNI (W/m^2)	869.36	869.36
A_{net} (m^2)	17,296	9,810
Q_{EFF} (MW)	8.064	6.467
η_{SF} (%)	57.5%	75.8%

- Annual Generated Electricity

The annual generated electricity can be determined by the following formula:

$$Electricity = (Q_{Gen} - Q_{Aux}) * 8760\ hr \tag{7.4}$$

Where:

- Electricity: the annual generated amount of electricity (MWh)
- Q_{Gen}: Power plant capacity (MW). Either 6, 7, or 8 MW in the proposed models
- Q_{Aux}: The sum of the other electrical consumption equipment in the plant. Such as pumps and air-cooled condenser fans.

As per the simulation results. Table 7.7 introduces the calculated amounts of electricity

Table 7.7: Annual generated electricity for all capacities based on both LFR and PT.

Power Plant Capacity	8 MW		7 MW		6 MW	
Solar Field Type	LFR	PT	LFR	PT	LFR	PT
Annual Generated Electricity (MWh)	68,951	68,872	60,321	60,251	51,691	51,629

In terms of annual generated capacity, LFR and PT are very close to each other. That demonstrates the fact that PT modules installed are far less than LFR modules. But the PT compensates using its superior concentration ratio and better solar field thermal efficiency.

7.4 Levelized Cost of Energy (LCOE) Calculation

At this point, all the technical framework of the proposed hybrid olive pomace-CSP power plant was introduced and explained. Simulations were run to extract different outcomes for assessing the plant performance.

Since all plant parameters are known, Economic analysis is now feasible. All the costs incurred in building the proposed models physically and their running costs during the plant lifetime are considered, to estimate the LCOE generated from the proposed models.

The incurred costs are divided into three main categories:

- Direct costs (DC): which are the costs that are paid to erect the power plant, purchase equipment, and all other costs that are paid for the power plant itself or its related works such as site preparations and infrastructure works.
- Indirect cost (IDC): costs that come as overheads, technical works, and land cost. Such as insurance, engineering, and construction management.
- Running costs: They are mainly Operation and Maintenance (O&M), annual insurance, and the cost of fuel feedstock (olive pomace).

Financing options for plant erection are either using Capital Recovery Factor (CRF) or Islamic financing. CRF is a factor that determines the annual due payment based on the number of years and an interest rate by the following formula (Masters, 2013):

$$CRF = \frac{i(1+i)^n}{(1+i)^n - 1} \tag{7.5}$$

Where:

- i: the interest rate
- n: number of years

So that:

$$AN = The\ Principle\ Borrowed\ Investment\ Cost\ * CRF \tag{7.6}$$

Where:

AN: the annual due payment from the borrowed investment cost

The Islamic financing using direct profit (Murabaha) is applying a selected profit rate that increases by the years of payment plan. The following formulas describe the mechanism. Pr stands for the profit intended in a deal (بوجلال and 2010 ,بورقبة):

$$Pr = TC * r_m * n \tag{7.7}$$

$$Sp = Pr + TC$$

(7.8)

Where:

- Pr: profit amount
- TC: the required finance amount for Investment (Total investment Cost)
- r_m: average profit (rate) percentage
- n: number of years
- Sp: the bank selling price used to calculate the annual payment

So that:

$$r_m = \frac{Sp - TC}{TC * n} * 100\%$$

(7.9)

r_m has a range that follows every Islamic financing institution. Also, in Islamic financing there is an exchange insurance amount that is added for contingencies and protection, the amount of exchange insurance rate is determined by the following formula:

$$I = TC * i_{ex} * n$$

(7.10)

i_{ex} stands for the applied percentage for exchange insurance. Where I is the added exchange insurance amount to the financed amount beside profit. So that:

$$Total\ Financed\ Amount\ = TC + Pr + I$$

(7.11)

Thus, the annual installments are by dividing the number above by the number of years (n). the profit percentage in Islamic banks differs from one bank to another and starts from 3% up to 6%. The exchange insurance rate also the same, it starts from 0.5% to 1% (JIB, 2021). These percentages depend on the policy of the financing institution, risk assessment, and other factors related to the policies of the monetary authority. 4% value of profit percentage will be considered and 0.75% for exchange insurance rate to establish the main outline of the LCOE, then sensitivity analysis will be presented to study how these and

other factors affect the LCOE of electricity produced from an LFR or PT hybrid olive pomace 7 MW plant model. Tables 7.8 and 7.9 represent the LCOE calculation for both Hybrid LFR and PT-Olive pomace at 7 MW capacity.

Table 7.8: LFR-Olive pomace hybrid 7 MW LCOE calculation summary(Askari and Ameri, 2018, Kincaid et al., 2018, Kurup and Turchi, 2015)

Direct Costs (DC)	**Unit**	**Unit Price**	**Quantity**	**Total**
Site Improvement works	Per m²	$20.00	50,000.00	$1,000,000.00
Solar Field Reflectors (LFR)	Per m²	$180.00	30,000.00	$5,400,000.00
HTF System and Filling - Using Therminol VP-1	Per m²	$60.00	30,000.00	$1,800,000.00
Power Block - dry cooling considered	Per kWe	$1,280.00	7,000.00	$8,960,000.00
Total of Direct Costs				***$17,160,000.00***
Indirect Costs (IDC)	**Unit**	**Unit Price**	**Quantity**	**Total**
Land Cost	Per m²	$15.00	50,000.00	$750,000.00
Engineering and Construction	% of DC	15.0%	1.00	$2,574,000.00
Project Contingencies and Construction Insurance	% of DC	10.0%	1.00	$1,716,000.00
Total of Indirect Costs				***$5,040,000.00***
Total Construction Costs Estimation				**$22,200,000.00**
Islamic Financing Costs (Murabaha)				
Investment Duration (years)				30
Islamic profit percentage				4%
Exchange insurance percentage				0.075%
Profit amount				$26,640,000.00
Exchange insurance amount				$499,500.00
Total Construction Costs Financed Amount				**$49,339,500.00**
Annual installments based on 30 years payments plan				**$1,644,650.00**

Running Costs (IDC)	**Unit**	**Unit Price**	**Quantity**	**Total**
Annual Insurance	% of DC	1.0%	1.00	$171,600.00
Annual O&M	Per kWe	$66.00	7,000.00	$462,000.00
Consumed Olive Pomace	Ton	$90.00	39,613.80	$3,565,242.00
Total of Annual Running Costs				***$4,198,842.00***

Annual payment and operating cost	**$5,843,492.00**
Annual Generated Electricity (MWh)	**60,321**
LCOE for kWh	**$0.0969**

Table 7.9: PT-Olive pomace hybrid 7 MW LCOE calculation summary. (Kurup and Turchi, 2015, Kincaid et al., 2018, Hagos, 2011)

Direct Costs (DC)	**Unit**	**Unit Price**	**Quantity**	**Total**
Site Improvement works	Per m²	$20.00	50,000.00	$1,000,000.00
Solar Field Concentrators (PT)	Per m²	$170.00	30,000.00	$5,100,000.00
HTF System and Filling - Using Therminol VP-1	Per m²	$60.00	30,000.00	$1,800,000.00
Power Block - dry cooling considered	Per kWe	$1,280.00	7,000.00	$8,960,000.00
Total of Direct Costs				***$16,860,000.00***
Indirect Costs (IDC)	**Unit**	**Unit Price**	**Quantity**	**Total**
Land Cost	Per m²	$15.00	50,000.00	$750,000.00
Engineering and Construction	% of DC	15.0%	1.00	$2,529,000.00
Project Contingencies and Construction Insurance	% of DC	10.0%	1.00	$1,686,000.00
Total of Indirect Costs				***$4,965,000.00***
Total Construction Costs Estimation				**$21,825,000.00**
Islamic Financing Costs (Murabaha)				
Investment Duration (years)				30
Islamic Profit Rate percentage				4%
Exchange insurance percentage				0.075%
Profit amount				$26,190,000.00
Exchange insurance amount				$491,062.50
Total Construction Costs Financed Amount				**$48,506,062.50**
Annual installments based on 30 years payments plan				**$1,616,868.75**

Running Costs (IDC)	**Unit**	**Unit Price**	**Quantity**	**Total**
Annual Insurance	% of DC	1.0%	1.00	$168,600.00
Annual O&M	Per kWe	$66.00	7,000.00	$462,000.00
Consumed Olive Pomace	Ton	$90.00	40,021.70	$3,601,953.00
Total of Annual Running Costs				***$4,232,553.00***

Annual payment and operating cost	**$5,849,421.75**
Annual Generated Electricity (MWh)	**60,251**
LCOE for kWh	**$0.0971**

The kWh is sold in Palestine from 0.5 NIS/kWh or more. Considering USD at 3.3 NIS. Then the levelized costs of energy for LFR and PT hybrid models are 0.3237 and 0.3244 NIS/kWh respectively. Which is below the general selling price of electricity in Palestine.

7.5 Sensitivity Analysis of the Levelized Cost of Unit Energy (LCOE)

LCOE can be affected by many parameters. Any change in the inputs of the proposed models changes the LCOE by different rates. In this study, the sensitivity analysis will be examined vs the cost of olive pomace, profit rate, and the land cost.

- Olive pomace price

Table 7.10 represents the modified values of LCOE based on different costs that may be incurred for a ton of olive pomace. These values consider that all other input values kept the same as in Table 7.8 and 7.9.

Table 7.10: LCOE values corresponding to different costs of olive pomace.

Olive Pomace Price ($)	LCOE of LFR ($)	LCOE of PT ($)
80	0.0903	0.0904
90	0.0969	0.0971
100	0.1034	0.1037
110	0.11	0.1104
120	0.1166	0.117

The maximum value of the LCOE that can be reached, so that produced electricity still could be sold with profit, is 0.1212 $/kWh (0.4 NIS/kWh) (PENRA, 2020). As per the table, the model could still make profits and pays off its installments up to 120$ for a ton of olive pomace. Figure 7.27 depicts the relation.

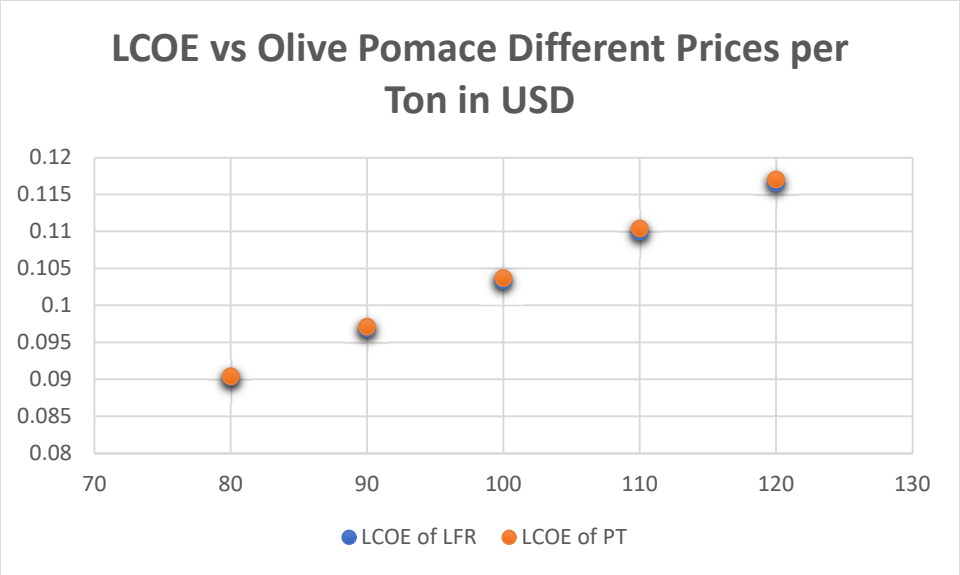

Figure 7.27: LCOE vs price of olive pomace in USD

- Islamic Financing Profit Rate:

Table 7.11 shows the modified values of LCOE based on different financing profit rate. These values consider that all other input values kept the same as in Table 7.8 and 7.9.

Table 7.11: LCOE values corresponding to different financing profit rates.

Average Profit Rate r_m (%)	LCOE of LFR ($)	LCOE of PT ($)
3%	0.0932	0.0935
4%	0.0969	0.0971
5%	0.1006	0.1007
6%	0.1042	0.1043
7%	0.1079	0.108

The model could still be functional even at high-profit rates. Even at a 7% profit rate, the LCOE still viable for production. Figure 7.28 illustrates the relation between them.

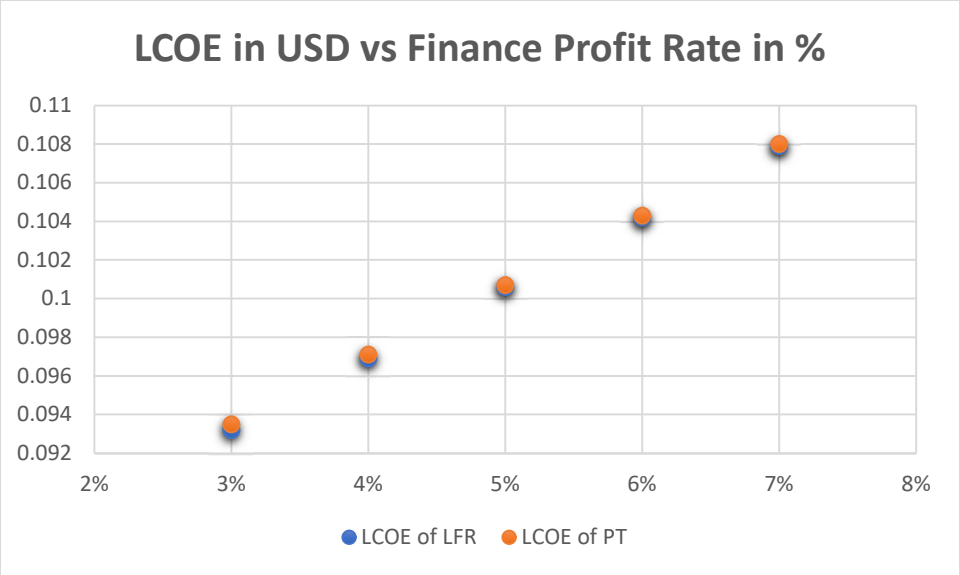

Figure 7.28: LCOE in USD vs finance profit rates in %

- Land Purchase Cost:

Table 7.12 shows the modified values of LCOE based on different prices for flatlands in the study designated location. These values consider that all other input values kept the same as in Table 7.8 and 7.9.

Table 7.12: LCOE values corresponding to different land purchase costs.

Land Cost ($ /m²)	LCOE of LFR ($)	LCOE of PT ($)
15	0.0969	0.0971
20	0.0972	0.0974
25	0.0975	0.0977
30	0.0978	0.098
35	0.0981	0.0983

The model could still be functional even at prices higher than the collected data for real estate prices in the area. Even at a 40 $/m^2 rate, the LCOE still didn't reach the threshold of 0.1212 $/kWh. Figure 7.29 illustrates the relation between them.

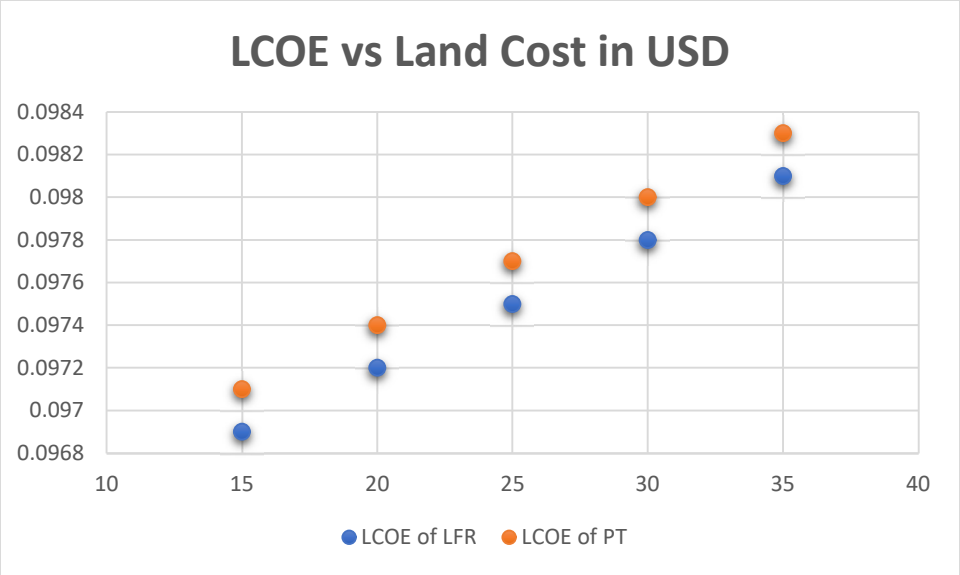

Figure 7.29: LCOE vs land purchase cost in USD.

As per the presented information, the hybridization model can produce energy at an affordable price. Making the hybrid power plant model feasible in terms of engineering and economic perspectives. In the following chapter, these results will be used to formulate the outcomes and recommendations of this study.

CHAPTER 8

Conclusions and Future Work

8.1 Conclusions

Authentic renewable resources play a vital role in contributing to the progress of societies. It is abundant, clean, and environmentally friendly. Solar-powered and biomass-powered power plants are increasing annually. Employing the sola and biomass resources in Palestine can be considered a step to mitigate the vast reliance on energy importation, and strengthen the energy sector in Palestine

In this research, an investigation was carried out to study the potential of using hybrid olive pomace-CSP power plants for electricity generation in Palestine. Complete survey and data collection were performed to gather all the required data that is needed for the analysis. An optimized power plant model was developed using EBSILON for hybridizing olive pomace with LFR powered and PT-powered solar fields. A simulation where run over an annum, with changing all the weather and sun parameters. Results were obtained and assessment was carried out.

The results show that for the same considered land area, the LFR and PT annual contribution is very close. Although the LFR installed aperture area was higher compared to the PT, the PT compensated using its superior optical efficiency. The most appropriate power generation capacity according to the considered inputs of land area and live pomace quantities is 7 MWe. The LCOE values were close in both LFR and PT hybrid models. The LCOE was 0.0969 and 0.0971 $/kWh respectively, which is lower than the maximum LCOE threshold in Palestine which is 0.1212 $/kWh. Sensitivity analyses were run to study the effect of changing the olive pomace price, Islamic profit rate, and the land cost, of the LCOE. It was found that the LCOE can be kept under the threshold by changing these variables at considered realistic rates, proving the economic feasibility of the project. the generated energy via the proposed 7 MW models can secure 1.07% of electricity consumption according to the consumed electricity in 2018.

8.2 Future Works and Recommendations

- Considering hybridization between LFR and PT solar power systems with other biomass resources that are suitable for combustion available in Palestine.
- Studying larger power generation capacities in part-load operation.
- Expand the study using more land area. And assess the techno-economic performance.

References

1- ABDO, Z. T. & KHATIB, I. 2018. *Potential of biogas production from biomass and organic waste materials in the West Bank of Palestine*, LAP LAMBERT Academic Publishing, Germany.

2- ABU HAMED, T., FLAMM, H. & AZRAQ, M. 2012. Renewable energy in the Palestinian Territories: Opportunities and challenges. *Renewable and Sustainable Energy Reviews,* 16**,** 1082-1088.

3- 3ABU HAMED, T., ISMAIL, L. & ALSHARE, A. 2017. The potential of using olive cake in power generation in the Palestinian territories. *International Journal of Sustainable Energy,* 36**,** 368-378.

4- AJLOUNI, E. & ALSAMAMRA, H. A Review of Solar Energy Prospects in Palestine. 2019. 49-62.

5- AMRO, M. A. 2016. Olives Pomace as Renewable Energy Source. *Journal of Multidisciplinary Engineering Science Studies (JMESS),* Vol. 2

6- ASKARI, I. B. & AMERI, M. J. R. E. 2018. Solar Rankine Cycle (SRC) powered by linear Fresnel solar field and integrated with Multi Effect Desalination (MED) system. 117**,** 52-70.

7- ASME 2007. Air-Cooled Steam Condensers - Performance and Test Codes. USA.

8- ATIMTAY, A. T. & VAROL, M. 2009. Investigation of co-combustion of coal and olive cake in a bubbling fluidized bed with secondary air injection. *Fuel,* 88**,** 1000-1008.

9- BARTSCH, U., MÜLLER, B., AAHEIM, A., BARNES, P., KOLSHUS, H. & MABRO, R. 2000. *Fossil fuels in a changing climate: impacts of the Kyoto Protocol and developing country participation*, Oxford University Press Oxford.

10- BURKHOLDER, F. & KUTSCHER, C. 2009. Heat Loss Testing of Schott's 2008 PTR70 Parabolic Trough Receiver. *In:* NREL (ed.).

11- ÇENGEL, Y. A. 2008. *Thermodynamics : an engineering approach*, Sixth edition. Boston : McGraw-Hill Higher Education, [2008] ©2008.

12- CHAANAOUI, M., VAUDREUIL, S. & BOUNAHMIDI, T. 2016. Benchmark of Concentrating Solar Power Plants: Historical, Current and Future Technical and Economic Development. *Procedia Computer Science,* 83**,** 782-789.

13- CLIFFE, K. R. & PATUMSAWAD, S. 2001. Co-combustion of waste from olive oil production with coal in a fluidised bed. *Waste Management,* 21**,** 49-53.

14- DA ROCHA, A. M. 2010. *Analysis on Solar Retrofit in Combined Cycle Power Plants.* Master thesis. Fakultät für Maschinenwesen und Betriebswissenschaften ….

15- DALLY, B. & MULLINGER, P. 2002. Utilization of Olive Husks for Energy Generation: A Feasibility Study. South Australian State Energy Research Advisory Committee: University of Adelaide.

16- DINCER, I. 2000. Renewable energy and sustainable development: a crucial review. *Renewable and sustainable energy reviews,* 4**,** 157-175.

17- DRAIDI, O. I. S. 2016a. *Feasibility Study of Implementing CSP Technology in Palestine.*

18- DRAIDI, O. S. 2016b. *Feasibility Study of Implementing CSP Technology in Palestine.* M.Sc, Al-Najah University.

19- DRBAL, L., WESTRA, K. & BOSTON, P. 2012. *Power Plant Engineering*, Springer Science & Business Media.

20- ELSHAZLY, R. 2011. *FEASIBILITY OF CONCENTRATED SOLAR POWER UNDER EGYPTIAN CONDITIONS.* Master in Sciences M.Sc, Kassel University, Cairo University.
21- FELDHOFF, J., SCHMITZ, K., ECK, M., SCHNATBAUM-LAUMANN, L., LAING-NEPUSTIL, D., ORTIZ-VIVES, F. & SCHULTE-FISCHEDICK, J. 2011. *Comparative System Analysis of Parabolic Trough Power Plants with DSG and Oil using Integrated Thermal Energy Storage*.
22- FELDHOFF, J. F. 2012. Linear Fresnel Collectors - A technology Overview. *In:* DLR (ed.).
23- FEMP, F. E. M. P. 2016. *Biomass For Electricity Generation* [Online]. PWDG. Available: https://www.wbdg.org/resources/biomass-electricity-generation#:~:text=Most%20biopower%20plants%20use%20direct,processes%20or%20to%20heat%20buildings. [Accessed 2016].
24- GHANNAM, M., AL-SA'ED, R. & ZIMMO, O. 2005. Assessment of recycling perspectives for olive mill solid waste in Palestine. *Proc. Int. Conf. on Water: Values and Rights, May 2-4, 2005, .* Ramallah, Palestine.: PALESTA.
25- GIOVANNELLI, A. 2015. State of the Art on Small-Scale Concentrated Solar Power Plants. *Energy Procedia,* 82**,** 607-614.
26- HAGOS, D. A. 2011. Techno-Economic Assesment of Parabolic Trough Steam Generation for Hospital.
27- IMRAISH, A. & SAFA, A. A. 2017. *Experimental and Simulation of Biomass Conversion by Gasification and Biodigestion: Potential of Bioenergy in Palestine.* An-Najah National University.
28- INDUSTRIALSOLAR 2020a. LF-11 LFR Datasheet.
29- INDUSTRIALSOLAR 2020b. Solar Field Design Instruction - LF-11 LFR Model.
30- ISLAM, M. T., HUDA, N., ABDULLAH, A. B. & SAIDUR, R. 2018. A comprehensive review of state-of-the-art concentrating solar power (CSP) technologies: Current status and research trends. *Renewable and Sustainable Energy Reviews,* 91**,** 987-1018.
31- ISMAIL, M. S., MOGHAVVEMI, M. & MAHLIA, T. M. I. 2013. Energy trends in Palestinian territories of West Bank and Gaza Strip: Possibilities for reducing the reliance on external energy sources. *Renewable and Sustainable Energy Reviews,* 28**,** 117-129.
32- JEBRIL, A. & KHATIB, I. 2018. Bio-energy in Palestine between reality and potential. *LAP LAMBERT Academic Publishing*.
33- JIB. 2021. *Murabaha and Ijara Calculation Procedures* [Online]. Available: https://www.jordanislamicbank.com/

[Accessed].
34- JINGZHI, D. 2014. Modeling for a 700 MW heat and power plant using EBSILON software. *Huadian Technology***,** 03.
35- JUAIDI, A., MONTOYA, F. G., IBRIK, I. H. & MANZANO-AGUGLIARO, F. 2016. An overview of renewable energy potential in Palestine. *Renewable Sustainable Energy Reviews*

65**,** 943-960.
36- KINCAID, N., MUNGAS, G., KRAMER, N., WAGNER, M. & ZHU, G. 2018. An optical performance comparison of three concentrating solar power collector designs in linear Fresnel, parabolic trough, and central receiver. *Applied Energy,* 231**,** 1109-1121.
37- KRUNAL H. SIYATAR, A. A. C., KIRTI J. VASANIYA, RAHUL B. CHANDEGARA 2017. Concentrated Solar Power Plant. *International Research Journal of Engineering and Technology (IRJET),* 4**,** 2395-0072.

38- KURUP, P. & TURCHI, C. S. 2015. Parabolic Trough Collector Cost Update for the System Advisor Model (SAM). *In:* NREL (ed.).
39- LI, P., NORD, N., ERTESVÅG, I. S., GE, Z., YANG, Z., YANG, Y. & MANAGEMENT 2015. Integrated multiscale simulation of combined heat and power based district heating system. *Energy Conversion,* 106**,** 337-354.
40- MAJDOUB, M. 2018. Olive pomace as biomass power plant in Tunisia: from simulation to application. *Waste and Biomass Valorization*.
41- MAKHLOUF, N., ALIAN, I. & ABUAWWAD, I. 2017. Potential of Using Concentrated Solar Power in Plastic Industry.
42- MASTERS, G. M. 2013. *Renewable and efficient electric power systems*, John Wiley & Sons.
43- MOSER, M., TRIEB, F. & FICHTER, T. 2013. Potential of Concentrating Solar Power Plants for the Combined Production of Water and Electricity in MENA Countries. *Journal of Sustainable Development of Energy, Water and Environment Systems,* 1.
44- MUSALAM, A. M., QARAMAN, A. F. A. & EL-HASSAYNA, I. 2017a. Thermal Properties of Pomace Olives in a Composite Mixture. *IUG Journal of Natural Studies*.
45- MUSALAM, A. M., QARAMAN, A. F. A. & EL-HASSAYNA, I. M. 2017b. Thermal Properties of Pomace Olives in a Composite Mixture. *Islamic University - Gaza: Journal of Natural Studies,* 25**,** 191-197.
46- NAG, P. K. 2015. *Engineering Thermodynamics, 5e*, Tata McGraw-Hill Education.
47- NIXON, J., DEY, P. & DAVIES, P. 2012. The feasibility of hybrid solar-biomass power plants in India. *Energy,* 46**,** 541–554.
48- OKTAY, Z. 2006. Olive Cake as a Biomass Fuel for Energy Production. *Energy Sources, Part A: Recovery, Utilization, and Environmental Effects,* 28**,** 329-339.
49- PABLO DEL RÍO, PEÑASCO, C. & MIRARTIGUES, P. 2018. RES policy framework for 2030. *In:* EUROPE, I. (ed.). University of Lleida (Spain): Intelligent Energy - Europe, ALTENER.
50- PCBS 2018. Quantity of Electricity Imported and Purchased in Palestine by Month and Source, 2018. *In:* STATISTICS (ed.). http://www.pcbs.gov.ps/: Palestinian Authority - PCBS.
51- PCBS 2020. Palestinian Central Bureau of Statistics.
52- PENRA 2020.
53- PETERSEIM, J. H., TADROS, A., WHITE, S., HELLWIG, U., LANDLER, J. & GALANG, K. 2014. Solar Tower-biomass Hybrid Plants – Maximizing Plant Performance. *Energy Procedia,* 49**,** 1197-1206.
54- POWER, E. 2019. *Improved boiler efficiency for large industrial boilers* [Online]. Available: https://www.explosionpower.ch/en/improved-boiler-efficiency-in-just-a-few-steps-for-large-industrial-boilers/ [Accessed].
55- QARAMAN, A. F., MUSALAM, A. & EL-HASSAYNA, I. 2017. *Thermal Properties of Pomace Olives in a Composite Mixture*.
56- RĂBOACĂ, M. S., BADEA, G., ENACHE, A., FILOTE, C., RĂSOI, G., RATA, M., LAVRIC, A. & FELSEGHI, R.-A. 2019. Concentrating Solar Power Technologies. 12**,** 1048.
57- SCHENK, H., HIRSCH, T., FELDHOFF, J. & WITTMANN, M. 2012. Energetic Comparison of Linear Fresnel and Parabolic Trough Collector Systems. *Journal of Solar Energy Engineering,* 136.
58- SERVERT, J. & SAN MIGUEL, G. 2011. Hybrid solar - Biomass plants for power generation; technical and economic assessment. *Global Nest Journal,* 13.
59- SIEMENS 2021. Siemens SST-300. *In:* AG, S. (ed.).

60- SOARES, J. Study of different solutions for solar/biomass hybrid electricity generation systems. 2018.
61- SOARES, J., OLIVEIRA, A. C., DIECKMANN, S., KRÜGER, D. & ORIOLI, F. 2018. Evaluation of the performance of hybrid CSP/biomass power plants. *International Journal of Low-Carbon Technologies,* 13**,** 380-387.
62- SOLARGIS. 2020. *Palestine DNI Values 1999-2018* [Online]. Available: https://solargis.com/ [Accessed].
63- SOLUTIA 2020. Therminol VP-1 Technical Data Leaflet.
64- SRINIVAS, T. & REDDY, B. V. 2014. Hybrid solar–biomass power plant without energy storage. *Case Studies in Thermal Engineering,* 2**,** 75-81.
65- STEAG-ENERGY 2015. EBSILON®Professional
66- The Planning Tool for the Power Plant Process. *In:* GMBH, S. (ed.).
67- STSMED 2015. *CONCENTRATED SOLAR THERMAL ENERGY SYSTEMS HANDBOOK*, ENPI CBC Mediterranean Sea Basin Programme.
68- SWAT, S. 2020. *Thermal cycle diagram calculation with Ebsilon Professional V14 - introduction example*.
69- ŚWIERZEWSKI, M. & KALINA, J. Modelling of Commercial Biomass-fired ORC System Using EBSILON Professional Software. 5th International Seminar on ORC Power Systems, 2019. 1-11.
70- TALEB, N. 2014. *Robust Design of Thermal Solar Power Station Using System Advisor Model (SAM) Software as the First Pilot Project in Palestine.* M.Sc, Islamic University of Gaza.
71- TAWARAH, K. M. & RABABAH, R. 2013. Characterization of some Jordanian crude and exhausted olive pomace samples. *Green sustainable chemistry,* 2013.
72- TOPAL, H., ATIMTAY, A. T. & DURMAZ, A. 2003. Olive cake combustion in a circulating fluidized bed☆. *Fuel,* 82**,** 1049-1056.
73- VOURDOUBAS, J. 2017. Possibilities of Energy Generation from Olive Tree Residues, by-products and Waste in Crete, Greece. *Journal of Agricultural Studies,* 5**,** 110.
74- WAEL AL-KOUZ, A. A., NIDAL ABU-LIBDEH, JAMAL NAYFEH, ALBERTO BORETTI 2020. A 140 MW Solar Thermal Plant in Jordan. *MDPI Processes,* 3.
75- WHITFOOT, J. 2018. Design of a Steam Power Plant - Cost Analysis. *In:* PITTSBURG, U. O. (ed.).
76- WOŁOWICZ, M., MILEWSKI, J., FUTYMA, K. & SZCZĘŚNIAK, A. The construction of the mathematical model of supercritical CO2 cycles using EBSILON software. AIP Conference Proceedings, 2019. AIP Publishing LLC, 450085.
77- YASIN, A. M. 2019a. The Impact of Dispatchability of Parabolic Trough CSP Plants over PV Power Plants in Palestinian Territories. *International Journal of Photoenergy,* 2019.
78- YASIN, A. M. 2019b. The Impact of Dispatchability of Parabolic Trough CSP Plants over PV Power Plants in Palestinian Territories. *International Journal of Photoenergy,* 2019**,** 4097852.
79- بوجلال, م. & بورقبة, ش. 2010. تكلفة التمويل في البنوك التقليدية والبنوك الإسلامية: دراسة مقارنة. مجلة جامعة الملك عبد العزيز.

Appendices

Appendix – 1: Thermal Efficiency Improvement Tables

Model I

For model configuration, I, reheat, and bleed pressures are changed while keeping all other parameters constant (P, T of live steam and the condensing pressure is selected previously and constant). In appendix 1, the thermal efficiency improvement is listed.

Power Block Model I pressure optimization

Reheat and Bleed Pressure	Thermal Efficiency
40	34.68%
30	35.56%
25	35.96%
20	36.34%
18	36.47%
16	36.58%
14	36.68%
12	36.75%
11	36.77%
10	36.75%
9	36.72%
8	36.64%
6	36.30%

- Model II

For model configuration II, reheat pressure and bleed pressure are changed one vs other. Resulting the following table that determines the combination that yields the best model efficiency.

Power Block Model II pressures optimization

Bleed Pressure P = 2 bar		Bleed Pressure P = 3 bar		Bleed Pressure P = 4 bar		Bleed Pressure P = 5 bar	
Reheat Pressure	Thermal Efficiency	Reheat Pressure	Thermal Efficiency	Reheat Pressure	Thermal Efficiency	Reheat Pressure	Thermal Efficiency
40	35.90%	40	36.20%	40	36.30%	40	36.40%
30	36.40%	30	36.70%	30	36.80%	30	36.80%
25	36.70%	25	36.90%	25	37.00%	25	37.00%
20	36.90%	20	37.00%	20	37.10%	20	37.10%

18	36.90%	18	37.10%	18	37.10%	18	37.10%
16	37.00%	16	37.10%	16	37.10%	16	37.10%
14	37.00%	14	37.10%	14	37.10%	14	37.10%
12	37.00%	12	37.00%	12	37.00%	12	37.00%
11	36.90%	11	37.00%	11	37.00%	11	36.90%
10	36.90%	10	36.90%	10	36.90%	10	36.80%
9	36.80%	9	36.80%	9	36.80%	9	36.70%
8	36.60%	8	36.70%	8	36.60%	8	36.50%
6	36.10%	6	36.10%	6	36.10%	6	35.90%
Bleed Pressure P = 6 bar		**Bleed Pressure P = 7 bar**		**Bleed Pressure P = 10 bar**		**Bleed Pressure P = 15 bar**	
Reheat Pressure	**Thermal Efficiency**	**Reheat Pressure**	**Thermal Efficiency**	**Reheat Pressure**	**Thermal Efficiency**	**Reheat Pressure**	**Thermal Efficiency**
40	36.40%	40	36.40%	40	36.40%	40	36.10%
30	36.80%	30	36.80%	30	36.70%	30	36.40%
25	37.00%	25	36.90%	25	36.80%	25	36.50%
20	37.10%	20	37.00%	20	36.80%	20	36.50%
18	37.10%	18	37.00%	18	36.80%	18	36.40%
16	37.10%	16	37.00%	16	36.80%	16	36.40%
14	37.00%	14	36.90%	14	36.70%	*	*
12	36.90%	12	36.80%	12	36.60%	*	*
11	36.90%	11	36.80%	11	36.50%	*	*
10	36.70%	10	36.70%	10	36.40%	*	*
9	36.60%	9	36.50%	*	*	*	*
8	36.40%	8	36.30%	*	*	*	*
*	*	6	35.70%	*	*	*	*

- Model III

For model configuration III, reheat pressure and bleed pressure are changed one vs other. Resulting the following table that determines the combination that yields the best model efficiency.

Power Block Model III pressures optimization

Bleed Pressure = 2 bar		Bleed Pressure = 3 bar		Bleed Pressure = 4 bar		Bleed Pressure = 5 bar	
Reheat Pressure	Thermal Efficiency	Reheat Pressure	Thermal Efficiency	Reheat Pressure	Thermal Efficiency	Reheat Pressure	Thermal Efficiency
40	35.40%	40	36.00%	40	36.30%	40	36.40%
30	36.60%	30	36.90%	30	37.10%	30	37.20%
25	37.10%	25	37.30%	25	37.40%	25	37.50%
20	37.50%	20	37.60%	20	37.70%	20	37.60%
18	37.60%	18	37.70%	18	37.70%	18	37.70%
16	37.70%	16	37.80%	16	37.70%	16	37.60%
14	37.80%	14	37.80%	14	37.70%	14	37.60%

12	37.70%	12	37.70%	12	37.60%	12	37.50%
11	37.70%	11	37.60%	11	37.50%	11	37.30%
10	37.60%	10	37.50%	10	37.40%	10	37.20%
9	37.50%	9	37.40%	9	37.20%	9	37.00%
8	37.30%	8	37.20%	8	37.00%	8	36.80%
6	36.80%	6	36.50%	6	36.20%	6	36.00%
Bleed Pressure = 6 bar		Bleed Pressure = 7 bar		Bleed Pressure = 10 bar		Bleed Pressure = 15 bar	
Reheat Pressure	Thermal Efficiency	Reheat Pressure	Thermal Efficiency	Reheat Pressure	Thermal Efficiency	Reheat Pressure	Thermal Efficiency
40	36.50%	40	36.60%	40	36.50%	40	36.30%
30	37.20%	30	37.20%	30	37.00%	30	36.60%
25	37.40%	25	37.40%	25	37.20%	25	36.70%
20	37.60%	20	37.50%	20	37.20%	20	36.60%
18	37.60%	18	37.50%	18	37.10%	18	36.50%
16	37.50%	16	37.40%	16	37.00%	16	36.40%
14	37.40%	14	37.30%	14	36.80%	*	*
12	37.30%	12	37.10%	12	36.60%	*	*
11	37.20%	11	37.00%	11	36.50%	*	*
10	37.00%	10	36.80%	10	36.40%	*	*
9	36.80%	9	36.60%	*	*	*	*
8	36.50%	*	*	*	*	*	*
*	*	*	*	*	*	*	*

- Model IV

For model configuration IV, reheat pressure and bleed pressure are changed one vs other. Resulting the following table that determines the combination that yields the best model efficiency.

Power Block Model IV pressures optimization

Bleed Pressure = 2 bar		Bleed Pressure = 3 bar		Bleed Pressure = 4 bar		Bleed Pressure = 5 bar	
Reheat Pressure	Thermal Efficiency	Reheat Pressure	Thermal Efficiency	Reheat Pressure	Thermal Efficiency	Reheat Pressure	Thermal Efficiency
40	36.40%	40	36.70%	40	36.80%	40	36.80%
30	37.20%	30	37.40%	30	37.40%	30	37.40%
25	37.50%	25	37.60%	25	37.70%	25	37.60%
20	37.80%	20	37.90%	20	37.80%	20	37.70%
18	37.90%	18	37.90%	18	37.80%	18	37.80%
16	37.90%	16	37.90%	16	37.80%	16	37.70%
14	37.90%	14	37.90%	14	37.80%	14	37.70%
12	37.90%	12	37.80%	12	37.70%	12	37.50%
11	37.80%	11	37.70%	11	37.60%	11	37.40%
10	37.80%	10	37.60%	10	37.50%	10	37.30%
9	37.60%	9	37.50%	9	37.30%	9	37.10%

8	37.50%	8	37.30%	8	37.10%	8	36.90%
6	36.90%	6	36.60%	6	36.40%	6	36.10%
Bleed Pressure = 6 bar		Bleed Pressure = 7 bar		Bleed Pressure = 10 bar		Bleed Pressure = 15 bar	
Reheat Pressure	Thermal Efficiency	Reheat Pressure	Thermal Efficiency	Reheat Pressure	Thermal Efficiency	Reheat Pressure	Thermal Efficiency
40	36.80%	40	36.80%	40	36.70%	40	36.40%
30	37.40%	30	37.30%	30	37.10%	30	36.70%
25	37.60%	25	37.50%	25	37.20%	25	36.70%
20	37.70%	20	37.50%	20	37.20%	20	36.60%
18	37.60%	18	37.50%	18	37.20%	18	36.50%
16	37.60%	16	37.50%	16	37.10%	16	36.40%
14	37.50%	14	37.40%	14	36.90%	14	*
12	37.40%	12	37.20%	12	36.70%	12	*
11	37.30%	11	37.10%	11	36.60%	11	*
10	37.10%	10	36.90%	10	36.40%	10	*
9	36.90%	9	36.70%	9	*	9	*
8	36.60%	8	36.40%	8	*	8	*
6	*	6	*	6	*	6	*

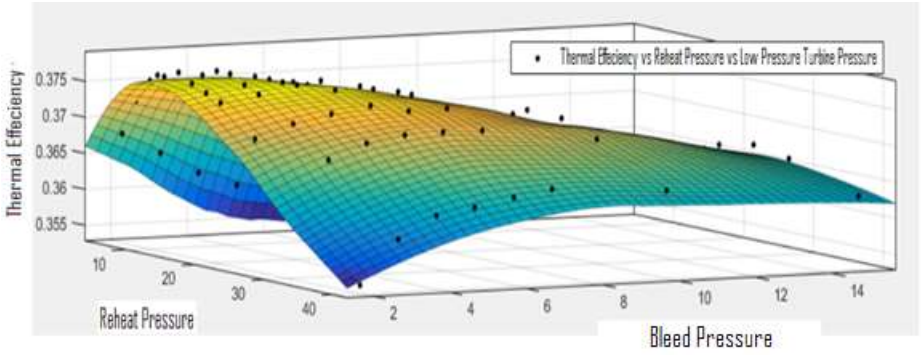

Reheat and bleed pressure turbine pressures vs thermal efficiency relation (Extracted from Model III but applies with small errors for other models except for Model I).

Appendix – 2: Industrial Solar LFR Module Technical Data

INDUSTRIAL SOLAR
renewables onsite

Fresnel Collector LF-11 Datasheet

The LF-11 Fresnel collector uses high-quality components from the concentrating solar power (CSP) industry, such as safety glass mirrors and thermally efficient vacuum absorber tubes. The collector operates safely and with minimum human intervention, guaranteeing the highest yields from the solar resource.

General data of a single module

Module width: 7.5 m
Module length: 4.06 m
Aperture surface of primary reflectors: 23 m²
Ground surface of a single module: 30.45 m²
Receiver height above primary reflector: 4.0 m
Height of primary reflector above ground level: 0.5 m
Minimum clearance between parallel rows: 0.2 m
Specific weight: 26.2 kg/m² (per installation area)
Maximum operational wind speed: 100 km/h
Maximum wind speed in stow position: 180 km/h
Life expectancy: +25 years

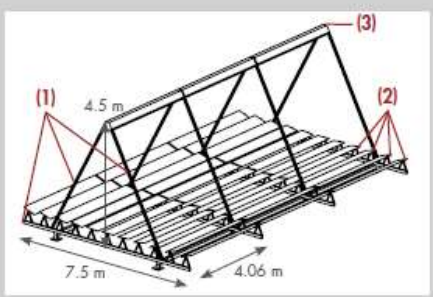

- *1. Support structure*
- *2. Primary reflectors*
- *3. Receiver, consisting of secondary reflector and vacuum absorber tube*

Optical performance characteristics

Angle-independent optical efficiency *(with 100% clean primary and secondary reflectors and receiver glass tube)*

- η_0 = 0.686 (for sun in zenith)
- η_{max} = 0.709 (for sun at 5° transversal zenith angle)

INDUSTRIAL SOLAR
renewables onsite

Thermal performance characteristics

Due to the vacuum absorber tube, thermal performance is independent of wind speed.

- ✔ **Maximum operating temperature: 400°C**
- ✔ **Thermal loss per m² of primary reflector** (according to DLR):
  - u1 = 0.032913 W/(m²K)
  - u4 = 1.4838 x 10^{-9} W/(m²K⁴)
- ✔ **Thermal output (under reference conditions*)**
  - 13.82 kW per standard module
  - 601 W/m² in terms of aperture surface area of primary reflectors
  - 454 W/m² in terms of total installation surface area

reference conditions:

30°C ambient temperature	*900 W/m² direct normal radiation*
160°C inflow temperature	*Azimuth angle 90°*
180°C outflow temperature	*Zenith angle 30°*

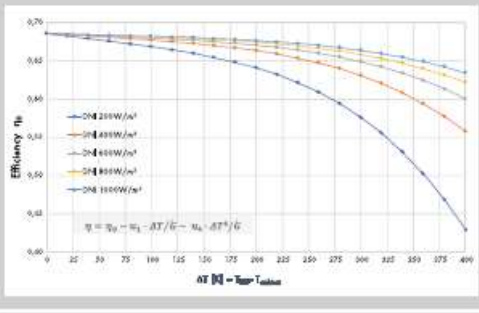

Characteristic curve of the LF-11 Fresnel collector

Correction factor (IAM – Incident Angle Modifier)

ANGLE	TRANSVERSAL	LONGITUDINAL
0	1.000	1.000
5	1.033	0.973
10	0.995	0.947
15	1.022	0.914
20	0.986	0.872
25	1.000	0.823
30	0.982	0.767
35	0.957	0.702
40	0.937	0.632
45	0.954	0.553
50	0.911	0.469
55	0.832	0.380
60	0.738	0.288
65	0.629	0.196
70	0.514	0.112
75	0.394	0.046
80	0.270	0.010
85	0.150	0.000
90	0.069	0.000

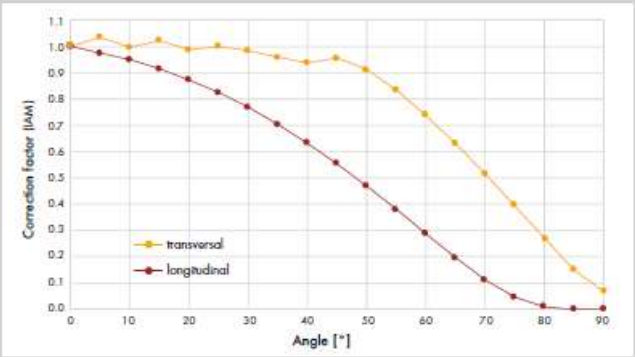

Correction factor

Additional features

- ✔ Lightweight structure
- ✔ Stow position for self-cleaning
- ✔ Good accessibility for maintenance
- ✔ Automatic mirror calibration system
- ✔ High ground usage efficiency
- ✔ Touchscreen HMI
- ✔ Electrical system according to steam boiler standards
- ✔ Optional automatic cleaning

Industrial Solar GmbH
Basler Str. 115
D-79115 Freiburg
T +49 761 767111-0
F +49 761 767111-99
info@industrial-solar.de
www.industrial-solar.de

Appendix – 3: HTF Therminol VP-1 datasheet

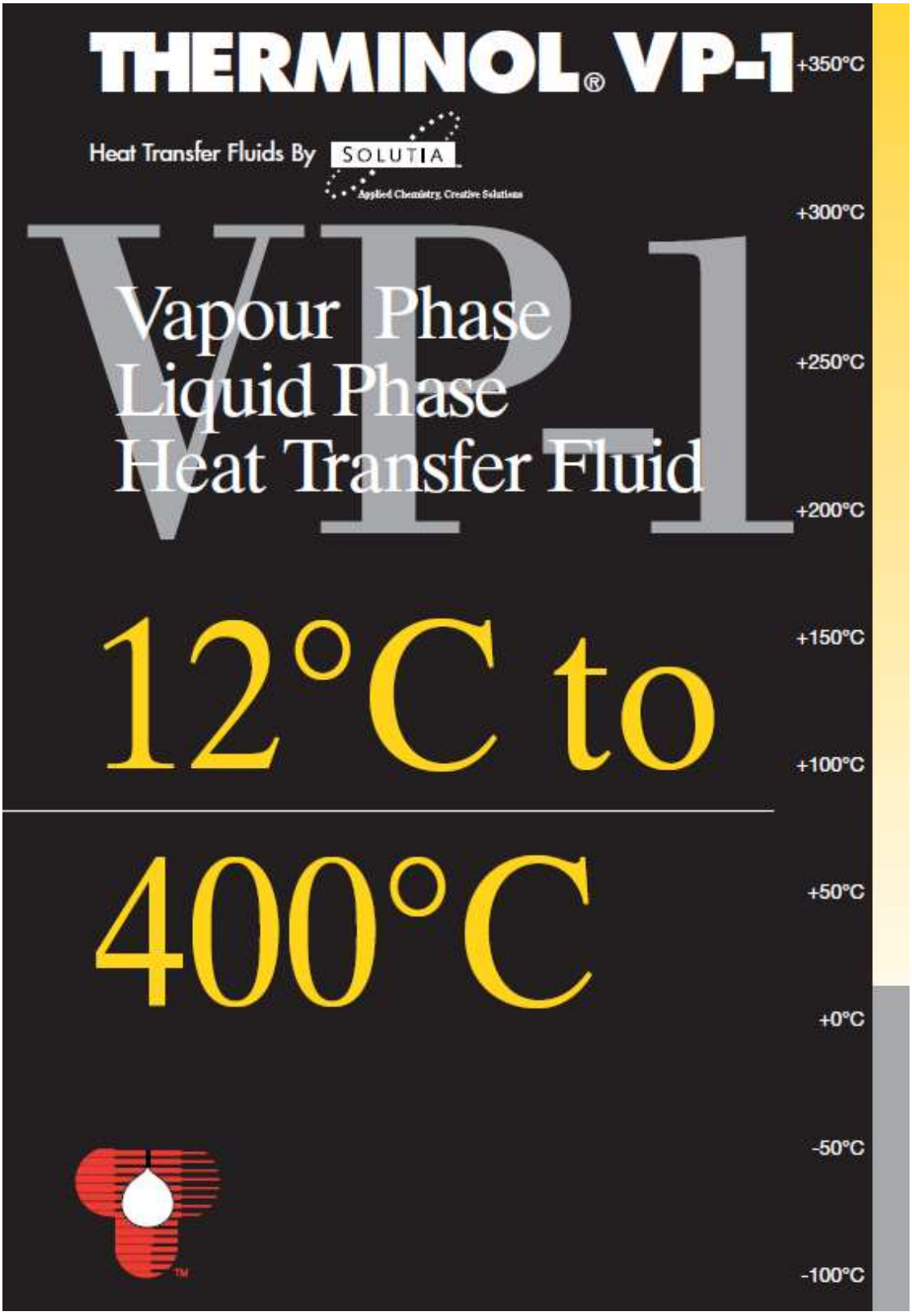

Therminol VP-1 liquid/vapour phase heat transfer fluid, is a stable, high temperature medium that delivers process heat at temperatures up to 400°C with reliability and precise control.

Therminol VP-1 is a eutectic mixture of 73.5% diphenyl oxide / 26.5% diphenyl, and as such can be used in existing liquid, or vapour phase systems, for top-up or replacement of heat transfer fluids of the same composition. Vapour phase operation is possible at temperature above 257°C.

Heat Tracing System

Since Therminol VP-1 heat transfer fluid solidifies at 12°C, precautions must be taken to ensure lines do not freeze, particularly in outdoor installations. Heat tracing must be installed wherever lines run a danger of cooling below this point. All pipelines and equipment which may contain stagnant liquid should be traced, including all streams, vapour, drain and charge lines.

Thermal Stability at 400°C

Thermal stability of a heat transfer is one of the most important considerations in the selection of a fluid for operation under specific heat transfer conditions. Therminol VP-1 has a reputation for outstanding stability in operation.

Therminol VP-1 is based on raw materials of high purity produced by a first intent manufacturing process. This results in a reduced level of high boiler formation, superior thermal stability and benefits to the user in terms of extended fluid life and dependable trouble-free system operation.

Therminol VP-1 is thermally stable and suitable for operation over long periods at bulk temperatures up to 370-400°C.

Flammability

Although the DP/DPO eutectic can burn at elevated temperature, its chemical nature is such that its use as heat transfer medium in a properly designed and operated system does not normally constitute a serious fire or explosion hazard. Vapour freed into the air rapidly cools to below the fire point. High pressure mists, however, can form an explosive mixture with air.

Typical Physical, Chemical and Thermal Properties of Therminol VP-1

Composition		Diphenyl oxide/diphenyl
Appearance		Clear, sediment free liquid
Max. bulk temperature		400°C
Max. film temperature		430°C
Kinematic viscosity @ 40°C	DIN 51562 - 1	2.48 mm^2/s (cSt)
Density @ 15°C	DIN 51757	1068 kg/m^3
Flash point	DIN EN 22719	110°C
	DIN 51376	124°C
Fire point	ISO 2592	127°C
Autoignition temperature	DIN 51794	621°C
Pour point	ISO 3016	12°C
Boiling point @ 1013 mbar		257°C
Coefficient of thermal expansion		0.00097/°C
Moisture content	DIN 51777 - 1	< 300 ppm
Total acidity	DIN 51558 - 1	< 0.2 mg KOH/g
Chlorine content	DIN 51577 - 3	< 10 ppm
Copper corrosion	EN ISO 2160	<< 1a
Average molecular weight		166

Note: Values quoted are typical values obtained in the laboratory from production samples. Other samples might exhibit slightly different data. Specifications are subject to change. Write to Solutia for current sales specifications.

Properties of Therminol VP-1 vs Temperatures - Liquid Phase

Temperature	Density	Thermal Conductivity	Heat Capacity	Viscosity		Vapour pressure (absolute)	Enthalpy	Latent Heat vap.
				Dynamic	Kinematic			
°C	kg/m³	W/m.K	kJ/kg.K	mPa.s	mm²/s**	kPa*	kJ/kg	kJ/kg
12	1071	0,137	1,523	5,48	5,12	-	0	419,0
20	1064	0,136	1,546	4,29	4,03	-	12,3	414,7
30	1056	0,135	1,575	3,28	3,10	-	27,9	409,3
40	1048	0,134	1,604	2,60	2,48	-	43,8	403,9
50	1040	0,133	1,633	2,12	2,03	-	60,0	398,6
60	1032	0,132	1,662	1,761	1,707	-	76,4	393,3
70	1024	0,131	1,690	1,492	1,458	-	93,2	388,1
80	1015	0,130	1,719	1,284	1,265	-	110,3	382,9
90	1007	0,129	1,747	1,119	1,111	-	127,6	377,8
100	999	0,128	1,775	0,985	0,986	0,5	145,2	372,7
110	991	0,126	1,803	0,875	0,884	0,8	163,1	367,6
120	982	0,125	1,831	0,784	0,798	1	181,3	362,6
130	974	0,124	1,858	0,707	0,726	2	199,7	357,5
140	965	0,123	1,886	0,642	0,665	3	218,4	352,6
150	957	0,121	1,913	0,585	0,612	5	237,4	347,6
160	948	0,120	1,940	0,537	0,566	7	256,7	342,7
170	940	0,118	1,968	0,494	0,526	9	276,2	337,7
180	931	0,117	1,995	0,457	0,491	13	296,0	332,8
190	922	0,115	2,021	0,424	0,460	18	316,1	327,9
200	913	0,114	2,048	0,395	0,432	24	336,5	323,0
210	904	0,112	2,075	0,368	0,407	32	357,1	318,0
220	895	0,111	2,101	0,345	0,385	42	378,0	313,0
230	886	0,109	2,128	0,324	0,366	54	399,1	308,0
240	877	0,107	2,154	0,305	0,348	68	420,5	303,0
250	867	0,106	2,181	0,288	0,332	86	442,2	297,9
260	857	0,104	2,207	0,272	0,317	108	464,1	292,7
270	848	0,102	2,234	0,258	0,304	133	486,3	287,5
280	838	0,100	2,260	0,244	0,292	163	508,8	282,2
290	828	0,098	2,287	0,232	0,281	198	531,6	276,8
300	817	0,096	2,314	0,221	0,271	239	554,6	271,2
310	806	0,095	2,341	0,211	0,262	286	577,8	265,6
320	796	0,093	2,369	0,202	0,254	340	601,4	259,7
330	784	0,091	2,397	0,193	0,246	401	625,2	253,8
340	773	0,089	2,425	0,185	0,239	470	649,3	247,6
350	761	0,086	2,454	0,177	0,233	548	673,7	241,3
360	749	0,084	2,485	0,170	0,227	635	698,4	234,7
370	736	0,082	2,517	0,164	0,222	732	723,4	227,8
380	723	0,080	2,551	0,158	0,218	840	748,8	220,7
390	709	0,078	2,588	0,152	0,214	959	774,4	213,2
400	694	0,076	2,628	0,146	0,211	1090	800,5	205,3
410	679	0,073	2,674	0,141	0,208	1230	827,0	197,0
420	662	0,071	2,729	0,137	0,206	1390	854,0	188,0
425	654	0,070	2,760	0,134	0,205	1470	867,7	183,3

* 1 bar = 100kPa ; ** 1 mm²/s = 1 cSt

Note: Values quoted are typical values obtained in the laboratory from production samples. Other samples might exhibit slightly different data. Specifications are subject to change. Write to Solutia for current sales specifications.

Physical Property Formulae of Liquid

Density (kg/m³) = - 0,90797 * T(°C) + 0,00078116 * T²(°C) - 2,367 * 10^{-6} * T³(°C) + 1083,25

Heat capacity (kJ/kg.K) = + 0,002414 * T(°C) + 5,9591 * 10^{-5} * T²(°C) - 2,9879 * 10^{-8} * T³(°C) + 4,4172 * 10^{-11} * T⁴(°C) + 1,498

Thermal Conductivity (W/m.K) = - 8,19477 * 10^{-5} * T(°C) - 1,92257 * 10^{-7} * T²(°C) + 2,5034 * 10^{-11} * T³(°C) - 7,2974 * 10^{-15} * T⁴(°C) + 0,137743

Kinematic viskosity (mm²/s) = $e^{\left(\frac{544,149}{T(°C)+114,43} - 2,59578\right)}$

Vapour pressure (kPa) = - 0,190859 * T(°C) + 4,35824 * 10^{-3} * T²(°C) - 3,6106 * 10^{-5} * T³(°C) + 1,08408 * 10^{-7} * T⁴(°C) + 2,12329

Properties of Therminol VP-1 vs Temperatures - Vapour Phase

Temperature °C	Density kg/m³	Thermal Conductivity W/m.K	Heat Capacity kJ/kg.K	Enthalpy* kJ/kg	Dynamic Viskosity mPa.s
12	-	0,0081	0,975	419,0	0,0057
20	-	0,0085	1,003	427,0	0,0059
30	-	0,0090	1,037	437,2	0,0061
40	-	0,0095	1,070	447,7	0,0063
50	-	0,0100	1,104	458,6	0,0065
60	-	0,0105	1,137	469,7	0,0067
70	-	0,0110	1,170	481,3	0,0069
80	-	0,0116	1,203	493,2	0,0071
90	-	0,0121	1,235	505,4	0,0073
100	-	0,0126	1,267	517,9	0,0075
110	0,042	0,0132	1,299	530,7	0,0077
120	0,065	0,0137	1,331	543,9	0,0079
130	0,099	0,0143	1,362	557,2	0,0081
140	0,148	0,0149	1,393	571,0	0,0083
150	0,214	0,0154	1,424	585,0	0,0085
160	0,303	0,0160	1,454	599,4	0,0087
170	0,422	0,0166	1,484	613,9	0,0089
180	0,575	0,0171	1,514	628,8	0,0091
190	0,772	0,0177	1,543	644,0	0,0094
200	1,02	0,0183	1,572	659,5	0,0096
210	1,33	0,0189	1,601	675,1	0,0098
220	1,71	0,0195	1,629	691,0	0,0100
230	2,17	0,0201	1,657	707,1	0,0102
240	2,72	0,0207	1,685	723,5	0,0104
250	3,38	0,0213	1,712	740,1	0,0106
260	4,17	0,0220	1,739	756,8	0,0108
270	5,09	0,0226	1,766	773,8	0,0110
280	6,17	0,0232	1,792	791,0	0,0112
290	7,42	0,0238	1,819	808,4	0,0114
300	8,86	0,0245	1,845	825,8	0,0116
310	10,5	0,0251	1,871	843,4	0,0118
320	12,4	0,0258	1,897	861,1	0,0120
330	14,6	0,0264	1,923	879,0	0,0122
340	17,0	0,0271	1,948	896,9	0,0124
350	19,8	0,0277	1,974	915,0	0,0126
360	22,9	0,0284	2,001	933,1	0,0128
370	26,5	0,0291	2,027	951,2	0,0130
380	30,5	0,0298	2,054	969,5	0,0132
390	35,0	0,0304	2,082	987,6	0,0134
400	40,1	0,0311	2,111	1005,8	0,0136
410	45,8	0,0318	2,142	1024,0	0,0138
420	52,4	0,0325	2,175	1042,0	0,0140

* the enthalpy basis is ideal gas at 12 °C

Note: Values quoted are typical values obtained in the laboratory from production samples. Other samples might exhibit slightly different data. Specifications are subject to change. Write to Solutia for current sales specifications.

Physical Property Formulae of Vapour

Density (kg/m³) = - 0,0303917 * T(°C) + 4,34615 * 10^{-4} * T²(°C) - 2,41006 * 10^{-6} * T³(°C) + 5,33458 * 10^{-9} * T⁴(°C) + 0,553905

Heat Capacity (kJ/kg.K) = + 0,003703 * T(°C) - 3,0274 * 10^{-6} * T²(°C) + 2,9324 * 10^{-9} * T³(°C) + 0,92709